



NATIONAL TECHNICAL UNIVERSITY OF ATHENS

School of Naval Architecture and Marine Engineering  
Division of Ship Design and Maritime Transport

Diploma Thesis

Parametric Roll Resonance in Random Waves

*Alexandra Fanouraki*

July 10, 2022

*Supervisor: K. J. Spyrou, Professor NTUA*

## Abstract

This work deals with parametric resonance which poses a great danger especially for container ships sailing in following or head seas. As a parametric resonance phenomenon, parametric roll is characterized by a periodical alteration of one of its characteristics, in this case the restoring ability of the ship. In this diploma thesis, important parameters that affect the instability of the ship are discussed. Also, the way in which the problem is modeled to find the ship's response to roll is presented. The ship used for this study, as a sample ship, is a large containership, with  $L_{oa} = 250 \text{ meters}$ .

The response of the ship is found by solving the one degree of freedom differential equation of rolling motion. The value of the righting arm, hence the restoring term, is derived from the equilibrium of the ship in the pitch and heave motions (pseudo-static model or else called 1.5 D.O.F.), for each specific time instant and position of the ship on the wave.

After constructing the numerical model and selecting the appropriate discretization of the hull geometry to solve the hydrostatic equilibrium at each position, the information on the form of the free surface is selected. The waves are irregular one-directional following waves. The free surface elevation is approximated by the random phase model. The different harmonic frequencies are correlated with the corresponding wave heights by a specific energy spectrum (in particular the Jonswap spectrum).

Specific cases were selected for consideration in order to construct a stability diagram, with the values of the significant height and the ratio  $a = \frac{4\omega_0^2}{\omega_{ep}^2}$  with the encounter frequency corresponding to the peak period. The diagrams were constructed for a different range of ship's forward speed and sea states. The results showed that, there are regions of instability, of which a few are cases of capsizing. These regions are narrower and generally shorter than those found in regular waves. From the data extracted we could say that the areas of instability correspond to lower ship speeds. In addition, for speeds over 12 knots there was no parametric roll observed at all.

Parametric resonance is a dangerous phenomenon that can lead to large roll angles, and cause severe container losses and economic damage. From the results of this thesis it is obvious that in irregular waves parametric roll occurs at a lower frequency. However, in cases where it occurs it can cause large roll angles and even capsizing.

As the phenomenon of wave randomness in combination with dynamic stability is a complex one, further studies are needed to provide a more complete picture of the occurrence of parametric roll in random waves.

# Acknowledgements

This diploma thesis has been carried out at the Division of Ship Design and Maritime Transport at the School of Naval Architecture and Marine Engineering of the National Technical University of Athens, under the supervision of Professor K. J. Spyrou.

First and foremost, I would like to thank Professor K. J. Spyrou for accepting me to conduct this thesis and at the same time gave me the opportunity to work on such an interesting topic and to get an insight into the ocean of knowledge concerning dynamic stability and, thus, parametric roll. I would also like to sincerely thank him for his constant guidance, support and his knowledge and experience that he shared with me.

I would like to thank Doctoral Candidate Ioannis Kontolefas for his invaluable assistance, as well as his patience, support and understanding. His valuable advice on understanding and developing the code helped me overcome obstacles at various stages of my diploma thesis.

In addition, I would like to thank all my friends, who supported me, each in their own special way, and were by my side throughout my academic journey. In particular I want to thank Kostas for his infinite support and for always standing by my side. Also, my friends Chris, Margaret, Myrsini and Antonia, for their patience and emotional support.

Last but not least, I would like to deeply thank my family for their patience and understanding in every decision I made and for providing me with everything I needed to get to this point.

# List of Figures

- 1.1 Pictures of the casualties from the APL CHINA and Svendborg Maersk containerships . . . . . 1
  - 1.1a Disasters from the APL CHINA accident [1] . . . . . 1
  - 1.1b Svendborg Maersk, aft deck at arrival in Malaga [2] . . . . . 1
- 1.2 Examples of lashing bridge damages and container losses, occurred in MAERSK ESSEN accident [4] . . . . . 2
  
- 3.1 Stevin’s Law [33] . . . . . 10
- 3.2 Righting Moment generation . . . . . 12
- 3.3 The stable and unstable equilibrium . . . . . 13
- 3.4 IMO Regulations for Intact Stability . . . . . 15
  - 3.4a General Regulations[16] . . . . . 15
  - 3.4b Regulations for Severe Wind and Rolling Criteria (Weather Criteria)[11] . . . . . 15
- 3.5 Difference in the waterplane for crest trough the midship, calm water and for wave trough amidship. . . . . 17
- 3.6 Time series of a roll decay motion[39] . . . . . 18
- 3.7 Example of GZ curves for calm water, wave crest amidship and wave trough amidship for a C11 type container ship [43]. . . . . 20
- 3.8 Stability Chart of solutions of the Mathieu Equation [3] . . . . . 21
- 3.9 Examples of swell ocean and wind generated waves . . . . . 23
  - 3.9a Swell ocean [45] . . . . . 23
  - 3.9b Waves generated by wind [46] . . . . . 23
- 3.10 Irregular wave from sum of regular waves . . . . . 24
  - 3.10a Multi-directional waves . . . . . 24
  - 3.10b Unidirectional waves [47] . . . . . 24
- 3.11 Comparison of PM and JONSWAP spectra [47] . . . . . 26
  
- 4.1 Definition of motions in 6DOF (surge, sway, heave, roll, pitch and yaw) [51] 29
- 4.2 Example of Buoyancy calculation- graphic representation of the position of the ship for specific  $(r_s^e, q_s^e)$  position vector . . . . . 32
  - 4.2a Position vector  $(r_s^e, q_s^e) = (0, 0, 0, 0, 0, 0)$  . . . . . 32
  - 4.2b Position vector  $(r_s^e, q_s^e) = (0, 0, 8.1, -\pi/12, \pi/180, 0)$  . . . . . 32
- 4.3 Rhino Tri-Mesh with different number of elements . . . . . 35
  - 4.3a Discretization with 1,000 elements . . . . . 35
  - 4.3b Discretization with 10,000 elements . . . . . 35



4.3c	Discretization with 20,000 elements . . . . .	35
4.4	Mathematica Quad-Mesh with different number of elements . . . . .	36
4.4a	Discretization with 2,320 elements . . . . .	36
4.4b	Discretization with 4,382 elements . . . . .	36
4.4c	Discretization with 6,694 elements . . . . .	36
4.5	Validation with Trim & Stability data and Aveva model of LCB and Displacement in Calm Water with Trim =0 . . . . .	38
4.6	Validation with Trim & Stability data and Aveva model of LCB and Displacement in Calm Water with Trim by Head . . . . .	38
4.7	Validation with Trim & Stability data and Aveva model of LCB and Displacement in Calm Water with Trim by Stern . . . . .	39
4.8	Validation with Trim & Stability data and Aveva model of GZ curve in Calm Water . . . . .	41
4.9	Positioning of a ship on a regular wave . . . . .	44
4.9a	Wave phase $\epsilon = 0\pi$ , . . . . .	44
4.9b	Wave phase $\epsilon = 0.5\pi$ , . . . . .	44
4.9c	Wave phase $\epsilon = 1\pi$ , . . . . .	44
4.9d	Wave phase $\epsilon = 1.5\pi$ . . . . .	44
4.10	Validation with Aveva model of GZ curve in sinusoidal Wave for LC 18 . . . . .	45
5.1	Polynomial fitting of data for approximation of $GM_0$ . . . . .	48
5.1a	Loading Condition 18 . . . . .	48
5.1b	Loading Condition 27 . . . . .	48
5.2	Comparison of Stability Charts for regular following wave (Type A) for LC -18 . . . . .	54
5.2a	Dousia's stability chart [26] . . . . .	54
5.2b	Stability Chart with data produced by the model developed in this diploma thesis . . . . .	54
5.3	Stability Chart for regular following wave (Type B) for LC-18 . . . . .	55
6.1	Scatter diagram for North Atlantic operation with $H_s$ in m and $T_p$ in s . . . . .	57
6.2	Jonswap spectrum discretization for $T_p = 6.5$ sec . . . . .	59
6.2a	$H_s = 0.5 m$ . . . . .	59
6.2b	$H_s = 4.5 m$ . . . . .	59
6.2c	$H_s = 9 m$ . . . . .	59
6.3	Jonswap spectrum discretization for $T_p = 8.$ sec . . . . .	59
6.3a	$H_s = 0.5 m$ . . . . .	59
6.3b	$H_s = 4.5 m$ . . . . .	59
6.3c	$H_s = 9 m$ . . . . .	59
6.4	Jonswap spectrum discretization for $T_p = 11.$ sec . . . . .	60
6.4a	$H_s = 0.5 m$ . . . . .	60
6.4b	$H_s = 4.5 m$ . . . . .	60
6.4c	$H_s = 9 m$ . . . . .	60
6.5	Jonswap spectrum discretization for $T_p = 14.$ sec . . . . .	60
6.5a	$H_s = 0.5 m$ . . . . .	60
6.5b	$H_s = 4.5 m$ . . . . .	60

6.5c	$H_s = 9 m$	60
7.1	Stability Chart for constant $V_s = 6.5$ knots and threshold =2 deg	63
7.2	Stability Chart for constant $V_s = 6.5$ knots and threshold =5 deg	63
7.3	Stability Chart for constant $V_s = 6.5$ knots and threshold =10 deg	64
7.4	Stability Chart for constant $V_s = 6.5$ knots and threshold =15 deg	64
7.5	Stability Chart for constant $V_s = 12.5$ knots and threshold =1 deg	65
7.6	Stability Chart for constant $V_s = 12.5$ knots and threshold =10 deg	66
7.7	Stability Chart for constant $V_s = 12.5$ knots and threshold =20 deg	66
7.8	Stability Chart for constant $V_s = 12.5$ knots and threshold =40 deg	67
7.9	Stability Chart for constant $T_p = 11$ sec and threshold =1 deg	68
7.10	Stability Chart for constant $T_p = 11$ sec and threshold =5 deg	69
7.11	Stability Chart for constant $T_p = 11$ sec and threshold =10 deg	69
7.12	Stability Chart for constant $T_p = 11$ sec and threshold =15 deg	70
7.13	Stability Chart for constant $T_p = 8.5$ sec and threshold =1 deg	71
7.14	Stability Chart for constant $V_s = 0$ knots and threshold =1 deg	71
A.1	Validation with Aveva model of GZ curve in sinusoidal Wave for LC 15	82
A.2	Validation with Aveva model of GZ curve in sinusoidal Wave for LC 27	83
A.3	Validation with Aveva model of GZ curve in sinusoidal Wave for LC 30	84
A.4	Validation with Aveva model of GZ curve in sinusoidal Wave for LC 36	85
B.1	Comparison of the three different cases with $V_s = 10$ knots	88
B.2	Comparison of the three different cases with $V_s = 11$ knots	89
B.3	Comparison of the three different cases with $V_s = 14$ knots	89
B.4	Comparison of the three different cases with $V_s = 15$ knots	89
B.5	Comparison of Parametric Roll Resonance in irregular waves ( $T_{peak} = 11.5$ sec, $V_s = 12$ knots) with 4 differential solvers	91
B.6	Comparison of Parametric Roll Resonance in irregular waves ( $T_{peak} = 12.5$ sec, $V_s = 12$ knots) with 4 differential solvers	92
B.7	Comparison of Parametric Roll Resonance in irregular waves ( $T_{peak} = 12.5$ sec, $V_s = 13$ knots) with 4 differential solvers	93
B.8	Comparison of Parametric Roll Resonance in irregular waves ( $T_{peak} = 13.5$ sec, $V_s = 12$ knots) with 4 differential solvers	94
B.9	Comparison of Parametric Roll Resonance in irregular waves ( $T_{peak} = 13.5$ sec, $V_s = 13$ knots) with 4 differential solvers	95
C.1	Jonswap spectrum discretization for $T_p = 11$ . sec and $H_s = 4.5$ m with 23 and 43 components respectively	96
C.2	Autocorrelation function and water surface elevation for spectrum discretization with $N = 23$ components	98
C.3	Autocorrelation function and water surface elevation for spectrum discretization with $N = 43$ components	99
C.4	Autocorrelation function and water surface elevation for spectrum discretization with $N = 84$ components	99
C.5	Diagram for maximum angle response for every seed - constant $V_s = 6.5$ knots	102

---

C.6 Diagram for maximum angle response for every seed-constant  $V_s = 12.5$  knots . . . . . 103

C.7 Diagram for maximum angle response for every seed - constant  $T_p = 11$  sec 104

C.8 Diagram for maximum angle response for every seed - constant  $T_p = 8.5$  sec 105

C.9 Diagram for maximum angle response for every seed - constant  $V_s = 0$  knots 106

C.10 Parametric roll resonance for  $H_s = 9$  m - constant  $V_s = 12.5$  knots . . . . . 107

C.11 Parametric roll resonance for  $H_s = 8$  m - constant  $V_s = 12.5$  knots . . . . . 108

C.12 Parametric roll resonance for  $H_s = 5$  and  $H_s = 6$  m - constant  $T_p = 11$  sec 109

C.13 Parametric roll resonance for  $H_s = 7$  and  $H_s = 7$  m - constant  $T_p = 11$  sec 110

# List of Tables

- 4.1 Principal Dimensions of the sample ship . . . . . 34
- 4.2 Loading Conditions of the sample ship from the Trim & Stability Booklet . 40
- 4.3 Parameters for the ship’s position in wave for calculation of Gz curve . . . 43
  
- 5.1 Data necessary to derive the Stability Chart for two types of regular fol-  
 lowing waves for LC 18 . . . . . 52
  
- B.1 Parameters for solving the differential equation with the three approaches . 87
- B.2 Parameters for solving the differential equation with the three approaches . 90
  
- C.1 Range of data and total computation time-constant  $V_s = 6.5$  knots . . . . . 100
- C.2 Range of data and total computation time-constant  $V_s = 12.5$  knots . . . . . 100
- C.3 Range of data and total computation time for the other 3 cases . . . . . 101
  - C.3a Constant  $V_s = 0$  knots . . . . . 101
  - C.3b Constant  $T_p = 11$  sec . . . . . 101
  - C.3c Constant  $T_p = 8.5$  sec . . . . . 101

# Nomenclature

$m_0$	Zero-order spectrum moment	$[m^2]$
$(\phi, \theta, \psi)$	Orientation angles of $s$ -frame with respect to $e$ -frame	$[rad]$
$(\xi, \eta, \zeta)$	Coordinates of $s$ -frame origin with respect to $e$ -frame	$[m]$
$(c_x, c_y, c_z)$	Coordinates of the centroid of each element of a mesh	$[m]$
$(e_x, e_y, e_z)$	Unit vectors along $x$ -, $y$ and $z$ directions	—
$(n_x, n_y, n_z)$	$x, y, z$ - components of the surface unit normal vector	—
$(x_b, y_b, z_b)$	Coordinates of the center of buoyancy	$[m]$
$(x_g^s, y_g^s, z_g^s)$	Coordinates of the center of gravity of the ship with respect to $s$ -frame directions	$[m]$
$\bar{F}_B$	Buoyancy force	$[N]$
$\Delta$	Ship's displacement	$[kg]$ or $[tons]$
$\epsilon$	Wave phase	$[rad]$
$\eta_w$	Surface elevation of sea	$[m]$
$\gamma$	Peak enhancement, parameter for JONSWAP spectrum	—
$\lambda$	Wave length	$[m]$
$\mu$	Encounter angle between wave and ship	$[deg]$ or $[rad]$
$\nabla$	Volume of displacement	$[m^3]$
$\omega_0$	Natural roll frequency of the ship	$[rad/sec]$
$\omega_e$	Encounter frequency	$[rad/sec]$
$\omega_w$	Radial frequency of the wave	$[rad/sec]$
$\overline{BM}$	Metacentric radius	$[m]$
$\overline{GM}$	Metacentric height with respect to the center of gravity G	$[m]$

---

$\overline{GZ}(\phi)$	Hydrostatic roll righting lever curve with respect to the center of gravity G	[m]
$\overline{KB}$	Vertical position of the center of buoyancy B	[m]
$\overline{KG}$	Vertical position of the center of gravity G	[m]
$\phi$	Roll angle (dots represent derivatives with respect to time)	[rad]
$\rho$	Water density	[kg/m <sup>3</sup> ]
$\sigma^2$	Statistical variance of the water surface elevation	[m <sup>2</sup> ]
$\sigma_a, \sigma_b$	Spectral width parameters for JONSWAP spectrum	[—]
$\vec{n}$	Surface unit normal vector	—
$\zeta$	Damping ratio	—
$a$	Wave amplitude	[m]
$A_{44}$	Hydrodynamic added moment of the inertia	[kg m <sup>2</sup> ]
$B_1$	Linear damping coefficient	[kg m <sup>2</sup> /s]
$E_w$	Wave energy per unit area of the sea	[J/m <sup>2</sup> ]
$g$	Gravitational acceleration equal to 9.80665	[m/s <sup>2</sup> ]
$GM_0$	Initial metacentric height	[m]
$H$	Wave height	[m]
$H/\lambda$	Wave steepness	—
$H_s$	Significant wave height	[m]
$I_T$	Transverse waterplane moment of inertia about the axis of inclination	[m <sup>4</sup> ]
$I_x$	Roll moment of the inertia	[kg m <sup>2</sup> ]
$k$	Wave number	[1/m]
$m$	Mass of the object under study	[kg]
$M_D$	Damping Moment	[kN]
$M_{IN}$	Moment from the inertia of the ship around its longitudinal axis	[kN]
$M_R$	Restoring Moment	[kN]
$q_{f_i}^{f_j}$	Orientation vector of $f_i$ -frame origin with respect to $f_j$ -frame	[rad]
$R(\tau_j)$	Autocorrelation function	[m <sup>2</sup> ]

---

$R_{f_i}^{f_j}$	Transformation matrix corresponding to three consecutive rotations about the axes of $f_i$ -frame origin with respect to $f_j$ -frame	—
$r_{f_i}^{f_j}$	Position vector of $f_i$ -frame origin with respect to $f_j$ -frame	[ $m$ ]
$S$	Submerged (Wetted) hull surface	[ $m^2$ ]
$S_{\eta_w}$	Wave Spectrum	[ $m^2 * sec$ ]
$T_0$	Natural roll period of the ship	[ $sec$ ]
$T_p$	Peak period	[ $sec$ ]
$T_{sim}$	Total duration of the simulation for the ship's roll resonance	[ $sec$ ]
$V_s$	Ship's forward speed	[ $knots$ ]

# Contents

<b>Nomenclature</b>	<b>vii</b>
<b>1 Introduction</b>	<b>1</b>
<b>2 Literature Review and Thesis Objective</b>	<b>5</b>
2.1 Literature Review . . . . .	5
2.2 Thesis Objective-Contributions . . . . .	7
2.3 Thesis Structure . . . . .	8
<b>3 Theoretical background</b>	<b>9</b>
3.1 Definition of Equilibrium and Stability of a ship . . . . .	9
3.1.1 Equilibrium of a floating body . . . . .	9
3.1.2 Initial Stability and Stability Criteria . . . . .	11
3.2 Parametric Roll Resonance . . . . .	16
3.2.1 Physics of Parametric Roll . . . . .	16
3.2.2 The Differential Roll Equation . . . . .	18
3.3 Irregular Waves . . . . .	23
<b>4 Hydrostatic Equilibrium and Hull Discretization</b>	<b>28</b>
4.1 Calculation of Hydrostatic equilibrium in Mathematica . . . . .	28
4.2 Discretization of hull's geometry . . . . .	33
4.2.1 Sample ship Data . . . . .	33
4.2.2 Rhino Model and hull discretization . . . . .	34
4.3 Validation of Mathematica code with Aveva and Trim & Stability data . . . . .	37
4.3.1 Displacement and LCB hydrostatic calculations . . . . .	37
4.3.2 GZ curve in calm water . . . . .	40
4.3.3 GZ curve in sinusoidal longitudinal wave . . . . .	42
<b>5 Differential Equation Model</b>	<b>46</b>
5.1 Differential Roll Equation in Longitudinal waves . . . . .	46
5.1.1 Damping term . . . . .	47
5.1.2 Natural roll frequency and transverse moment of inertia . . . . .	47
5.1.3 Righting arm . . . . .	49
5.1.4 Numerical Integration of the Roll equation . . . . .	49
5.2 Application of developed model in Regular Waves . . . . .	50
5.2.1 Parameters for the Stability charts . . . . .	51
5.2.2 Stability Charts . . . . .	53



---

<b>6</b>	<b>Modelling Irregular waves</b>	<b>56</b>
6.1	Spectrum Characteristics and Discretization . . . . .	56
6.2	Parameters of Stability Charts . . . . .	60
<b>7</b>	<b>Results and Discussion</b>	<b>62</b>
7.1	Forward ship's speed $V_s = 6.5$ knots constant . . . . .	62
7.2	Forward ship's speed $V_s = 12.5$ knots constant . . . . .	65
7.3	Peak period $T_p = 11$ sec constant . . . . .	68
7.4	Peak period $T_p = 8.5$ sec constant . . . . .	70
7.5	Forward ship's speed $V_s = 0$ knots constant . . . . .	70
7.6	Discussion . . . . .	72
<b>8</b>	<b>Conclusion and Future Work</b>	<b>73</b>
8.1	Conclusions . . . . .	73
8.2	Future Work . . . . .	75
<b>A</b>	<b>Validation of GZ curve in wave with Aveva model</b>	<b>81</b>
<b>B</b>	<b>Equation of Roll</b>	<b>86</b>
B.1	Study for the three approaches of solving the differential equation . . . . .	86
B.2	Roll resonance while reducing the initial time step of solver in Mathematica . . . . .	90
<b>C</b>	<b>Irregular Waves</b>	<b>96</b>
C.1	Self-Repeating Effect . . . . .	96
C.2	Data sets for Stability Charts and their Computation time . . . . .	100
C.3	Stability Charts for every seed . . . . .	101
C.4	Ship Responses for different cases . . . . .	107

# Chapter 1

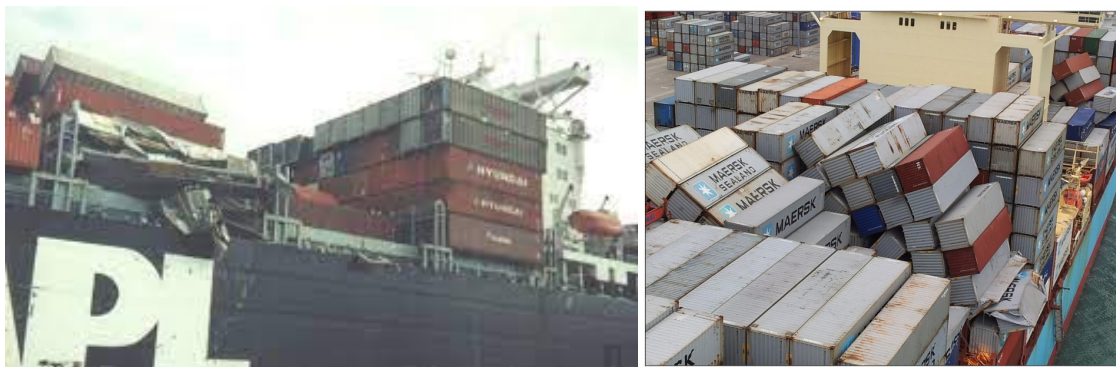
## Introduction

In the last decades, we have seen many big vessels (most of them being containers), suffer from sudden severe rolling motion. Potential effects of this phenomenon are: unpleasant accelerations for the crew members, the containers and lashing system are placed under extreme stress, container loss, exposure of the vessel's propulsion system to varying loads and even can lead to capsizing of the vessel.

This phenomenon is called parametric rolling and it belongs to the family of parametric resonance phenomena of the dynamic stability of the ship. What is this phenomenon but also why and under what circumstances is it considered a problem?

Parametric roll has been recognized by naval architects for more than fifty years. It is described by spontaneous rolling motions when the ship travels in head or following seas. Although the disturbance is in the longitudinal direction (following or head seas) of the ship, the ship's response to roll is in the transverse direction. This is a result of dynamic instability of the motion of the ship, due to the variation in the transverse stability of the ship as it moves in these types of waves. So when a small initial disturbance occurs in roll (i.e. gust wind), an oscillatory rolling can be triggered. This, as already mentioned, can grow to amplitudes that may cause the ship to capsize.

At first, parametric rolling has historically been of practical concern for smaller vessels



(a) Disasters from the APL CHINA accident [1]

(b) Svendborg Maersk, aft deck at arrival in Malaga [2]

Figure 1.1: Pictures of the casualties from the APL CHINA and Svendborg Maersk containerships

(such as coasters and fishing vessels) of low or marginal stability in following seas. In the 1990s, however, there has been an increase in accidents due to parametric instability of larger ships, such as containerships, and even cruise ships. These ships had a hull form characterized by great flare in bow, and wide flaring in stern sections. One of the major accidents that occurred was the APL CHINA in October 1998. APL CHINA was a post-Panamax, C11 class containership, which encountered extreme weather and sustained extensive loss and damage to deck stowed containers, as the ship reached as great as 35 deg to 40 deg rolling angles, while extreme pitching occurred simultaneously. This accident was one of the first to initiate research model tests and numerical analyses [3].



Figure 1.2: Examples of lashing bridge damages and container losses, occurred in MAERSK ESSEN accident [4]

And even in more recent accidents, losses have been reported on ships linked to parametric instability. Some examples include the accident of the Svendborg Maersk on 14 February 2014, when it was sailing under heavy weather conditions [5]. At first, the master reduced speed and changed heading into the wind and sea to minimize rolling. After two hours the vessel suddenly rolled to extreme angles of 38 deg three to four times, without any warning. And even after three hours had passed, the vessel experienced again rolling over 41 deg. After investigation, the casualties were up to 600 damaged containers, more than 500 lost at sea and damage to other equipment was also reported. Later studies showed that the master unknowingly exposed the ship to conditions that led to parametric instability.

More recent incidents include the accident of the containership CMA CGM G. Washington [6]. During heavy weather on the passage from Xiamen to Los Angeles on 20 January 2018. The containership lost 137 containers as three container bays collapsed. The loss was due to a 20 deg rolling angle, which was later investigated and found to be due to parametric instability. Another incident occurred on a voyage from China to Los Angeles on the ship Maersk Essen on 16 January 2021 [7]. The number of lost containers was reported at 750. The investigation later done, conclude that the ship most likely experienced parametric resonance with large rolling angles building up during a six-minute period.

These accidents, and many others, were the beginning for the marine community to reflect and start to consider parametric instability as a real risk. Over the years, many

theoretical and experimental papers have focused on dynamic stability in general and parametric rolling in particular, as discussed to some extent in the literature review.

So as a brief mention, the factors that may cause parametric roll to occur are:

1. The direction of the waves (following, head, or quartering sea),
2. The wavelength concerning the length of the ship,
3. The hull geometry of the ship. For instance a flared hull increases the variation in changes in the stability when the position of the waves (crest and trough) changes the waterplane area and buoyancy,
4. Low roll damping due to small or no bilge keels,
5. The loading condition of the ship, and
6. Vessel's speed (corresponding to the encounter period of the ship)

In more detail, parametric roll can be explained by the following phenomenon. The stability of the ship is somewhat different for following or head waves than in beam waves. When the middle of a ship is on the crest of the wave, the surface area of its waterplane is reduced compared to still sea state. In contrast, the surface area of the waterplane increases when the ship is in a wave trough. In both cases, this effect is most pronounced when the length of the wave is almost equal to the length of the ship. This, somewhat periodically variation of the waterplane area, affects the restoring energy in rolling motion. So as stated above, a small distribution may lead to big rolling angles, due to the dynamic instability of the motion of the ship.

The above condition is mainly satisfied when the wave is regular and has a clear periodicity and alternation between crest and trough. But in a real sea state, normal waves are not encountered frequently. Waves in reality are one of the most complex and unpredictable phenomena in nature. As harmonious and peaceful as they can be, they can also become destructive and tumultuous. This is why it is not easy to achieve a complete understanding of the fundamental characteristics and behavior of waves. If we wanted to observe the waves of the sea, we would find that they have an irregular form. There consists of small and large peaks, which have different directions, collide and create foam or merge harmoniously and create different wave patterns.

The foundation of a better understanding and modelling of the waves was introduced by Sverdrup and Munk [8], who clearly understood that sea waves are composed of large and small waves. They introduced the concept of the significant wave, which was based upon the understanding of sea waves as a random process. Later on, in the early 1950's a group of American oceanographers, headed by Pierson, formed the basis for the recognition of the irregular nature of waves, as they introduced the idea of the energy spectrum as a basic tool for describing the irregular sea. At first, while the idea of the spectrum was common knowledge among oceanographers, it was considered complex among the wide circle of engineers. Over time, however, this idea became recognized for its importance and assimilated into the engineering community, to the point that it is now commonly used. The use of this method in applications involving floating or fixed platforms and ships can now give a clearer picture of the actual phenomenon and is widely used in studies and numerical simulations.

Finally, it would be impossible not to mention the regulatory background. Initially, the stability criteria covered only the static behavior of the ship (A.167 [9]). But it was subsequently shown that the static-type criteria do not cover all the ship's conditions satisfactorily. In 1985, the so-called 'weather criterion' was introduced, which took into account the effect of the wind and the ship's inclination angle to some extent. All of the above were assimilated into a single code (the Intact Stability Code) in November 1993 (resolution A.749(18))[10]. Later in 2008, the Maritime Safety Committee adopted the International Code in Intact Stability[11], which contains the above for the intact stability of the ship, including both mandatory requirements and recommended provisions. The code describes, in addition to the mandatory regulations, proposals concerning the dynamic stability of the ship. There are also guidelines for masters on how to avoid parametric instability in following and quartering seas [12]. Until recently, the IMO has been working on the creation of performance-based criteria concerning dynamic phenomena, in order to assess the stability of the ship in conditions regarding parametric roll, excessive acceleration, pure loss of stability, surf-riding/broaching and others [13].

Although awareness of dynamic stability has increased in recent years, because it is a multifaceted and challenging problem, there is still room for research and progress towards a better understanding of it.

# Chapter 2

## Literature Review and Thesis Objective

### 2.1 Literature Review

A general reference has already been made to what parametric instability is and what factors affect it in a general sense. As early as 1860's, researchers such as Froude and Reed had observed the change in the righting arm when ships were traveling in large waves [14]. William Froude spotted a ship roll-heave coupling, a phenomenon similar to parametric roll. This phenomenon was consisting of heave oscillations at the heave natural period, stimulated by the small changes in buoyancy force caused by rolling motion, which occurred at twice the roll frequency.

Later, in 1938, Kerf in Germany stated that in a following seaway the roll-righting-arm of a ship can become seriously dependent on its position relatively to the following waves [15]. This observation was based on the change of the stability, which decreases when the mid of the ship is on the crest of a wave, and increases when it is on a wave trough. This theory was subsequently confirmed by experiments until, in the 1950's, Professors Paulling (in the USA) and Wendel (in Germany) attributed some accidents to the phenomenon of righting arm variation combined with a reduction in the restoring torque when large rolling angles occur [16].

Paulling *et al.* in 1959 [17], investigated the nonlinear equations of motion of a ship having three degrees of freedom (heave, pitch, and roll). The nonlinear parts were all of second order. His study showed that instability can occur in any of the three degrees of freedom, when a distribution occurs in one of the other two degrees. Instabilities occur when the natural frequency in the unstable motion is almost half the natural frequency of the excitation motion or when these natural frequencies are almost equal.

Around the same time, Professors Grim [18] and Kerwin observed that there is a periodic variation of the metacentric height in following waves. Their observation resulted in a description of the rolling motion by the differential equation of "Mathieu's", or else called parametric. This equation is amenable to numerical solution and assumes a linear relationship between the rolling angle and the metacentric height.

The first experimental observation of parametric roll was done by Paulling, Kastner, Sigismund, *et al.* (1972) [19] in San Francisco Bay. These experiments shed a light on the mechanism of capsizing in heavy seas. The models examined were strongly influenced by the effect of quartering or following seas, as they were appeared to be affected by pure loss of stability, and broaching.



Initially the concern with parametric roll was mostly for smaller ships. For example in the work by Umeda, Hamamoto, Takaishi, *et al.* (January 1995) [20], models of two types of ships were examined, a pure seiner and a small containership with length of 150 meters. The experiments were carried out in both long and short-crested irregular waves and the results showed a link in capsizing in the cases of short-crested following and quartering seas. However, when the post-Panamax APL China (Type C11) containership encountered a severe storm and suffered heavy losses of containers and damage to machinery, due to the casualties, further research and investigations were initiated by researchers and regulatory authorities. These investigations were either related to the ship itself or to ships of similar shape and size. The study by Pesman and Taylan [21] indicated that a 261 meter long containership can exhibit parametric instability in both head and following seas with response angles of 30 and 20 degrees respectively.

In further studies, researchers such as Spyrou (2000) [15], Neves and Rodriguez (2006) [22], Bulian (2005) and Neves, Perez, Lorca, *et al.* [24] focused on nonlinear aspects and effect of changing frequency range on parametric roll motion. A model with 3 degrees of freedom could be used to estimate the ship's response. Most of the above authors have worked on 3-DOF nonlinear models. In this case, all three equations of motion are solved, which are coupled (assuming surge, sway and yaw to be restrained). In this case the resulting equation contains a large number of parameters (related to geometric and hydrodynamic aspects of the problem), the precise and simple determination of which is questionable [24]. A highly non-linear 3-DOF analytical system, although suitable for rapid scheduling numerical simulations, can hardly be addressed by analytical technique, due to the cumbersome calculations required.

Other researchers have devoted their attention to finding the most appropriate form for introducing the restoring term into the differential equation of roll. In addition to Mathieu's model which considers that the GM varies sinusoidally between two extreme values, there are other approaches that can be used. It is not always necessary for GM to be approached sinusoidally, as long as its variation is periodic. An example of this assumption is the study done by Shin, Blenky, Paulling, *et al.* [25], where they consider the linear relationship between the rolling angle and the metacentric height, but calculated individually the GM values for successive instantaneous wave positions along the ship. This is possible by calculating the basic characteristics of the varying stability as the ship moves through longitudinal waves. In that study the heave and pitch motions of the ship are neglected in the calculations. Only the geometry under the wave and how it changes form as the ship moves through, is considered.

A similar logic to Shin, Blenky, Paulling, *et al.* [25], was followed by Ms. Dousia [26] in her diploma thesis, of which the present study can be considered a continuation. Ms. Dousia proceeded in numerical calculations, which provided the local value of metacentric height while the ship passes through each position on the wave. Later a single-degree of freedom in roll with linear damping, characterized by linear restoring term was used for the calculations. The resonance of the ship was calculated for linear and for higher orders Stokes waves (up to 5th order).

A different approach is, instead of changing the metacentric height, to directly address the righting arm of the ship. The simplest approximation formulas, like for instance  $GZ(\phi) = GM\phi(1 - \phi^2)$ , see Belenky, Bassler, and Spyrou (2011) [27], produces so rough estimation of the GZ characteristic that applied in the rolling equation they cannot

achieve a sufficient accuracy of the results of rolling simulation. One of the most popular approach is the application of a polynomial power series. Many authors use the fifth to ninth order polynomials (Contento, Francescutto, and Piciullo, 1996 [28]; Surendran and Venkata Ramana Reddy[29], 2003; Taylan 2000 [30]) with only odd powers of the angle of heel due to a symmetrical character of the GZ curve. A limited number of authors, such as Bulian [23], apply higher order polynomials like seventh or ninth, and rarely even higher.

Perunovic [31] calculated the parametric roll response in a container sailing in irregular head seas. She uses a a single degree of freedom rolling differential equation. For the calculation of the restoring term, she also estimates GZ as a function of angle. She examines three methods for the computation of the restoring term.

1. The first method, is by calculating the instantaneous GZ obtained by the equilibrium of gravity and buoyancy forces at each time step.
2. With the second method, the GZ curve is fitted with fifth order, non-linear function of roll and relative position the ship according to the wave's crest.
3. Finally, the third method is by using the effective Grim wave.

In addition, for the representation of the irregular waves, she uses the energy spectra approach (for methods 1, and 2), and most specific the JONSWAP wave spectrum. For the third approach she uses the effective wave spectrum.

In this study it was chosen to use a pseudo-static model (similar to Bulian analysis). The GZ, is calculated from the equilibrium (by heave and pitch), for each time instant and entered into the differential equation (as stated in the paper Perunovic [31]). Finally, the differential equation of roll with one degree of freedom is solved for following seas. The remaining terms of the differential equation (terms of inertia and damping) are calculated in the same way as in the work of Ms.Dousia [26]. The irregular waves are calculated with the energy spectral approach as already done by many researchers, such as Shin, Blenky, Paulling, *et al.*, [25], and Bulian, Francescutto, and Lugni [32].

## 2.2 Thesis Objective-Contributions

The phenomenon of parametric instability is a dynamic phenomenon. And while for regular waves, there are methods for finding the instability regions, in real sea states the whole picture is not yet clear. There are guidelines for captains to understand the phenomenon and to take precautions to avoid the occurrence of large angles [12]. However, accidents still happen, as the shipbuilding community still relies more on the human factor to avoid such cases. This is why the second generation criteria have been developed in an attempt to reduce the occurrence of parametric instability, but now with a regulatory background, which requires knowledge and expertise.

In this thesis, an attempt is made to construct the so-called stability diagrams or otherwise Ince-Stutt diagrams, but for irregular seas. These diagrams will show the areas of instability as derived from the ship's response to random waves. However, to find the responses of the ship in rolling motion, it is essential to construct a numerical model to solve the differential motion of the ship. It is therefore chosen to use a pseudo-static



model, in which instead of solving all three coupled equations of motion of the ship (heave, pitch, and roll), the roll motion is modelled dynamically using a single degree of freedom, whereas the additional half DOF indicates that the coupling with heave and pitch is taken into account by means of hydrostatic calculations without considering dynamic effects. In this way, the model of the differential equation will have a non-linear relationship between the inclination angle and the righting arm.

This approach is interesting because the actual righting arm will be implied at each point in time. Also because the model is nonlinear it will be possible to calculate the maximum response angle of the ship. In this way, the intensity of the instability and whether it leads to capsizing or not will be shown.

Further, the random phase model will be used to represent the irregular wave. Due to the randomness of the phenomenon, 16 ship responses are calculated for each case, resulting from 16 different runs of the experiment, i.e. 16 randomly generated lists of phase angles.

Therefore, in this thesis, all these aspects are explored, trying to bridge the non-linearity of the dynamic phenomenon called parametric roll with the randomness of the waves. This attempt is a small insight into the actual phenomenon, which is multidimensional, depends on many parameters and can be studied from many aspects.

## 2.3 Thesis Structure

In Chapter 3 ([Theoretical background](#)), the theoretical groundwork of this thesis is laid; which include the static stability, a brief description of the intact stability criteria, the physics underlying parametric roll and the corresponding differential equations describing it. Then there is a brief mention of the theoretical background of the random waves, and the energy spectra.

In Chapter 4 ([Hydrostatic Equilibrium and Hull Discretization](#)), the method for the computation of the hydrostatic equilibrium, the validation of the accuracy of the model and the procedure for selecting the appropriate discretization of the hull geometry are described.

Chapter 5 ([Differential Equation Model](#)), presents the form of the differential equation for the parametric roll, and how it was modelled in the code. Next, in section 5.2, the application of the model for regular waves is presented and two stability diagrams are obtained for specific cases.

Chapter 6 ([Modelling Irregular waves](#)) describes how random waves are modeled. In addition, the logic behind the choice of the spectrum and its characteristics is explained.

Finally, in Chapter 7 ([Results and Discussion](#)), the results for the different cases for which the stability diagrams were constructed are presented. An attempt is made to interpret the results. Overall, the conclusions and suggestions for future work are listed in Chapter 8.

# Chapter 3

## Theoretical background

### 3.1 Definition of Equilibrium and Stability of a ship

#### 3.1.1 Equilibrium of a floating body

A ship is a complicated structure that sails in the sea, but in fact, it is nothing less than a floating body that must follow specific equilibrium rules. A body is said to be in equilibrium if it is not subjected to accelerations. As dictated by Newton's second law <sup>1</sup>, the force on an object is equal to its mass times its acceleration. As a result, if the sum of all forces acting on that body is zero and the sum of the moments of those forces is also zero, then the body is in equilibrium. Regarding a floating body, such as a ship, two forces are always applied on it: the weight of the body and the buoyancy force. Two principles should be implemented, for equilibrium equations to be formed. The first condition for equilibrium, which is the one regarding the sum of forces, is expressed as Archimedes' principle. The second condition, regarding the sum of moments, is stated as Stevin's law [33]. In the paragraphs that follow, it will be explained how these principles lead to a better understanding of the ship's stability.

According to Archimedes's principle, a body immersed in a fluid is subjected to an upward force equal to the weight of the fluid displaced. Let's assume that a body is floating in a fluid and the wetted surface area is  $S$ . To find the force acting on the surface, it is necessary to integrate the pressure distribution over the surface. As the wetted surface is more likely to be curved, the integration will be done over a vector element  $\bar{ds}$ . The pressure force acting on the element of area  $\bar{ds}$ , is given by

$$d\bar{F}_B = -p \bar{ds} \quad (3.1.1)$$

, where the minus sign indicates that the force acts on the area in the direction opposite to the normal area. Therefore, the resultant force, called buoyancy, is calculated with the following formula [34]:

$$\bar{F}_B = - \iint_S p \bar{ds} \quad (3.1.2)$$

---

<sup>1</sup>  $\sum_{n=1}^{\infty} \vec{F} = m\vec{a}$ , Newton's second law states that, if there is a net force  $\vec{F}$  on a body with mass  $m$ , the body accelerates in the same direction as the net force with  $\vec{a}$

Using divergence theorem expression (3.1.2) can be written as a volume integral over the submerged volume of the floating body.

$$\bar{F}_B = - \iiint_V \nabla p dV \quad (3.1.3)$$

The proof of (3.1.3) formula exceeds the purpose of this diploma thesis. When the floating body is in hydrostatic equilibrium, the buoyancy equals the weight of the body. Assuming that the submerged body is a ship, then the weight of a ship, in any given loading condition, equals the weight of the fluid which is displaced, called Displacement  $\Delta$ . For the corresponding volume of the hull's underwater part, the symbol  $\nabla$  is used.

The second condition of equilibrium of a floating body is that the sum of the moments of all forces acting on it must be zero. By applying this principle, we can find the coordinates of the Center of Buoyancy ( $COB = (x_b, y_b, z_b)$ ). Let us assume that a floating body is in equilibrium and the waterline corresponding to this condition is  $W_0L_0$ , then the weight of the body,  $\Delta$ , and the buoyancy force,  $F_B$  are equal. Also, the two forces act along the same line, and as there is no righting arm, the sum of their moments about any reference is zero. If the position of the center of gravity changes,  $G_1$ , then the sum of the moments is no longer zero. This alteration causes a clockwise inclination of the body, by an angle  $\phi$ . A volume submerges at right, so another one emerges at left. The result is that the center of buoyancy moves to the right, to a new point that is marked by  $B_\phi$ , until it reaches a position of equilibrium in which the new waterline is  $W_\phi L_\phi$ . The floating body will find a position of equilibrium when the two points  $G_1$  and  $B_\phi$  will be on the same vertical line, perpendicular to the waterline  $W_\phi L_\phi$ . This situation is illustrated in Figure 3.1. Thus, in the case of a floating body, the second condition of equilibrium is satisfied if the center of gravity and the center of buoyancy are on the same vertical line. This condition refers to Simon Stevin's law. [33].

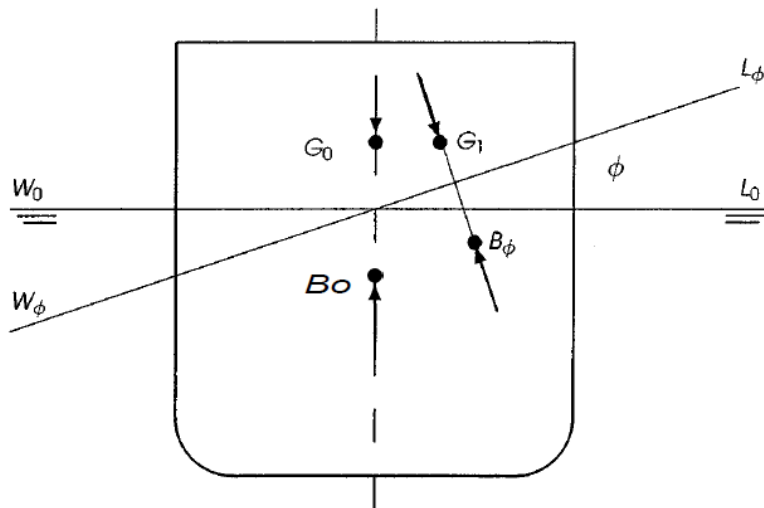


Figure 3.1: Stevin's Law [33]

There is only one thing left to be determined, and that is the application of the momentum theory of forces due to pressures, so that the Center of Buoyancy can be

calculated. These can be expressed as follows [35]:

$$M_x = g \iiint_V \rho(z)y dV = |\bar{F}_B|y_B \quad (3.1.4)$$

$$M_y = g \iiint_V \rho(z)x dV = |\bar{F}_B|x_B \quad (3.1.5)$$

$$M_z = 0 \quad (3.1.6)$$

In the equations (3.1.4), (3.1.5) and (3.1.6), symbol  $B$  indicates the center of mass of the displaced water. Assuming that the density is constant, then:

$$y_B = \frac{\iiint_V y dV}{\iiint_V dV} \quad (3.1.7)$$

$$x_B = \frac{\iiint_V x dV}{\iiint_V dV} \quad (3.1.8)$$

It is important to state that we cannot always give information about the  $z_B$  coordinate, as the point of application of the center of buoyancy does not necessarily coincide with the central of the submerged volume.

### 3.1.2 Initial Stability and Stability Criteria

In the preceding section, we learned the conditions of equilibrium of a floating body. But equilibrium alone is not enough. It should also be determined whether a condition of equilibrium is stable or not. So the concept of stability should be defined. Again the easiest way to approach it is by considering a floating body in equilibrium and assuming that some force or moment causes a small change in its position, such as a wind gust. With this change, the force of buoyancy and the weight no longer act on the same vertical line. Thus three situations can occur when that force or moment ceases to act.

1. The body returns to its initial position; The equilibrium is stable.
2. The position of the body continues to change. In this case the equilibrium is unstable. In practical terms, this can mean, for example, that the floating body capsizes.
3. The body remains in the displaced position until the smallest perturbation causes it to return to the initial position or to continue to move away from the initial position. We call this situation neutral equilibrium.

Considering that the displacement of the floating body is known, then with an external heeling moment, the body should react with a righting moment, for it to return to its initial condition, thus its condition is stable. Due to the fact, that the buoyancy and the weight of the body do not act on the same vertical line, a couple of equal and opposite forces is produced. The coupled moment that is created, depends on whether it tends to roll the body back to its initial condition or the other way. Let us see what happens in this case in more detail.



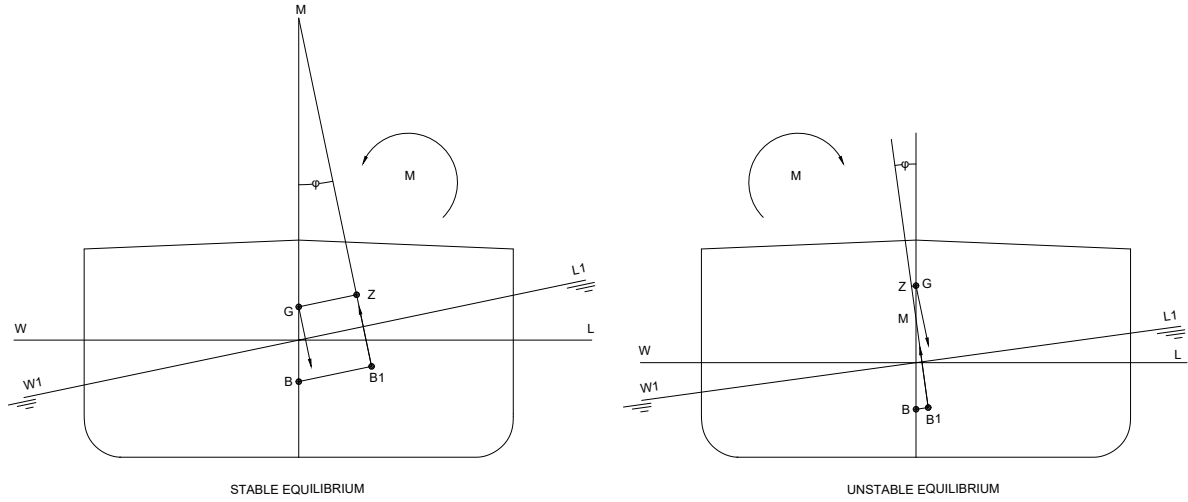


Figure 3.3: The stable and unstable equilibrium

the centerline and the baseline intersect. From this point, we measure any coordinates vertical from it, upwards. In the figure, the initial metacenter,  $M_0$ , is the one corresponding to the waterline  $WL$ , and for any other waterline the metacenter is expressed with the symbol  $M$ . So, to have a sense of the stability of the ship, we use the vector  $\overline{GM}$ , which can be calculated by the following formula:

$$\overline{GM} = \overline{KM} - \overline{KG} = \overline{KB} + \overline{BM} - \overline{KG} \quad (3.1.10)$$

, where

- the vector  $\overline{GM}$  is called metacentric height,
- the vector  $\overline{KB}$  is the  $z$ -coordinate of the centroid of the submerged hull (center of buoyancy), as a result of hydrostatic calculations,
- the vector  $\overline{KG}$  is the  $z$ -coordinate of the centroid of the center of gravity of the ship, thus it depends on the weight calculations and the Loading Condition (LC), and finally
- the vector  $\overline{BM}$  is called the metacentric radius and is equal to the ratio of the transverse waterplane moment of inertia  $I_T$ , about the axis of inclination, to the volume of displacement  $\nabla$ , and is calculated by equation 3.1.11.  $I_T$  is given by equation 3.1.12.

$$\overline{BM} = \frac{I_T}{\nabla} \quad (3.1.11)$$

$$I_T = \iint_{A_{WL}} y(x)^2 dx dy \quad (3.1.12)$$

The GM is also described as the gradient of the righting arm  $GZ(\phi)$  curve for inclination angle  $\phi = 0$ .

$$\overline{GM} = \left. \frac{d\overline{GZ}(\phi)}{d\phi} \right|_{\phi=0} \quad (3.1.13)$$

The equation (3.1.11) is fundamental for static stability and it is preferable for the  $\overline{BM}$  to be as large as possible, something that, for a given displacement, can be achieved by increasing the waterplane moment of inertia. Conversely, if the value of the waterplane area  $A_{WL}$  is low, then this leads to low  $\overline{BM}$  and consequently low or even negative  $\overline{GM}$  values.

With the calculation of the metacentric height, we can easily calculate the righting arm with the equation (3.1.9). Although, the knowledge of  $\overline{GM}$  can determine the righting moment, hence the stability for each angle, in bigger inclination angles, it does not remain in the same position [16]. As a result, other criteria are used to determine the static stability of the ship, at bigger rolling angles. Initially, the criteria used are the Intact Stability Criteria, where the whole  $GZ(\phi)$ , for a large range of heeling angles is taken into consideration. The information of  $\overline{GM}$ , alone is not able to determine the static stability of the ship.

The Intact Stability Criteria according to IMO 2008 Intact Stability Code [11] consists of two main parts; the Criteria regarding the righting lever curve properties and the Severe wind and rolling criterion (Weather Criterion). They evaluate the point where the ship becomes unstable, and the values of certain parameters that are obtained from the stability curve, are examined [37]. These parameters are the following:

1. Three areas should be calculated under the GZ curve. The area under the GZ curve between  $0^\circ$  and  $30^\circ$  of the heeling angle (gray area in Figure 3.4a). Additionally the area between  $30^\circ$  and  $40^\circ$  (or flooding angle, whichever is less) should be calculated. The sum of the areas above, that is the total area under the GZ curve between  $0^\circ$  and  $40^\circ$  (or flooding angle, whichever is less), should not be less than 0.09 meter-radians.
2. The righting lever at an angle of heel equal to or greater than  $30^\circ$ , ( $GZ(30^\circ) \geq 0.20 \text{ m}$ ).
3. The heeling angle where the maximum righting lever occurs (preferably more than  $30^\circ$ , but not less than  $25^\circ$ )
4. The initial metacentric height which takes into account the influence of the free surface of the liquid and should be more than 0.15 m.
5. Steady wind pressure on the ship causes a heeling arm,  $l_{w1}$ , according to the weather criterion, which is illustrated in Figure 3.4b. As a result, a steady heel angle  $\theta_0$  is generated to achieve equilibrium at the point of intersection of the heeling curve and static stability curve. This angle plays a major role not only in determining the safety of the crew, personnel, and cargo on board, but also helps in determining the angle at which the deck edge of the ship is likely to submerge. In other words, it helps evaluate a ship's resistance to capsizing, for a given loading condition.
6. The weather criterion examines also the heeling angle that is caused by the wave motion,  $\theta_1$  (see Figure 3.4b) against the wind. Moreover, due to the gust wind



pressure, the ship is subjected to an inclination with gust wind heeling lever  $l_{w2}$ . In this case, the area of "b" should be larger than the area of "a".

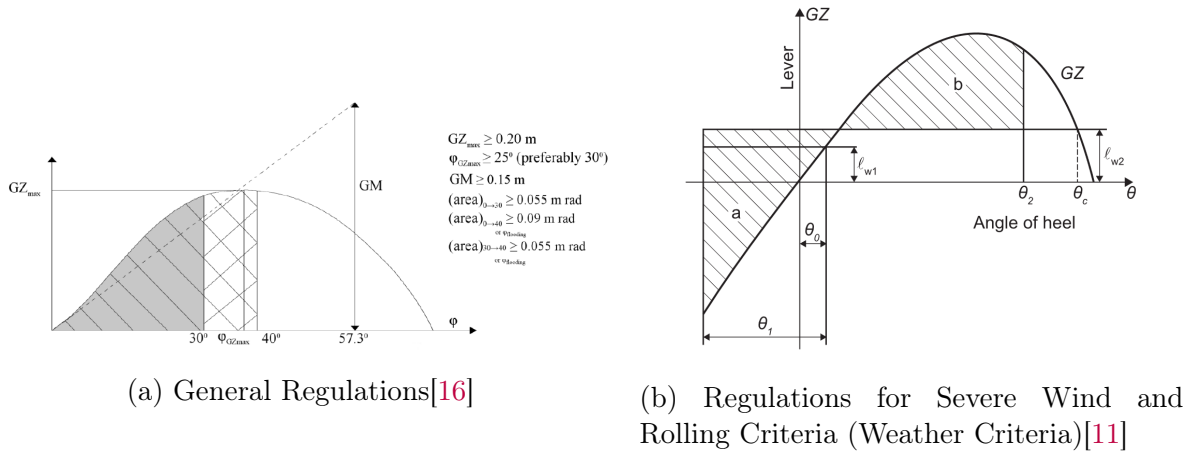


Figure 3.4: IMO Regulations for Intact Stability

As explained above, determining the stability of a ship is more complex than what it seems at first glance. According to IMO Regulations, an attempt is made to find out whether a ship is stable or not, considering many parameters. This is so that there is a general picture of the GZ curve's shape, which is obtained by meeting various criteria and does not depend solely on one value, such as  $\overline{GM}_0$ .

As a continuation of the general criteria, the Weather criterion evaluates the ability of a ship to withstand the combined effects of beam wind and rolling. This criterion was originally developed to guarantee the safety against capsizing for a ship losing all propulsive and steering power in severe wind and waves, which is known as a dead ship [38].

Second Generation Intact Stability Criteria (SGISC) [13] are (from December 2020 onwards) included in Chapter 2.3 of the I.S. Code as an extension and as an optional audit for understanding the dynamic stability characteristics of a ship. They use a multi-tiered approach that consists of three levels of successive assessment. Level 1 vulnerability criteria are intended as a simple assessment to identify loading conditions that are not vulnerable to the given failure mode. Level 2 is a more complex analytical assessment applied to those loading conditions that do not satisfy the Level 1 standard. Loading conditions that do not satisfy the Level 2 standard may be subject to the third level, called Direct Stability Assessment (DSA), which involve the application of sophisticated, proprietary computer software that meets IMO agreed specifications. These assessment levels should be consistent: an assessment outcome of "not vulnerable" for a loading condition in Level 1 should not have an opposite outcome for Level 2. Likewise, a "not vulnerable" Level 2 outcome should not have an opposite outcome for DSA.

The second generation of intact stability criteria consist of assessment for dynamic stability failure modes in waves, as requested in section 1.2 of part A of the 2008 Intact Stability (IS) Code [11]. These dynamic stability failure modes are as follows: dead ship condition, excessive acceleration, pure loss of stability, parametric rolling, and surf-riding/broaching. In this sense, the aim is to use the latest technology and knowledge on



ship dynamics, which is something that the previous stability criteria had not taken into consideration.

As already stated the dynamic stability of the ship is something that only lately has started to be taken into consideration in IMO Regulations. One of those dynamic phenomena is parametric roll, whose theoretical background will be discussed in the following subsection.

## 3.2 Parametric Roll Resonance

### 3.2.1 Physics of Parametric Roll

Not only the presence or absence of waves but also their direction, have a great influence on the ship's stability. In this subsection, the physics of parametric roll will be explained and how the stability of a ship changes in longitudinal waves. The stability of a ship in waves depends on three main parameters. The first parameter, and the most important, is the one regarding the changes in the submerged volume of a ship at any given time. The other two parameters are the effect of the non-hydrostatic component of the pressure distribution along the hull, and the effect due to the disturbance of the pressure field due to its movement, (e.g., heave or pitch motion). The first parameter, mainly revolves around the distribution of the hydrostatic pressure on the ship's hull, as a result of the ship's position on the wave.

When a ship is in equilibrium in calm water with a certain waterline, in this position the area of the waterplane is constant, and as the center of buoyancy and gravity do not change, this leads to a specific value of  $\overline{GM}$ . The  $\overline{GM}$  is calculated with equation (3.1.13), while the waterplane affects the transverse waterplane moment of inertia, thus the  $\overline{BM}$  (eq. 3.1.11), between the crest and trough of a large wave [25].

When the ship travels through waves, the waterline changes, and so does the waterplane area as shown in figure 3.5. This effect becomes more noticeable in large container-ships, which are designed with substantial bow flare and stern overhang that causes a great variation in waterline form, and therefore in transverse stability,

Provided that a typical containership travels through a regular wave with wavelength equal to the length of the ship, the waterline constantly changes. As the mid of the ship is located on a wave trough, the average waterplane width is greater than the one in calm water. In this position, the wave crest is found on the ship's bow and stern, where they are more deeply immersed. On the contrary, the draught in the midship, where the trough is located, decreases. This makes the mean instantaneous waterplane wider, so the waterplane area's second moment  $I_T$  increases, with the result that the value of  $\overline{BM}$  is greater than the one in calm water, assuming that the displacement of the ship is constant.

Thereafter, when the ship is located with the wave crest amidships, the immersed portion of the bow and stern sections are narrower than in calm water. Consequently, the mean waterplane is narrower, so the waterplane area's second moment decreases and the value of  $\overline{BM}$  is decreased in comparison to calm water.

In these positions, the value of  $\overline{KB}$  also changes. The value of  $\overline{KB}$  becomes insignificantly bigger when the wave crest is located on the midship, where there is the most

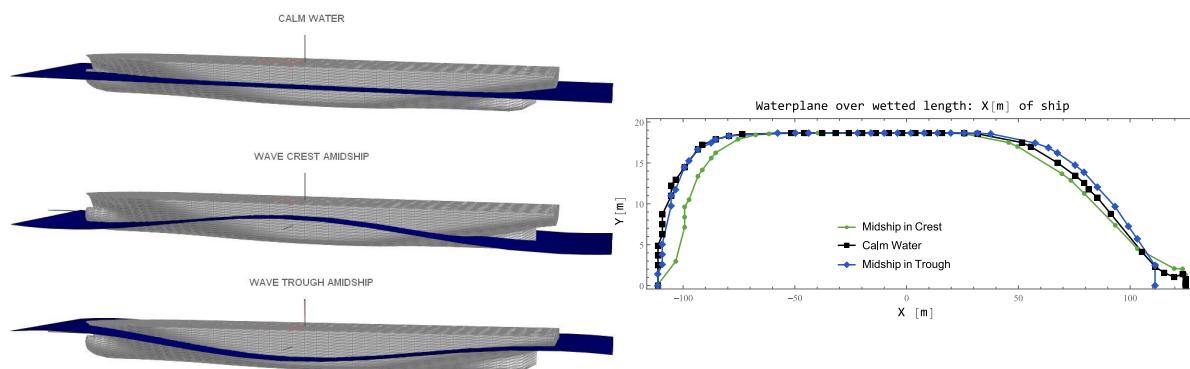


Figure 3.5: Difference in the waterplane for crest trough the midship, calm water and for wave trough amidship.

For a containership traveling through a longitudinal wave, with wavelength equal to the ship's length

volume of the ship. However, this increase in  $\overline{KB}$  has a hardly noticeable effect, as the change in  $\overline{BM}$  usually has a more significant effect on the decrease in  $\overline{GM}$ .

As stated above, when a ship is traveling in longitudinal waves, its stability increases when the trough is near amidship and decreases on the wave crest. When in such state, a small disturbance (e.g. wind gusts) is likely to cause a rolling motion with large angles as a result of parametric resonance. The most rapid increase of parametric roll can be observed when the ship encounters the waves at a frequency near twice the normal frequency of rolling motion, as will be explained further in this section. There are other factors, individually or cumulatively, that can influence the development of parametric resonance. Some of these factors are:

1. The presence of large enough waves, with wavelength close to the length of the ship, and waves of certain wave height cause big GM variation, else called wave steepness  $H/\lambda$ .
2. The direction of the ship in relation to the waves (head and following waves)
3. Low roll damping due to small or no bilge keels.
4. The geometry of the hull. For instance, a flared hull increases the waterline breadth when wave trough is amidship.
5. Encounter period of half that of the natural roll period, encounter period the same as natural roll period.
6. Sufficiently many encounters of similar types of waves for resonance to grow.

## 3.2.2 The Differential Roll Equation

### Free Rolling Equation

When a ship is in calm water, a sudden disturbance in roll or roll velocity (such as that caused by a wind gust) can set up an oscillatory roll motion. The period of such roll oscillations in calm water depends on the ship's stability or restoring moment properties and the mass properties, and is known as the "natural roll period" [39]. In such case, the ship motion is called free rolling and is often used in the roll amplitude decay test. A plot of a roll decay time series (Fig. 3.6) shows the main properties of a damped roll motion. In addition, the measured period of the damped (free) roll motion, can be approximately set equal to the ship's natural period of roll. The differential equation that describes the free rolling motion of the ship (eq.: 3.2.4) results from Newton's second law as shown in equation (3.2.1).

$$M_{IN}(\ddot{\phi}) + M_D(\dot{\phi}) + M_R(t, \phi) = 0 \quad (3.2.1)$$

The first term represents a moment from the inertia of the ship around its longitudinal axis as a function of angular acceleration. When a body moves in a fluid, the inertia of the fluid opposes the motion and that effects are equivalent to having a virtual mass added to the mass of the solid. For this reason, the term related to inertia can be divided into the term of the mass moment of inertia of the (dry) ship and the hydrodynamic (added) moment of inertia about the ship's roll axis that increases the mass moment of inertia of the ship by about 10 to 25% [40]. As a result, the term  $M_{IN}$  can be replaced by the following argument.

$$M_{IN}(\ddot{\phi}) = (I_x + A_{44})\ddot{\phi} \quad (3.2.2)$$

,where  $I_x$  is the transverse moment of ship inertia;  $A_{44}$  is the added mass due to water dragging by the rolling hull. Henceforth, when reference is made to  $I_x$ , it will be considered to include the added mass  $A_{44}$ .

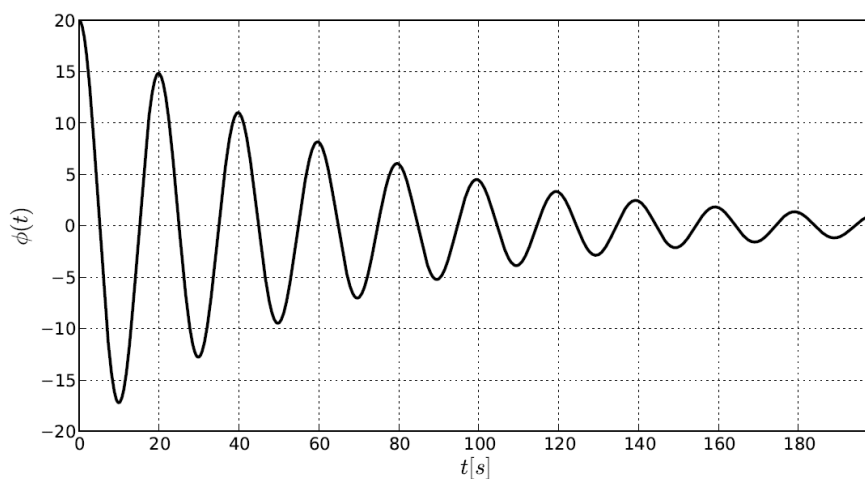


Figure 3.6: Time series of a roll decay motion[39]

The second term represents a moment due to the roll angle velocity of the system linked with damping. When the damping moment is based only of its linear (or "equivalent" linear) component, it takes the following form.

$$M_D(\dot{\phi}) = B_1 \dot{\phi} \quad (3.2.3)$$

where  $B_1$  can be the linear or linearized damping coefficient, but in this thesis  $B_1$  represents the linear roll damping coefficient, assumed to be dependent only on the instantaneous roll velocity  $\dot{\phi}$ .

The third term represents a moment due to the restoring moment when a ship rolls, as described above (Section 3.1.2: [Initial Stability and Stability Criteria](#)). This moment is the force of buoyancy from the displaced water of the ship times the righting arm  $\overline{GZ}$ .

After substitution of formulas (3.2.2) and (3.2.3) into equation (3.2.1) the rolling equation is the following:

$$(I_x + A_{44})\ddot{\phi} + B_1 \dot{\phi} + m g \overline{GZ}(\phi) = 0 \quad (3.2.4)$$

Further, by dividing both sides of equation (3.2.4) with  $(I_x + A_{44})$ , we introduce the commonly used notation for free rolling [41].

$$\ddot{\phi} + 2\zeta \omega_0 \dot{\phi} + \frac{\omega_0^2}{GM_0} \overline{GZ}(\phi) = 0 \quad (3.2.5)$$

where  $\omega_0$  denotes the natural roll frequency of the ship,  $GM_0$  is the initial metacentric height and  $\zeta$  is the damping ratio. From the damping ratio's value  $\zeta$  the magnitude of the damping that exists in the dynamic system can be easily determined. For the rolling motion damping ratio is usually about 0.05 and it does not become greater than 0.2 [16].

The natural roll frequency of the ship is defined by the following equation [40]:

$$\omega_0 = \sqrt{\frac{m g GM_0}{I_x + A_{44}}} \quad (3.2.6)$$

In the application of the above formula the main difficulty is the evaluation of the moment of inertia that includes the mass moment of inertia and the added hydrodynamic moment of inertia due to the acceleration of the fluid by the oscillating ship. Although we might find in the bibliography [40] many semi-empirical formulas to approximate the value of the moment of inertia, they all give quite different values for the same type of ship, as the value of the moment of inertia is not constant for a particular ship, but it also depends on its loading condition and the distribution of the weight on the ship.

### Differential Roll Equation in Longitudinal waves

The rolling motion of the ship in longitudinal waves (pure head or following seas), which neglects any couplings from motions taking place in other than the rolling degree of freedom, can be also expressed with Newton's second law by the equation (3.2.1). For parametric oscillations of a ship, no external roll moments are acting on the system so the second part of the formula is zero[42].

As already mentioned above, the value of the righting arm changes in compliance with the inclination angle of the ship. However, when the ship travels through a longitudinal

wave, the form of the GZ curve changes as the stability increases or decreases when the trough or the crest of a wave is near amidship, respectively. For this reason, the value of the righting arm  $\overline{GZ}$  is time-dependent, as it changes accordingly with the position of the ship on the wave, as shown in figure 3.7, so the restoring moment can be calculated by the equation (3.2.7).

$$M_R(t, \phi) = m g \overline{GZ}(t, \phi) \quad (3.2.7)$$

It is common for the righting arm GZ curve to be approximated as a polynomial power series with odd powers so that the curve that will be created will be an odd function. Finally, the differential equation of rolling motion of the ship in longitudinal waves, by applying the equations (3.2.5) and (3.2.6) becomes:

$$\ddot{\phi} + 2\zeta \omega_0 \dot{\phi} + \frac{m g \overline{GZ}(t, \phi)}{I_x + A_{44}} = 0 \quad (3.2.8)$$

### Mathieu's differential Roll Equation

The GZ curves vary between the trough amidship and crest amidship values as shown in Figure 3.7, as the waves move past the ship. In regular waves this change can be considered approximately sinusoidal between two extreme values. The single degree of freedom rolling motion of a ship in head or following seas may then be described by an equation of motion similar to that for still water, as in equation (3.2.5). However, the restoring moment is not only a function of heeling angle but also varies sinusoidally with time. For small amplitudes of motion, we may use the simplified form of the righting arm (eq. 3.1.9) expression with a time-varying metacentric height as follows.

$$\ddot{\phi} + 2\zeta \omega_0 \dot{\phi} + \frac{\omega_0^2}{GM_0} GM(t) \phi = 0 \quad (3.2.9)$$

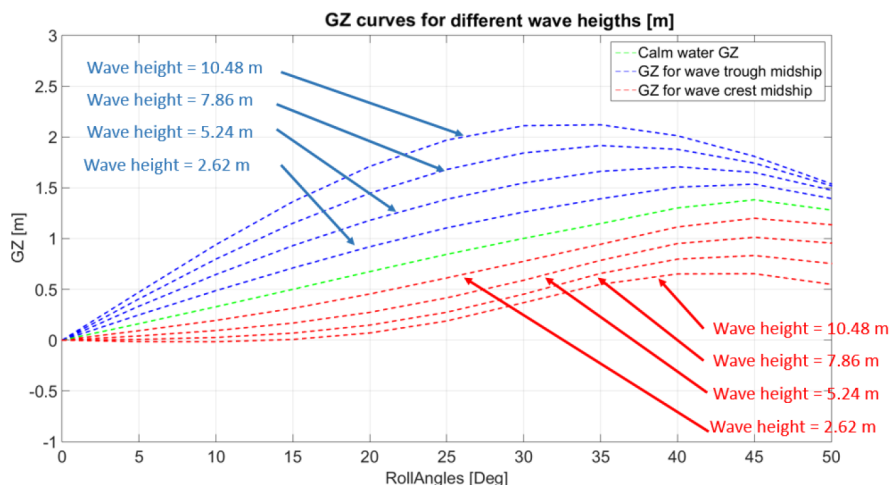


Figure 3.7: Example of GZ curves for calm water, wave crest amidship and wave trough amidship for a C11 type container ship [43].

Wave length equal to the ship length

Considering that the  $GM$  varies approximately sinusoidally between two extreme values, then it is modeled as:

$$GM(t) = GM_0 + \delta GM \cos(\omega_e t) \quad (3.2.10)$$

, where  $GM_0$  denotes the metacentric height of the ship in calm water,  $\omega_e$  is the frequency of variation of  $GM$  equals to the encounter frequency of waves and  $\delta GM$  is the variation of  $GM$  due to waves.

After substitution of formulas (3.2.10) into equation (3.2.9) the linear differential equation of roll becomes:

$$\ddot{\phi} + 2\zeta \omega_0 \dot{\phi} + \omega_0^2 [1 + h \cos(\omega_e t)] \phi = 0 \quad (3.2.11)$$

The form of (3.2.11) without the damping term is recognized as the Mathieu Equation even though the equation is seen to be a linear differential equation with a time-varying restoring coefficient, there is no closed-form analytic solution of Mathieu's equation. Studies and applications of this equation are inevitably fraught by numerical approximation schemes and nonlinear analysis of so-called Stability Charts or Ince-Stutt diagrams [3]. The solutions of Mathieu's equation have been studied extensively and are found to exhibit unstable behavior formula (3.2.12) satisfiable, for any  $n \in \mathbb{N}$ .

$$\frac{4\omega_0^2}{\omega_e^2} \approx n^2 \quad (3.2.12)$$

In figure 3.8 the shaded regions represent stable solutions to the equation and unshaded regions correspond to unstable solutions when the damping coefficient is zero. In the diagram the symbol  $\delta$  represents the ratio  $\frac{\omega_0^2}{\omega_e^2}$  and  $\epsilon$  equals to  $h \frac{\omega_0^2}{\omega_e^2}$ .

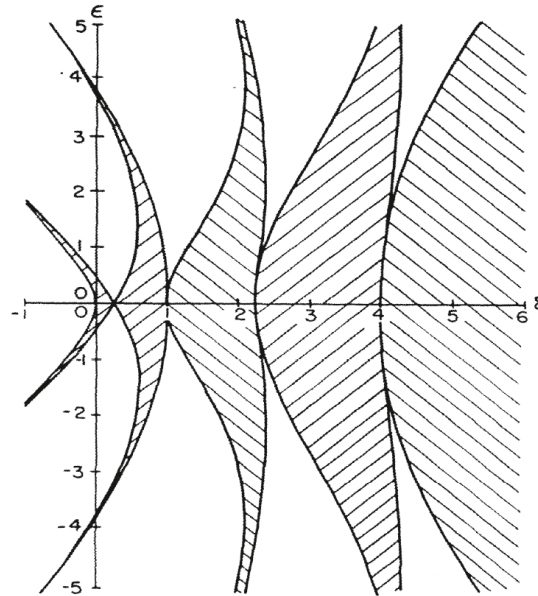


Figure 3.8: Stability Chart of solutions of the Mathieu Equation [3]

From Mathieu's Stability Chart, we can see that  $\delta$  is equal to the square of the ratio of the natural roll frequency of roll to the frequency of the time-varying  $GM$ , or else

the encounter frequency. Additionally,  $\epsilon$  is proportional to the fractional change in  $GM$ . The first unstable region is centered on a value  $\delta = 1/4$  (or else for  $n = 1$  from eq. (3.2.12) called the case of principle resonance). In principle resonance the ratio of natural frequency to frequency of  $GM$  variation is  $1/2$ . If the frequency of  $GM$  variation does not exactly satisfy this value, unstable motion can still take place if  $\epsilon$  is sufficiently large. It is also important to highlight that, the effect of linear damping is merely to raise the threshold value of  $\epsilon$  at a given frequency of variation,  $\omega$ . From this simplified analysis, when we examine regular waves, it is expected that, if the ship encounters regular head or following seas at a frequency near one-half the natural frequency of roll, a small disturbance in roll will grow to appreciable amplitude depending on the amplitude of the stability variation and the roll damping. In reality, for regular waves, it would be more correct to express the  $GM$  change with a periodic, but not necessarily sinusoidal function.

However, the simplification provided by Mathieu's model allows us to have a relatively small knowledge of the ship's instability areas at a relatively small computational cost. Things become even more uncertain in a sea state that is close to the real sea. For this reason, in this diploma thesis, an attempt will be made to calculate the change of the righting arm in random waves. Subsequently, the next section will refer to the theoretical background used to model the random sea waves.



### 3.3 Irregular Waves

Waves are the most important phenomenon to be considered among the environmental conditions, as they significantly affect the ship. Wave behavior is not always easy to understand, since the waves are one of the most complex and mutable phenomena in nature. Waves occur in many ways, they appear as the wind starts to blow, grow into mountainous waves amid storms, and completely disappear after the wind ceases blowing. An observer on a ship easily recognizes the pattern of waves consisting of large and small waves moving in many directions. In most cases, the waves are characterized by significant irregularity.

However, when reaching the shore a wave swell breaks as individual waves, giving the impression of regular repetition. Ocean swell refers to a series of ocean surface waves that were not generated by the local wind, but from a distant storm, as shown in figure 3.9a. Many swell oceans originate in the oceans around Antarctica where there are high winds with nearly infinite duration and fetch [44].

Another type of wave, widely known in fluid dynamics, is wind wave, or wind-generated wave, figure 3.9b. A wind wave is a water surface wave that results from the wind blowing over a fluid surface. More precisely wind wave is created by energy transferred from the wind to the water surface.



(a) Swell ocean [45]



(b) Waves generated by wind [46]

Figure 3.9: Examples of swell ocean and wind generated waves

In oceanography, a sea state is the general condition of the free surface on a large body of water, such as swell or wind-generated waves, at a certain location and moment. A sea state is characterized by statistics, including the wave height, period, and spectrum [8]. The sea state varies with time, as the wind conditions or swell conditions change. The resulting statistics are determined for a time interval in which the sea state can be considered to be constant. This duration has to be much longer than the individual wave period, but smaller than the period in which the wind and swell conditions vary significantly. Typically, records of one hundred to one thousand wave periods are used to determine the wave statistics. Usually, 20 to 30 minutes are enough for a sea state to be represented. Another term that is commonly used in oceanography, is the term of a fully developed sea. A fully developed sea has the maximum wave size theoretically possible for a wind of specific strength and duration.

At first, the simplest approach for describing ocean waves is to consider that the waves can be approximated by two-dimensional sinusoidal form, as called regular waves. De-



terminating the wave parameters is the first step in understanding and, later on, modeling the free surface of the sea. Wave height, wave period, and direction are the most relevant parameters to be studied for the modeling of waves. Additionally, there are other parameters, such as the wave number  $k$ , which refers to the number of waves per unit distance,  $k = 2\pi/\lambda$ . One important formula that includes the wave number is the dispersion relation which relates the wavelength or wave number of a wave to its frequency. It is expressed as the equation (3.3.1).

$$\omega^2 = g k \tanh(kh) \quad (3.3.1)$$

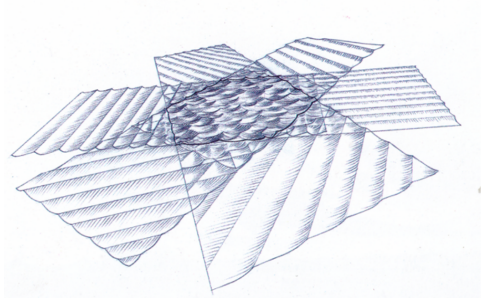
, where  $h$  is the water depth. For deep water, where  $h$  is large  $\tanh(kh) \approx 1$  the dispersion relation becomes:

$$\omega^2 = g k \quad (3.3.2)$$

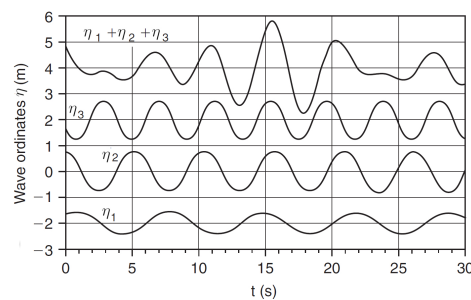
Thus, the free surface elevation of the sea,  $\eta_w$  is defined as:

$$\eta_w(x, t) = a \cos(kx - \omega t) \quad (3.3.3)$$

Although linear wave theory is useful and simplifies calculations in many cases, sinusoidal waves are never found in the natural environment as single wave forms. Picture 3.9b, clearly shows that they are many small and large wavelets with different lengths and heights moving in various directions, that all together combined resemble the real sea. So the natural seaway can be decomposed to a sum of partial sinusoidal waves, each having a relatively small steepness, even for a severe sea as depicted in picture 3.10a. Therefore, the spectral approach with a sum of partial waves is considered a valid representation for a random sea [47].



(a) Multi-directional waves



(b) Unidirectional waves [47]

Figure 3.10: Irregular wave from sum of regular waves

Wave spectrum  $S_{\eta_w}$  is defined, as the distribution of the total wave energy with respect to the circular wave frequency  $\omega$ . More precisely, the wave energy distribution with respect to the frequency alone, irrespective of wave direction, is called the frequency spectrum, while the energy distribution expressed as a function of both frequency and direction is called the directional wave spectrum [8].

Figure 3.10b gives an example of an unidirectional irregular wave profile which was constructed by adding three sinusoidal waves (component waves) of different heights and

periods. Although this example is rather simplistic, it already approaches the real representation of the sea. Further increase in the number of component waves, will create quite irregular profiles similar to those of the real sea. So the energy per unit area of the sea, for a single sine wave component is proportional to its height squared as shown in equation (3.3.4).

$$E_w = \frac{1}{2} \rho g a^2 = \frac{1}{8} \rho g H^2 \quad (3.3.4)$$

Adding the energy of each individual regular wave component, the average energy per unit area  $\bar{E}$  is as follows:

$$\bar{E} = \frac{\rho g}{8N} \sum_{i=1}^N H_i^2 \quad (3.3.5)$$

or

$$\frac{\bar{E}}{\rho g} = \frac{1}{2N} \sum_{i=1}^N a_i^2 = \sigma^2 \quad (3.3.6)$$

The value  $\sigma^2$  is the variance<sup>2</sup> of the water surface elevation record and it follows the form of equation (3.3.6). In the limit, for  $N \rightarrow \infty$ , the amplitude spectrum can be expressed as a continuous spectrum  $S_{\eta_w}$ , called frequency spectrum or omnidirectional spectrum (it does not depend on the direction of the wave). For every component  $i$ , the following equation applies [48].

$$S_{\eta_w}(\omega_i) \Delta\omega = \frac{a_i^2}{2} \quad (3.3.7)$$

In bibliography [49] the variance is linked with the zero-order spectrum moment of the stationary seaway  $m_0$  with the following equivalence,  $\sigma = \sqrt{m_0}$ . From integration of  $S_{\eta_w}$  for all positive frequencies  $\omega$ , we derive the value of  $m_0$ , which is also equal to the area under the wave spectrum:

$$m_0 = \int_0^\infty S_{\eta_w}(\omega) d\omega \quad (3.3.8)$$

Oceanographers have studied the ocean pattern extensively and tried to fit measurements into general formulas. One of the most popular wave spectrums for fully developed seas in deep water is Pierson and Moskowitz (PM) (1963). An alternated model of the Pierson and Moskowitz's seaway spectrum was also developed by Bretschneider (1952, 1961) [8]. Another commonly used spectrum is the Jonswap (Joint North Sea Wave Observation Project) spectrum, which is more narrow (peakier) than the pure open sea spectra. Last but not least, another worth mentioning type of spectrum is the Ochi-Hubble spectrum. It is a double-peaked spectra that represents sea states including both a remotely generated swell and a local wind-generated sea [50]. In figure 3.11, an example of Pierson and Moskowitz's and Jonswap, a higher peak, spectrum is shown.

After this brief reference to the definition of wave spectrums, we can follow the opposite procedure to determine the elevation of the sea. By decomposing a spectrum, for a certain sea state, the characteristics of the regular wave components can be calculated.

<sup>2</sup>The variance in statistics is calculated by taking the average of squared deviations from the mean.

For time history of the surface elevation  $\sigma^2 = \sum_{n=1}^N (a_i - \bar{a})^2 / N$

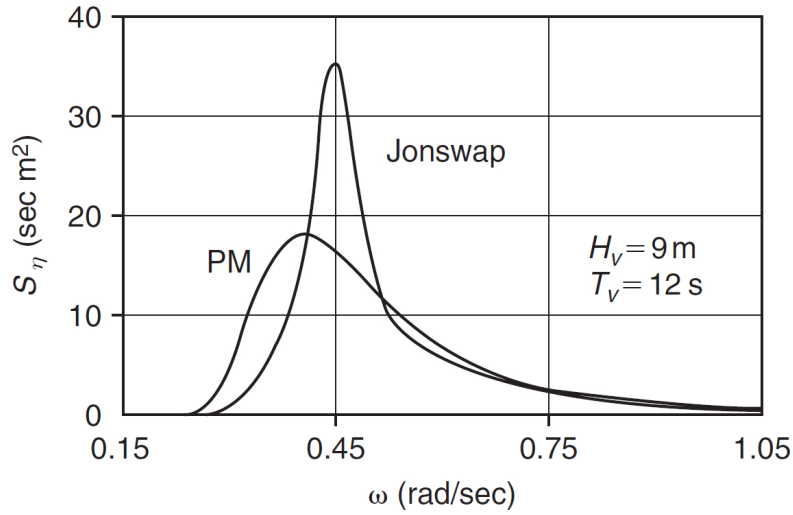


Figure 3.11: Comparison of PM and JONSWAP spectra [47]

The unidirectional, irregular wave pattern  $\eta_w$  is seen as the sum of regular partial waves, as shown in Figure 3.10b (at  $x=0$ ). Using Fourier analysis we can calculate the wave components of a sea state out of a record of sea elevation over time. An irregular record can be plotted again as a sum of the partial waves, according to the following equation for  $t \in \mathbb{R}$ .

$$\eta_w(x, t; \beta) = \sum_{n=1}^N a_n \cos(k_n x - \omega_n t + \Xi_n(\beta)) \quad (3.3.9)$$

swhere

- $\beta$ , is a selection variable, stochastic<sup>3</sup> argument, used to distinguish one outcome of an experiment from another.
- $\omega_n > 0, n = 1, 2, \dots, N$ , are deterministic values that represent the the frequencies of every wavelet component  $n$ .  $\omega_n$  in deep water is linked with the wave number with the equation (3.3.2)
- $a_n > 0, n = 1, 2, \dots, N$ , are also deterministic values that correspond to the amplitude of every wavelet component  $n$ .
- $\Xi_n(\beta)$ , are the random phases that have the same Probability density function (pdf). All wave phases have an equal probability of occurrence as they follow an uniform distribution, expressed by a constant probability density  $1/(2\pi)$  in the range  $[0, 2\pi)$ .

Randomization with phase means that every wavelet component of the sum is moved randomly with respect to the phase (i.e., to the beginning of the axes) as defined by

<sup>3</sup>Stochastic is the experiment which can be repeated many times under similar routines (uniform repetitions), yet the results of which vary irregularly from one test to another. However, certain "average" values and certain histograms of the results, after many repetitions show an obvious statistical regularity of the process. i.e., they show a clear tendency of stabilization, when the number of repetitions increases. For example the experiment of measurement of the free surface elevation is a stochastic experiment.

$\Xi_n(\beta)$ . In the end, to get the value of the surface elevation  $\eta_w(x, t; \beta)$  at a specific point  $x$ , all the partial waves will be added. For every experiment outcome,  $\beta$ , one set of random phases provides us with only one realization of irregular waves. Simulation with another realization of waves requires generation of another set of random phases (with each set containing  $N$  values) [42].

The spectral form  $S_{\eta_w}(\omega)$  acknowledges that the water surface is composed of components across a range of frequencies; however, it does not consider that these components could propagate in a variety of directions. An extension of (3.3.9) to account for direction would take the form [48]:

$$\eta_w(x, y, t; \beta) = \sum_{n=1}^N a_n \cos[k_n(x \cos e_i + y \sin e_i) - \omega_n t + \Xi_n(\beta)] \quad (3.3.10)$$

, where  $e_i$  is the angle between the  $x$ -axis and the direction of propagation of component  $i$ . The spectrum that describes the energy distribution among the wave frequencies, will now be defined, equation (3.3.11) as the directional frequency spectrum  $S_{\eta_w}(\omega, \epsilon)$ .

$$m_0 = \int_0^{2\pi} \int_0^\infty S_{\eta_w}(\omega, \epsilon) d\omega d\epsilon \quad (3.3.11)$$

However, in this diploma thesis the directional spectrums will not be used, as only the unidirectional irregular waves will be examined. So in this chapter, a small introduction has been made, of the spectral method and the use of the Fourier analysis in order to approach the free surface elevation, with the phase of each partial wave as a stochastic value.

## Chapter 4

# Hydrostatic Equilibrium and Hull Discretization

The first topic explained in Chapter 3.1.1 is the hydrostatic equilibrium of the ship. For this reason, in the current chapter, the method for the computation of the hydrostatic equilibrium will be described. For this diploma thesis, a code has been developed in Mathematica environment that calculates the longitudinal and transverse center of buoyancy of the ship for a specific loading condition. For these computations, the knowledge of the geometry of the hull is necessary. The data from a sample Post-Panamax Containership are used, and later on, the same data are used for the simulations. To make the appropriate calculations, the geometry of the hull must be introduced into the program in a format that simplifies the calculations. For this reason, a mesh was created with the appropriate discretization. From every cell of the mesh, specific data were extracted.

Finally, an analysis of the hydrostatic equilibrium of the ship was performed not only to confirm the accuracy of the code but also to examine which discretization of the mesh achieved the desired accuracy. This analysis shall consist of the calculation of the displacement and longitudinal centre of buoyancy for a range of draughts, and the construction of the GZ curve for specific loading conditions. For the validation of the code, two models were designed. The first model was designed in *Aveva<sup>TM</sup>* Initial Design Program and the second in Rhinoceros<sup>®</sup> Design Program. The mesh created of the hull's geometry with the Rhinoceros<sup>®</sup> was used as an input for the code. The data that were calculated with the code were compared with the data exported from Aveva and data from the Trim and Stability Booklet of the ship.

### 4.1 Calculation of Hydrostatic equilibrium in Mathematica

For the computation of the hydrostatic equilibrium and the righting arm of a ship in any position, a code was provided by Doctoral Candidate Ioannis Kontolefas, developed in Mathematica programming language. In this section, we will describe the development process of this code and its functions. Later on, these functions were used and modified accordingly for subsequent calculations as the ship moves in longitudinal waves.

It is common knowledge that when a ship floats in water, it is free to move in all six

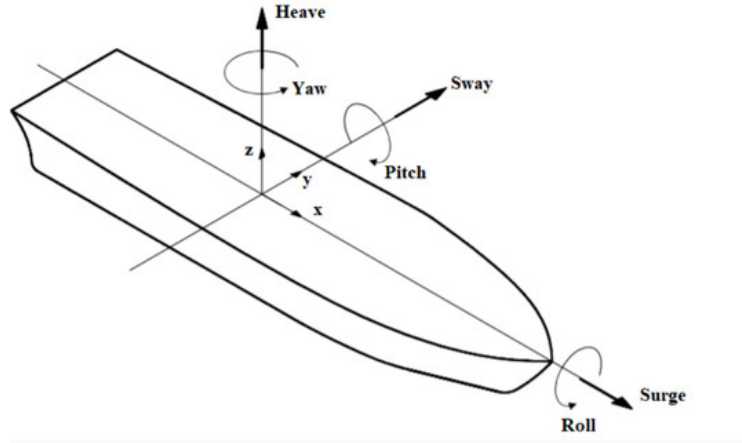


Figure 4.1: Definition of motions in 6DOF (surge, sway, heave, roll, pitch and yaw) [51]

possible degrees of freedom (6DOF) as illustrated in figure 4.1. The three of these motions describe translations in the three main perpendicular axes of the ship, the longitudinal axis (surge motion), the transverse axis (sway), and the vertical axis (heave). The other three movements describe the rotation around the respective axes (roll, pitch, and yaw). Two systems /frames of reference are used, one as an earth-fixed frame ( $\epsilon$ -frame) and the other as a ship-fixed frame (called  $s$ -frame). For later applications, we place the  $s$ -frame to always on the midship. The position of the ship is defined by the coordinates of the ship-fixed origin with respect to the earth-fixed frame as defined in (4.1.1). While the orientation by the ship-frame with respect to the earth frame is defined in (4.1.2)

$$r_s^e = (\xi, \eta, \zeta) \quad (4.1.1)$$

$$q_s^e = (\phi, \theta, \psi) \quad (4.1.2)$$

The coordinates of a point can be transferred from the ship-frame to the earth-frame with the use of the transformation matrix  $R_s^e(q_s^e)$ .

$$r_p^e = r_s^e + R_s^e(q_s^e) r_p^s \quad (4.1.3)$$

This equation refers to the transport by  $r_s^e$  and then the rotation of the point  $p$  with respect to the  $s$ -frame by multiplying it with the transformation matrix. The ship, as a 3D body, can be rotated about the three orthogonal axes as shown in 4.1.

The yaw, pitch and roll counterclockwise rotations about the  $z$ ,  $y$  and  $x$ -axis respectively are given by the following rotation matrices <sup>1</sup>.

$$R_z(\psi) = \begin{bmatrix} c\psi & -s\psi & 0 \\ s\psi & c\psi & 0 \\ 0 & 0 & 1 \end{bmatrix}, R_y(\theta) = \begin{bmatrix} c\theta & 0 & s\theta \\ 0 & 1 & 0 \\ -s\theta & 0 & c\theta \end{bmatrix}, R_x(\phi) = \begin{bmatrix} 1 & 0 & 0 \\ 0 & c\phi & -s\phi \\ 0 & s\phi & c\phi \end{bmatrix} \quad (4.1.4)$$

<sup>1</sup>Note that  $c\bullet = \cos(\bullet)$  and  $s\bullet = \sin(\bullet)$

The yaw, pitch, and roll rotations can be used to place a 3D body in any orientation. A single rotation matrix can be formed by multiplying the yaw, pitch, and roll rotation matrices to obtain the following rotation matrix [52].

$$R_s^e(q_s^e) = R_z(\psi) R_y(\theta) R_x(\phi) = \begin{bmatrix} c\psi c\theta & -s\psi c\phi + c\psi s\phi s\theta & s\psi s\phi + c\psi c\phi s\theta \\ s\psi c\theta & c\psi c\phi + s\psi s\phi s\theta & -c\psi s\phi + s\psi c\phi s\theta \\ -c\theta & c\theta s\phi & c\theta c\phi \end{bmatrix} \quad (4.1.5)$$

It is important to note that  $R_s^e(q_s^e)$  performs the roll first, then the pitch, and finally the yaw. If the order of these operations is changed, a different rotation matrix would result.

We now introduce a moving frame ( $m$ -frame) located at the  $s$ -origin and aligned with the  $e$ -frame, so that it change with the rotational movements of the ship. The decomposition of all vector quantities hereafter is performed with respect to the  $m$ -frame, unless otherwise stated. It is also assumed that the  $e_z$  axis is collinear with the gravitational acceleration vector. The hydrostatic pressure is calculated for each point on the ship by the following formula.

$$p = p(x, y, z, t) = \rho g [\eta_w(x, y, t) - z] = \rho g h \quad (4.1.6)$$

,where  $h$  is the vertical distance between any submerged point at the ship and the free surface  $\eta_w$ . Dividing the pressure into three components along the  $x$ -,  $y$  and  $z$  directions, with the unit vectors  $e_x, e_y, e_z$  respectively, the formula (3.1.3) results in:

$$\bar{F}_B = -e_x \iiint_V \rho g \frac{\partial \eta_w}{\partial x} dV - e_y \iiint_V \rho g \frac{\partial \eta_w}{\partial y} dV + e_z \iiint_V \rho g dV \quad (4.1.7)$$

Considering that the first two components of formula (4.1.7) are significant small, then we use (3.1.2) and (4.1.7) becomes:

$$\nabla = \iiint_V dV = \iint_S h n_z dS \quad (4.1.8)$$

Furthermore, by neglecting the  $x$ - and  $y$ -component of the buoyancy force and considering that the element forces are parallel to each other, the expressions (3.1.8), (3.1.7) and (4.1.8) can be described as

$$\nabla \cong \sum_{i=1}^N h_i n_{zi} \delta S_i \quad (4.1.9)$$

$$x_B \cong \frac{\sum_{i=1}^N c_{xi} h_i n_{zi} \delta S_i}{\sum_{i=1}^N h_i n_{zi} \delta S_i}, \quad y_B \cong \frac{\sum_{i=1}^N c_{yi} h_i n_{zi} \delta S_i}{\sum_{i=1}^N h_i n_{zi} \delta S_i} \quad (4.1.10)$$

,where

$N$  is the number of surface elements considered for the discretization of the submerged part of the hull,

$c_i$  is the centroid of the surface element with index  $i$ ,

$h_i$  is the distance of  $c_i$  from the free surface,

$n_{zi}$  is the  $z$ -component of the unit normal vector  $n$  at  $c_i$ , which points inwards and,

$\delta S_i$  is the area of the surface element with index  $i$

As has already been discussed in chapter 3.1.1, for a floating body to be in hydrostatic equilibrium, the buoyancy should equal its weight. Additionally, the center of gravity with the center of buoyancy should be on the same vertical line. Thus, the following equations should be satisfied.

$$\begin{aligned} \rho \nabla &= m \\ x_b &= x_g \\ y_b &= y_g \end{aligned} \quad (4.1.11)$$

When the ship has rotated around an axis then the coordinates of the center of gravity should be expressed with respect to the  $m$ -frame, by using the rotation matrix as shown in (4.1.12).

$$\begin{bmatrix} x_g \\ y_g \\ z_g \end{bmatrix} = R_s^e(q_s^e) \begin{bmatrix} x_g^s \\ y_g^s \\ z_g^s \end{bmatrix} \quad (4.1.12)$$

Finally, considering expressions (4.1.5), (4.1.9), (4.1.10) and (4.1.12) system (4.1.11) can be written in the following form.

$$\rho \sum_{i=1}^N h_i n_{zi} \delta S_i - m = 0 \quad (4.1.13)$$

$$\frac{\sum_{i=1}^N c_{xi} h_i n_{zi} \delta S_i}{\sum_{i=1}^N h_i n_{zi} \delta S_i} - (c\psi c\theta) x_g^s - (c\psi s\phi s\theta - s\psi c\phi) y_g^s - (s\psi s\phi + c\psi c\phi s\theta) z_g^s = 0 \quad (4.1.14)$$

$$\frac{\sum_{i=1}^N c_{yi} h_i n_{zi} \delta S_i}{\sum_{i=1}^N h_i n_{zi} \delta S_i} - (s\psi c\theta) x_g^s - (c\psi c\phi + s\psi s\phi s\theta) y_g^s - (s\psi c\phi s\theta - c\psi s\phi) z_g^s = 0 \quad (4.1.15)$$

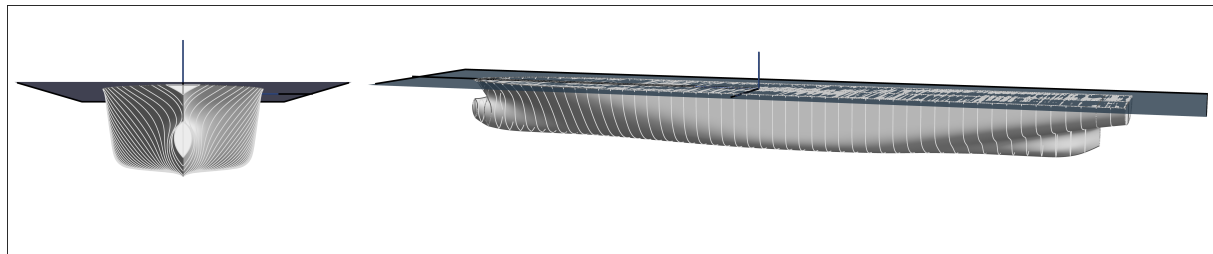
All points on the deck are assumed to be in the reference plane, with  $z = 0$ . Consequently, all other elements of the hull discretization will have negative  $z$ -coordinates. The sea surface is also considered at  $z = 0$ , as shown in figure 4.2a. In addition,  $\eta_w$  is the elevation of the free surface in case of regular or irregular waves. In the beginning, when the hydrostatic equilibrium is examined,  $\eta_w$ , is considered a wave with a height equal to zero.



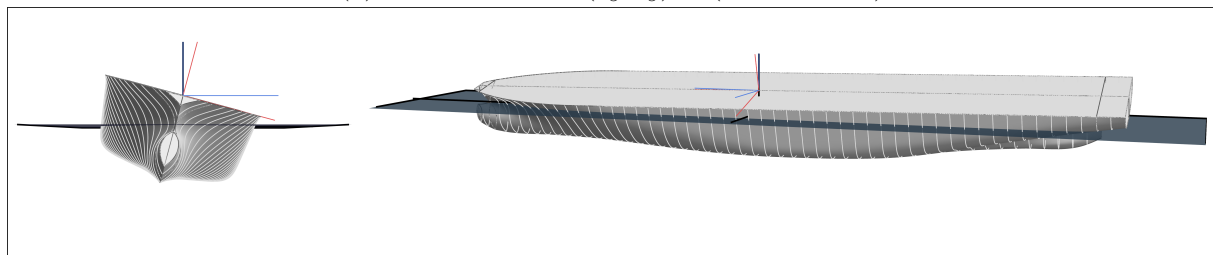
One of the inputs of the code is a vector with the generalized position of the ship

$$(r_s^e, q_s^e) = (\xi, \eta, \zeta, \phi, \theta, \psi) \quad (4.1.16)$$

Every transformation and rotation from (4.1.16), is applied from the  $s$ -frame, which is located in the midship and on the deck of the ship (Fig. 4.2b)



(a) Position vector  $(r_s^e, q_s^e) = (0, 0, 0, 0, 0, 0)$



(b) Position vector  $(r_s^e, q_s^e) = (0, 0, 8.1, -\pi/12, \pi/180, 0)$

Figure 4.2: Example of Buoyancy calculation- graphic representation of the position of the ship for specific  $(r_s^e, q_s^e)$  position vector

The black axes refer to the  $e$ -frame, whereas the blue and red axes refer to  $s$ - and  $m$ -frame respectively.

With the use of the formula (4.1.3), every centroid is transferred with respect to the  $m$ -frame. And every unit normal is rotated with the rotation matrix. Then formula (4.1.9) is applied to the elements that are under the free surface, in order to calculate the Displacement volume. Similarly, equations (4.1.14) and (4.1.15) can be used to calculate the longitudinal and transverse center of buoyancy from the midship. For the above calculation the function *Buoyancy.m*<sup>2</sup> is used.

Conversely, by using the functions that were created, the generalized position of the ship can be calculated. This time the coordinates of the center of gravity and the displacement of the ship for a given loading condition will be used as input. In the function *Equilibrium.m*<sup>3</sup>, the equations (4.1.13), (4.1.14), (4.1.15) can be solved as a 3x3 system to find the appropriate pair  $(\zeta, \phi, \theta)$  of the ship's position that satisfies the equations. Then the function searches for a numerical root of  $(\zeta, \phi, \theta)$ , starting from the point  $(\zeta_0, \phi_0, \theta_0)$ . For this reason, the initial position vector should be provided as input. With this sense, three functions were developed, *Equilibrium 3*, *Equilibrium 35* and *Equilibrium 345*. In each of the above functions, the equilibrium is resolved in only one degree of freedom (corresponding to heave response motion), two degrees of freedom (corresponding to heave

<sup>2</sup>//BuoyUp2Lite/Needs/Mathematica/BuoyUp/Buoyancy.m

<sup>3</sup>//BuoyUp2Lite/Needs/Mathematica/BuoyUp/Equilibrium.m

and pitch response motion), and finally three degrees of freedom (corresponding to heave, roll and pitch response motion) respectively.

Finally, combining the functions developed so far, the righting arm ( $GZ$ ) is calculated. Since the righting arm must be found for a particular loading condition, there is no equilibrium on the transverse axis. For a certain rolling angle, the function *Equilibrium 35* is used, so the solution for the ship's position  $(\zeta, \theta)$  is found. After knowing the position vector  $(r_s^e, q_s^e)$ , but with the equilibrium being applied only in the direction of the heave and pitch motion,  $y_b$  can be computed. After this process, the righting arm is calculated, for a given roll angle by the following formula.

$$GZ = y_b - y_g \quad (4.1.17)$$

As already mentioned that quantities  $y_b$  and  $y_g$  are considered with respect to the  $m$ -frame.

## 4.2 Discretization of hull's geometry

### 4.2.1 Sample ship Data

To calculate the righting arm, as described in the previous section, the ship's hull geometry must be input to the program. This is done via discretizing the hull surface into small elements. From each element, the coordinates of the centroid, its unit normal vector, and the area of the surface element are used. The coordinates of the elements are used with respect to the origin point in the  $s$ -frame, located in the middle of the ship.

As a sample for this study, a Post-Panamax Container Carrier is used. This ship is capable of worldwide trading, including Suez Canal and Panama Canal. The Containership's capacity is between 4275 TEU (10 t/TEU homogeneous) and 2366 TEU (18 t/TEU homogeneous) approximately, depending on the loading condition of the ship. The sample ship is a vessel with a block coefficient of around 0.65, no parallel midship section, a bow with a large flare and a bulb. It also has a pair of bilge keels with width of 0.415 m and length of about 30% of  $L_{pp}$ . The Containership appears to have a deckhouse in the stern section. The vessel's hull lines, bulbous bow, and bow flare are optimized by HSVA (The Hamburg Ship Model Basin).

For this ship, studies on parametric roll have been done in the past. The ship was investigated at design draught with a low transverse metacentric height of  $GM_t = 0.5m$ . The ship at this investigated load case has a natural roll period of  $T_0 = 41.5sec$ . At this condition, the ship suffers from low static stability and it is likely for parametric rolling to occur at medium ship speeds in following waves. According to the calculations of the HSVA report, severe roll motions can occur in a wide range of wave periods and ship speeds, and even capsizing is possible in following seas of 6 m significant wave height and wave periods between approximately 10 and 20 sec.

In this diploma thesis, this case will not be examined, as the purpose of the diploma thesis is not to evaluate whether or not this particular ship has sufficient stability. This ship is used as a typical sample ship so that the response to parametric roll in waves can be examined in general. In addition, the same ship was also used by Ms. Dousia in her diploma thesis [26]. So it is used so that a relative comparison can then be made between the results of Ms. Dousia's and this diploma thesis. In table 4.1 the main particulars of the ship, that was chosen for this study, are shown.

Table 4.1: Principal Dimensions of the sample ship

Length overall	$L_{oa}$	250	m
Length between perpendiculars	$L_{pp}$	238.35	m
Breadth (mld.)	$B$	37.3	m
Depth (mld.)	$D$	19.6	m
Design Draught (mld.)	$T_d$	11.5	m
Scantling Draught (mld.)	$T_{sc}$	12.5	m

## 4.2.2 Rhino Model and hull discretization

A model has been created with the Rhinoceros<sup>®</sup> Design Program. After creating the surface of the model by following the lines of the ship, a mesh is made with triangular elements (trimesh). The triangular mesh is then exported to a .raw file, consisting of a list of the coordinates of the 3 corners ( $p_{corn1}, p_{corn2}, p_{corn3}$ ) of each triangular element. The list consist of the  $x, y, z$ - coordinates for each corner, as shown below.

$$\begin{aligned}
 p_{corn1} &= (x_{corn1}, y_{corn1}, z_{corn1}), \\
 p_{corn2} &= (x_{corn2}, y_{corn2}, z_{corn2}), \\
 p_{corn3} &= (x_{corn3}, y_{corn3}, z_{corn3})
 \end{aligned}
 \tag{4.2.1}$$

Then the coordinates of the centroid of each element are calculated as follows.

$$\begin{aligned}
 c_x &= \frac{x_{corn1} + x_{corn2} + x_{corn3}}{3}, \\
 c_y &= \frac{y_{corn1} + y_{corn2} + y_{corn3}}{3}, \\
 c_z &= \frac{z_{corn1} + z_{corn2} + z_{corn3}}{3}
 \end{aligned}
 \tag{4.2.2}$$

In a triangle two vectors  $\vec{A} = p_{corn2} - p_{corn1}$  and  $\vec{B} = p_{corn3} - p_{corn1}$  are selected. The surface normal of each triangle can be calculated by taking the vector cross product of two edges of that triangle, as  $\vec{N} = \vec{A} \times \vec{B}$ . The order of the vertices used in the calculation will affect the direction of the normal (inwards or outwards of the face). After the calculation vector cross product, each vector component can be calculated as follows:

$$\begin{aligned}
 N_x &= A_y B_z - A_z B_y, \\
 N_y &= A_z B_x - A_x B_z, \\
 N_z &= A_x B_y - A_y B_x
 \end{aligned}
 \tag{4.2.3}$$

Finally, the unit vector  $\vec{n}$  is equal to the normal vector  $\vec{N}$  divided by its magnitude. The magnitude  $|\vec{N}|$  of the normal vector  $\vec{N}$  is equal to the square root of the sum of the squares of its components,  $|\vec{N}| = \sqrt{N_x^2 + N_y^2 + N_z^2}$ .

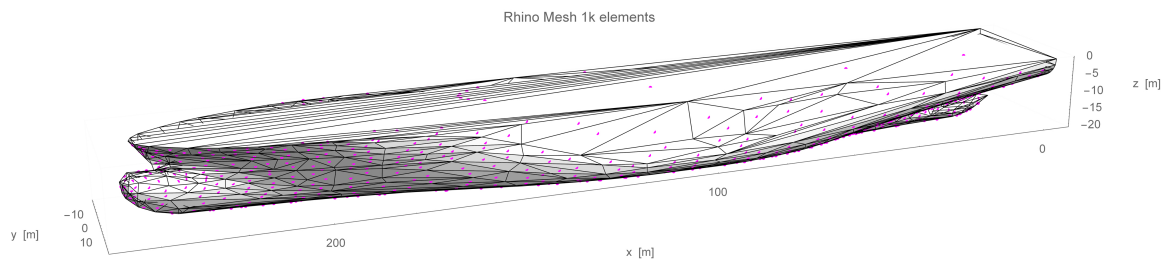
For all the above computations a function was created in Mathematica<sup>4</sup>, and the direction of the unit vector is checked so that it is always directed inwards to the ship's hull. The area of the surface of each element is also calculated. With the use of this

<sup>4</sup>//BuoyUp2Lite/Needs/Mathematica/BuoyUp/Discretization.m

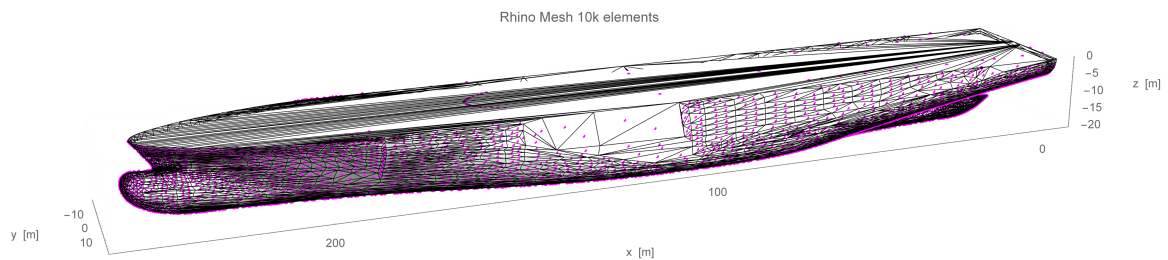
function, the unit normals, centroid, and area of each element are determined, in order to be used as input for the calculation of the Hydrostatic Equilibrium for the previous functions.

The mesh generated by the model designed in Rhino is shown in figure 4.3. Three different meshes were selected, with 1000, 10,000, and 20,000 elements respectively. The meshes are automatically generated by the Rhino program to capture the geometry of the ship as accurately as possible, according to the number of elements specified.

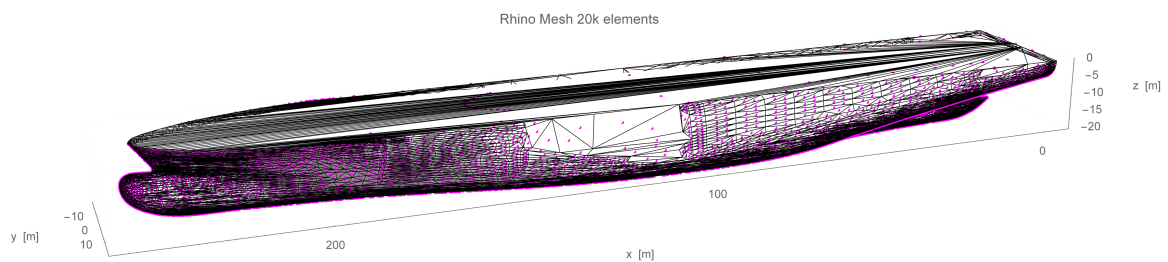
In figure 4.3, we notice that the elements that form the mesh are not of constant size and are sometimes larger and sometimes smaller. At positions where the geometry is complex, there are a more numerous but smaller elements. In areas where the hull surface is flat, e.g. FOS, FOB or the upper deck the mesh consists of larger elements.



(a) Discretization with 1,000 elements



(b) Discretization with 10,000 elements



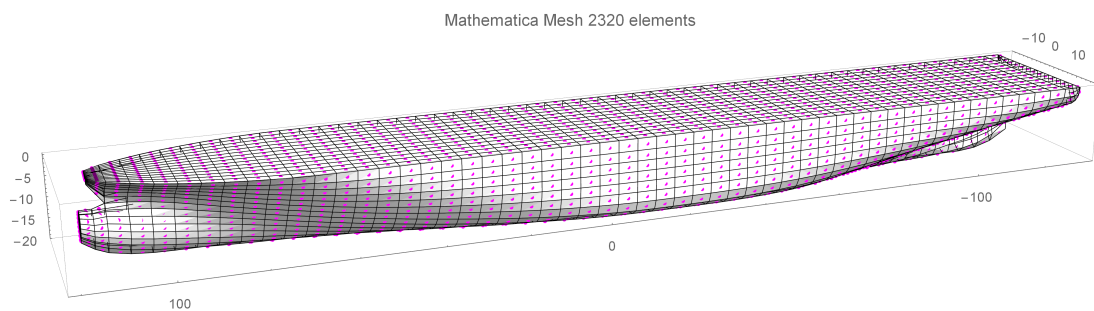
(c) Discretization with 20,000 elements

Figure 4.3: Rhino Tri-Mesh with different number of elements

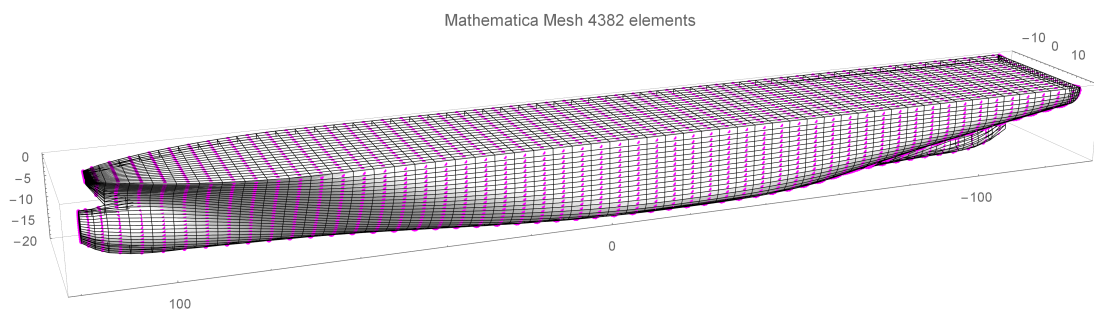
In particular, it is observed that in the deck the triangular elements have an elongated structure and are not evenly distributed over the entire surface. In every triangle one of

the three corners is fixed on the same point and this is what creates the elongated shape. As a result the centroids of the triangular elements in the deck are concentrated in one area only. This is a problem as the program recognizes the geometry by the location of the centroids and therefore may not produce accurate results for the equilibrium of the ship at large angles where the free surface will exceed the deck.

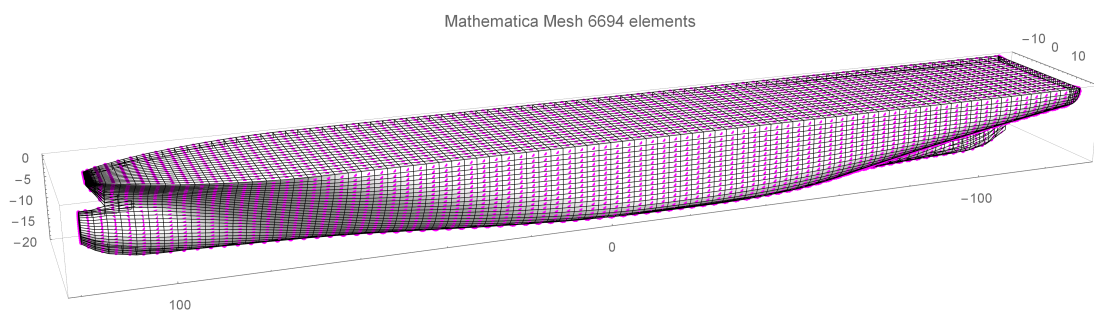
For the above reasons, another discretization of the hull was created in a slightly different way. The frames, taken from the ship's data, were placed at equal distances. Each frame was divided into a sufficient number of points. For each frame these points will be at an appropriate location so that they create quadrilateral elements as they line up with the points of the adjacent frame. Again, three different meshes were selected, with 2,320, 4,382, and 6,694 elements respectively, as shown in figure 4.4. Since the mesh is quadrilateral, the centroids, unit vectors and area for each element are calculated respectively.



(a) Discretization with 2,320 elements



(b) Discretization with 4,382 elements



(c) Discretization with 6,694 elements

Figure 4.4: Mathematica Quad-Mesh with different number of elements



## 4.3 Validation of Mathematica code with Aveva and Trim & Stability data

### 4.3.1 Displacement and LCB hydrostatic calculations

A model of the ship was then designed in *Aveva*<sup>TM</sup> Initial Design to validate the accuracy of the program in the hydrostatic calculations. A comparison of the created meshes will also be made to select the proper discretization with as few elements as possible in order to speed up the calculation process, but at the same time provide a sufficient level of accuracy.

First, the values of Displacement and LCB (from the Aft Peak) were calculated from Aveva and Mathematica for a range of drafts. The cases that are examined are for even keel (or else called zero trim), for trim by stern (trim=-1), and trim by head (trim=1) in still water. For the Mathematica calculations, the functions developed in Section 4.1 for the calculation in hydrostatic equilibrium are used, in function *TDisp.m*<sup>5</sup>. With the function *TDisp.m*, the ship's displacement is calculated for a given draught, to ensure the equilibrium in the three degrees of freedom (corresponding to heave, roll and pitch response motion respectively). Similarly, the longitudinal center of buoyancy is calculated from the AP, for variant draughts. For the computations, the generalized position of the ship is fed into the program as input data,  $(r_s^e, q_s^e) = (0, 0, \zeta_i, 0, \theta_{(0,-1,1)}, 0)$  (see equation (4.1.16)). The value  $\zeta_i$  is the vertical transformation corresponding to the desired drafts. The values  $\theta_{(0,-1,1)}$  in rad are the right rotation angles that the ship should be subjected in order to have zero trim, trim by stern, and trim by head accordingly.

The calculations of the ship's displacement and LCB are made with the six different hull meshes. The former are compared with the corresponding values from the hydrostatic table of the reference ship and the results from the Aveva model as presented in the figures 4.5, 4.7, and 4.6. For each case, the error is calculated from the real data, which is the data extracted from the Trim & Stability of the ship and are considered to be the most accurate. For each draft the deviation between the displacement calculated by Mathematica or Aveva and the actual one (Trim & Stability), is evaluated. The error is then divided by the real value, and finally, it is multiplied by 100 to obtain the percentage error, as shown in the following formula.

$$\text{Percentage Error} = \frac{\Delta_{CASE} - \Delta_{REAL}}{\Delta_{REAL}} 100 \quad (4.3.1)$$

In the same way, for the LCB, the error is presented as a percentage of the ship's  $L_{pp}$  which is always constant and equal to 238.35 metres, as follows.

$$\text{Error as percentage of } L_{pp} = \frac{LCB_{CASE} - LCB_{REAL}}{L_{pp}} 100 \quad (4.3.2)$$

From the graphs what we observe primarily, is that there are no extreme values nor logical errors. The LCB for zero trim calculated for each draught is between the corresponding values for the trim by stern and by head. This is to be expected, as when the ship has trim by stern, the stern of the ship is deeper submerged in the water. This results

<sup>5</sup>//BuoyUp2Lite/Needs/Mathematica/BuoyUp/TDisp.m

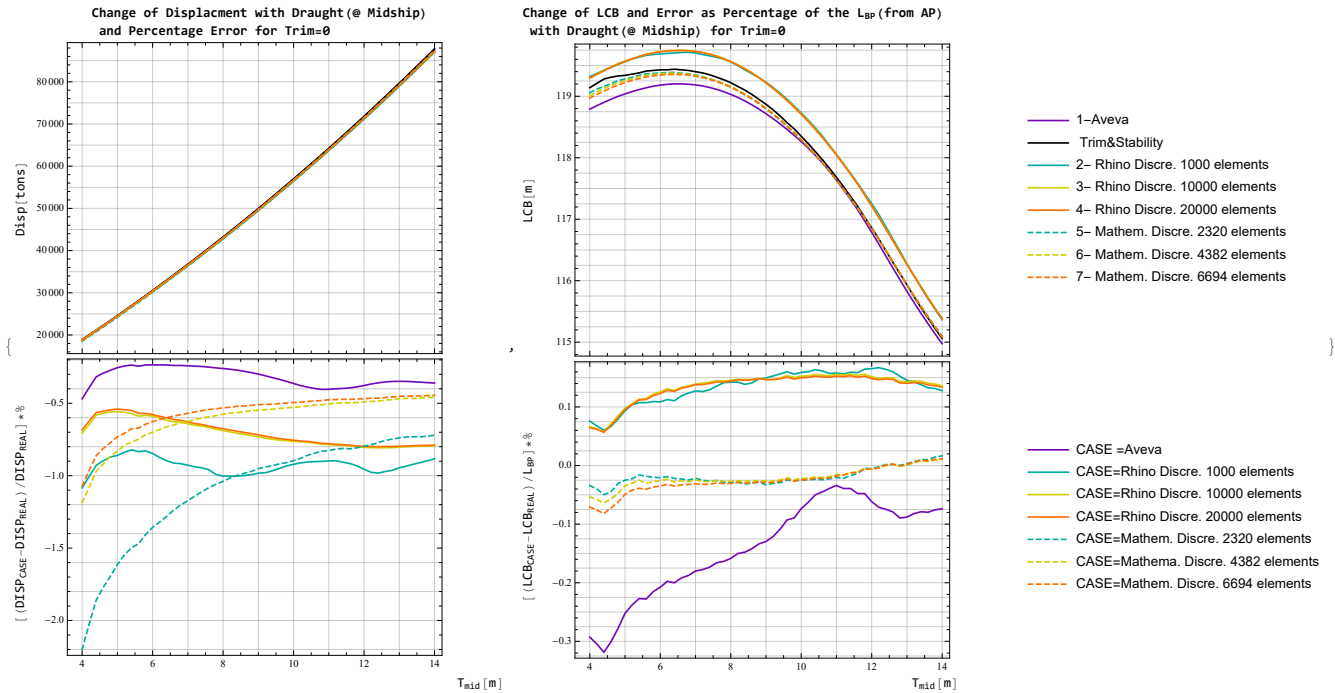


Figure 4.5: Validation with Trim & Stability data and Aveva model of LCB and Displacement in Calm Water with Trim = 0

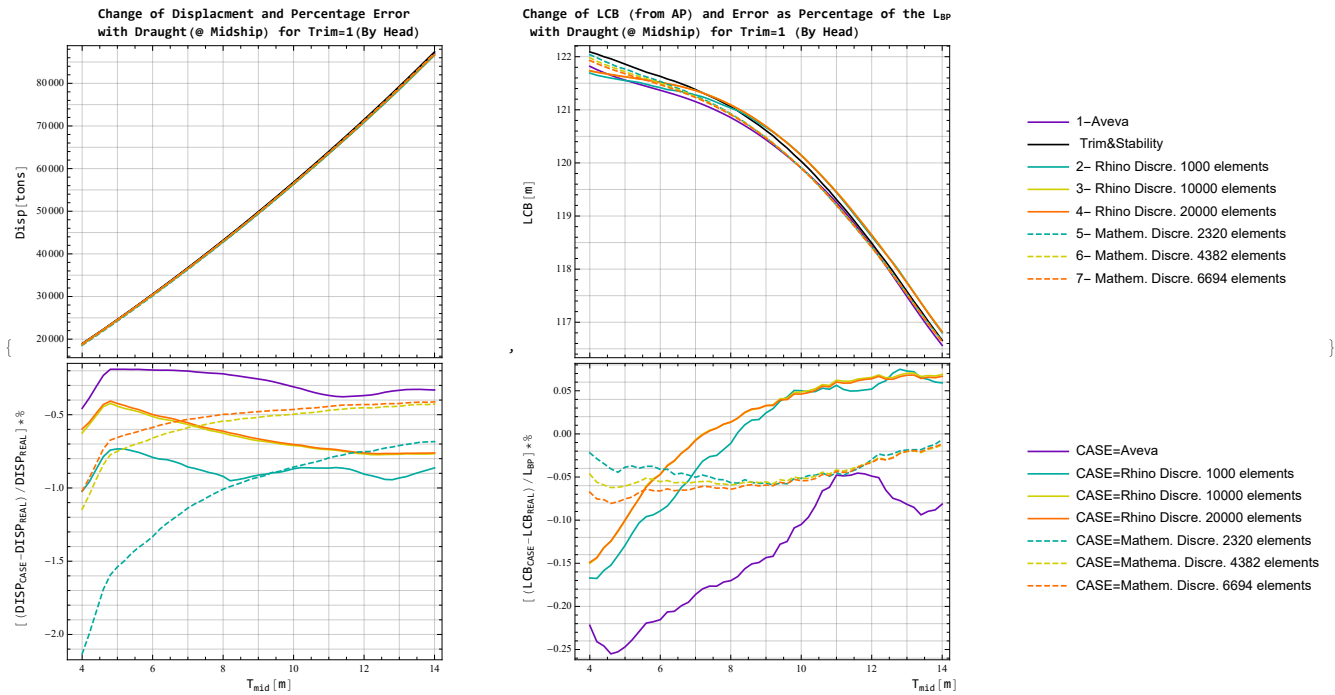


Figure 4.6: Validation with Trim & Stability data and Aveva model of LCB and Displacement in Calm Water with Trim by Head

in the submerged volume of the ship being more towards the stern and therefore the LCB is further aft than it would be for zero trim. The opposite applies when the ship has a

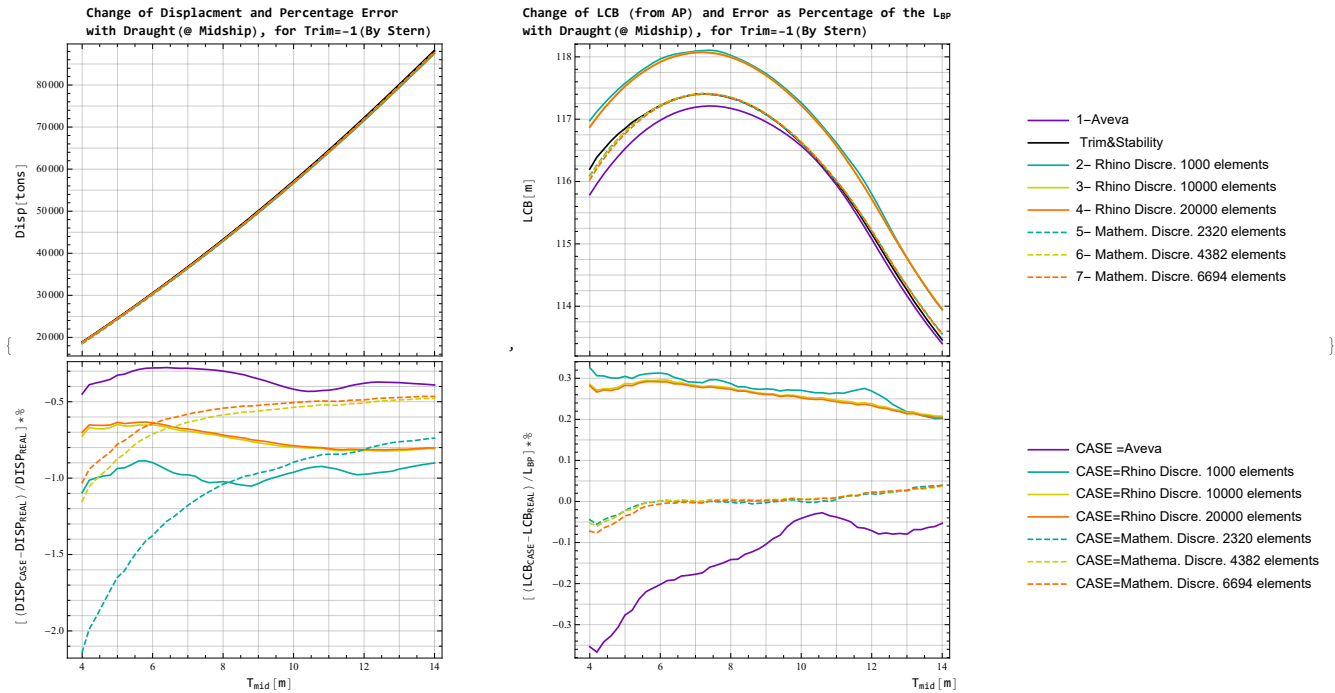


Figure 4.7: Validation with Trim & Stability data and Aveva model of LCB and Displacement in Calm Water with Trim by Stern

trim by head. Then the longitudinal center of buoyancy is further forward than it would be for the same situation at zero trim. By observing the diagrams above it is obvious that this happens in all cases, and for every draught. So the program in Mathematica approximates and understands well the changes that will occur with the alteration of the ship's position on the free surface of the sea.

For the condition of the ship with even keel, both the Mathematica and Rhino model discretizations have a modest error from the actual values. The error for the displacement calculation decreases further for larger draughts. For the calculation of the LCB, the error becomes almost close to zero. The same seems to occur for the trim by stern and by head.

For the displacement, the discretizations 2 and 5, with the fewest elements, both from the quadrilateral and triangular mesh, have the poorest accuracy. The models from Rhino (models no. 2, 3, and 4) have better accuracy for smaller draughts than the ones from Mathematica (models no. 5, 6, and 7). This may be due to the Rhino model having additional geometry detail in the bulb and the stern of the hull (see figure 4.4). As the draught increases the accuracy of Model 6 and 7 is better than the one of Model 3 and 4. This may be because of the larger elements in FOS that exist in the Rhino models (see figure 4.3). Either way, both models have acceptable levels of accuracy. The same is true for the LCB calculation. For bigger draughts, models no. 5, 6, and 7, both for trim by stern and by head, estimate the LCB with almost zero error (figures 4.6 and 4.7).

The Aveva model has the highest accuracy of all the examined models, as far as the calculation of the displacement is concerned. At smaller draughts, the error for calculating the LCB is as low as  $-0.3\%$  of  $L_{pp}$ . However, for larger draughts, the error is very close to zero.

As final findings, we can say that, for these hydrostatic calculations both discretiza-



tions (Rhino and Mathematica models) were acceptable. The mesh with 2,320 elements seems to be the least exact for calculations of the displacement, but without affecting the accuracy for calculating LCB. The next most inaccurate models are those derived from the Rhino model, especially for the LCB, where it results up to 0.7 meters larger than the actual LCB, as shown in figure 4.7. However, even the values with the largest deviation are considered to have acceptable errors.

In some cases, the Aveva model (model no. 1) has some noticeable error, but this is because it may have undergone the most processing during the geometry representation process. In this process, some of its details may have been altered. In contrast, with the Aveva model, we see that the absence of some vertices from the model in Mathematica does not significantly affect the hydrodynamic calculations. In general, for displacement and LCB, the Mathematica models have very good precision, although they are lacking a little at smaller draughts.

### 4.3.2 GZ curve in calm water

Next, the ability of the code to accurately calculate the righting arm in calm water for a given loading condition will be further investigated. This comparison is necessary as the main purpose of the code in Mathematica is to calculate the righting arm. As already discussed in section 4.1, the righting arm is calculated for a specific rolling angle, with the function *Equilibrium 35*. This function is used to find the solution for the ship's position  $(\zeta, \theta)$ , so that the equilibrium of the ship in the two degrees of freedom (corresponding to heave and pitch motion) is achieved.

For the calculation of the righting arm for a specific rolling angle, the function *GzEq35*<sup>6</sup> is used. The value of the righting arm depends on time, the ship's position on the  $x$ - and  $y$ - axis (generalized ship's position), the angle of inclination, the hull geometry, and the loading condition (hence the displacement and center of gravity, vertical and longitudinal). The GZ curves generated by Mathematica code in still water should be compared with the corresponding curves generated by Aveva and those in Trim & Stability booklet. The comparison will be made under 5 main loading conditions, the characteristics of which are presented in the following table.

Table 4.2: Loading Conditions of the sample ship from the Trim & Stability Booklet

Loading Condition		15	18	27	30	36
No. of Containers	[-]	3858	3118	3889	3262	2659
tons/TEU	[t]	12 hom.	16 hom.	10 hom.	12 hom.	16 hom.
Mean Draught	[m]	12.52	12.52	11.52	11.52	11.52
Displacement	[t]	75973.8	76078.1	68322.2	68192.8	68199.1
KG (Fluid)	[m]	17.17	16.21	16.88	15.62	14.83
LCG (from AP)	[m]	115.39	114.99	121.62	116.41	123.48

The GZ curves resulting from the six different discretizations of the hull for the loading conditions are shown in figure 4.8. For most models, the GZ is calculated accurately for small inclination angles. Only the Rhino model no. 2 has in certain loading conditions

<sup>6</sup>//BuoyUp2Lite/Needs/Mathematica/BuoyUp/NDSolve4.m

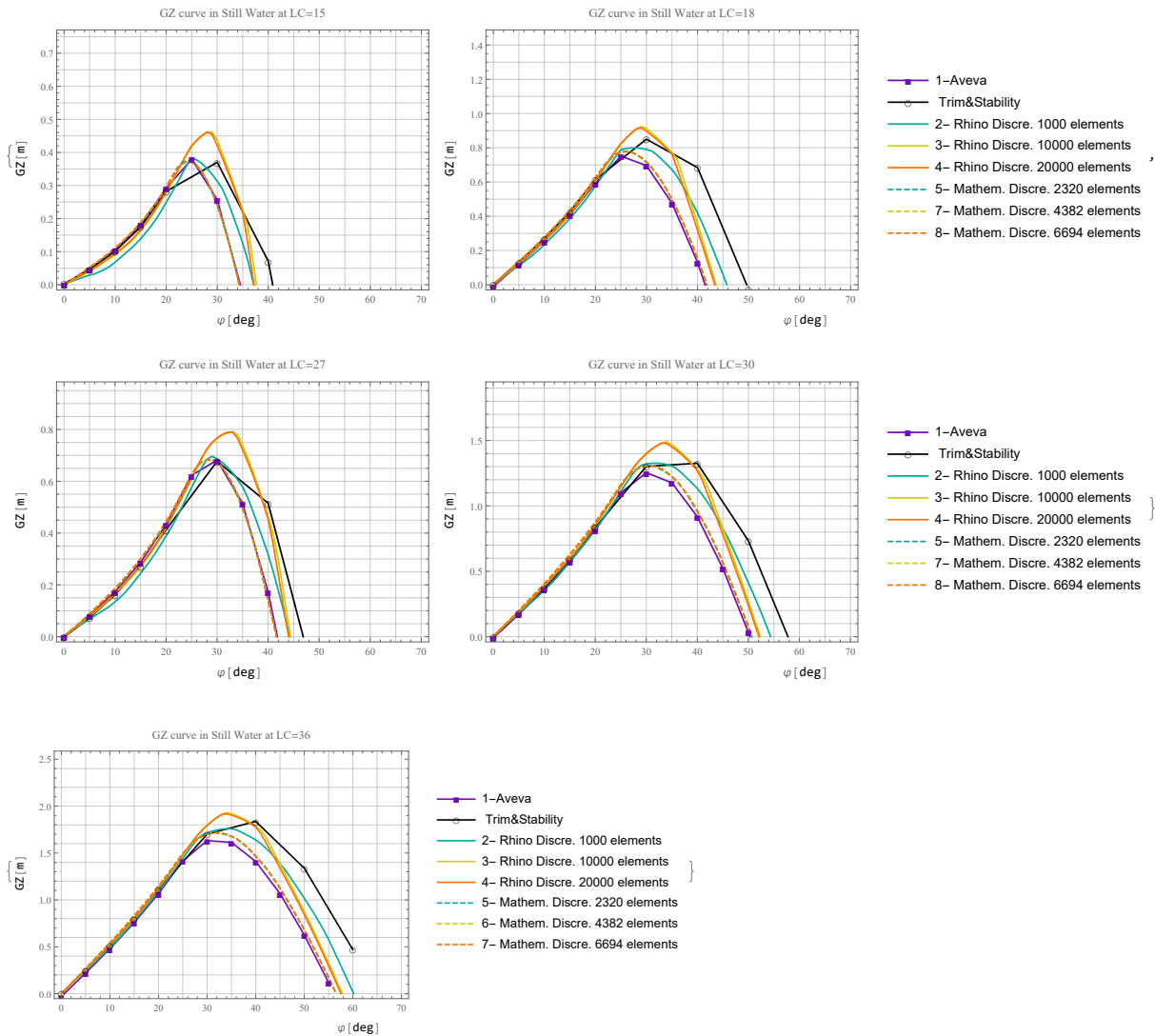


Figure 4.8: Validation with Trim & Stability data and Aveva model of GZ curve in Calm Water

a larger deviation for small angles, between the data from the Trim and Stability or the Aveva model. The other two Rhino models (models no. 3, and 4) have large deviations for bigger angles and higher inconsistencies in the calculation of maximum GZ and the capsizing angle. This could be partly due to the fact that in larger angles, the FOS gets wet and then parts of the upper deck may be immersed. Then the results may be distorted because of non-uniform discretization and the presence of large and non-uniform elements.

Because of the limited data available to produce the GZ charts from the ship's Trim and Stability, the generated curves are not smooth. But already from the few points, it is obvious that there are no obvious similarities with the other curves, for large roll angles. At this point, it should be noted that both for Aveva model and Mathematica/ Rhino models, the geometry of the bare hull has been recreated. This may be the reason why the GZ curve from the ship's Trim and Stability has a higher maximum righting arm and capsizing angle in all loading conditions. Apart from the above reason, the purpose of

this diploma thesis is not to evaluate the stability of the sample ship. Since the model in Aveva has sufficient accuracy, as already shown in figures 4.5, 4.6, and 4.7, it can be considered quite reliable.

Finally, models 5, 6, and 7, are the ones that calculate the GZ curve most accurately. In some loading conditions (LC 15, and 27) the calculated curve, falls exactly on the points of the Aveva. Moreover, the capsizing angle is predicted exactly in every case, and the position and value of the maximum righting arm are computed with acceptable accuracy.

At this stage, by examining the diagrams 4.8, it is interesting to observe how the loading condition affects the intact stability of the ship. As shown in table 4.2, depending on the number of containers loaded, and the weight of each one, the  $\overline{KG}$  decreases or increases accordingly. It seems that the loading conditions, where the  $\overline{KG}$  is higher, are less stable. Conversely, stability increases (both the maximum  $GM$  and capsizing angle have a higher value). This is consistent with the formula (3.1.10), as the  $\overline{KG}$  fluctuates, the metacentric height of the ship changes. For a constant displacement obviously, there are other factors affecting stability, such as the change in the waterline, the moment of inertia of the waterplane  $I_T$  or the  $\overline{KB}$ , but the effect of  $\overline{KG}$  is more pronounced here.

### 4.3.3 GZ curve in sinusoidal longitudinal wave

At this stage, the Aveva model is considered rather accurate. Further verification was made, using Aveva Hydrostatics and Hydrodynamics, to calculate the ship's GZ curve in a cosine longitudinal wave. Since there are no data for waves in the Trim and Stability Booklet, the Aveva model is used to check the accuracy of the calculations performed by the Mathematica code.

From Aveva the values of the GZ curves for the different Loading Conditions were calculated as shown in the table 4.2. Aveva can calculate the Intact Stability of the ship in a cosine wave, by entering the appropriate parameters. The wave was chosen to have wavelength equal to the ship's  $L_{pp}$ ,  $(\lambda/L_{pp})=1$ . Each time, calculations are made to shift the wave by  $\lambda/8$ , so that after 8 translations, the wave has traveled a distance equal to one wavelength. The reference point was chosen to be located at the ship's amidships, i.e. for Aveva, the parameter "Pivot Point" (P.P.) took the value  $L_{pp}/2 = 238.35/2 = 119.175 m$ . Therefore the distance of the wave crest from this reference point was shifted accordingly each time.

For the computations with the Mathematica code the only parameter that needed to be modified, was the formula for the description of the free surface elevation. Since the wave is a cosine wave, the free surface relation was expressed by the equation (3.3.3). In Mathematica, the change of the wave's position was done by changing its phase,  $\epsilon$ , from 0 to  $2\pi$  in steps of  $\pi/4$ . Therefore the wave equation was appropriately modified as below.

$$\eta_w(x, t) = a \cos(kx - \omega t + \epsilon) = a \sin(kx - \sqrt{k} g t + \epsilon) \quad (4.3.3)$$

In this application, the wave amplitude  $a$  is chosen to be equal to  $3 m$  and the wave direction angle is zero. The wavenumber  $k$  is defined as,  $k = 2\pi/L_{pp}$ .

As the wave was located in different positions, the GZ curve of the ship was calculated. The parameters of the wave, used for the Aveva to determine its position in each case are given in the table below.

Table 4.3: Parameters for the ship's position in wave for calculation of Gz curve

Wave phase		0	$\pi/4$	$\pi/2$	$3\pi/4$	$\pi$	$5\pi/4$	$3\pi/2$	$7\pi/4$
Wavelength	[m]	238.35	238.35	238.35	238.35	238.35	238.35	238.35	238.35
Height	[m]	6	6	6	6	6	6	6	6
Crest	[m]	0	-29.79	-59.59	-89.38	119.175	89.38	59.59	29.79
position from P.P.									
Dir. angle to C.L.	[deg]	0	0	0	0	0	0	0	0

The figures 4.9 show the representation of the free surface elevation and the ship for some of the phase  $\epsilon$  of the wave, according to relation (4.3.3). In 4.9c the wave trough is located amidship, so the restoring ability of the ship is better than when the wave crest is located amidship. In this condition, the restoring ability drastically decreases, as shown in 4.10.

Correspondingly, figure 4.10 shows the GZ curve as calculated for the 6 different hull discretizations, compared to the corresponding curve obtained from Aveva. As the wave passes through the ship, its equilibrium changes (in the 2 DOF, heave, and pitch motion). Therefore the ship for each differing rolling angle will have a different value of the righting arm. In this figure, the variance of GZ is presented only for LC 18. The rest diagrams, for LC 15, 27, 30, and 36, are shown in Appendix A.

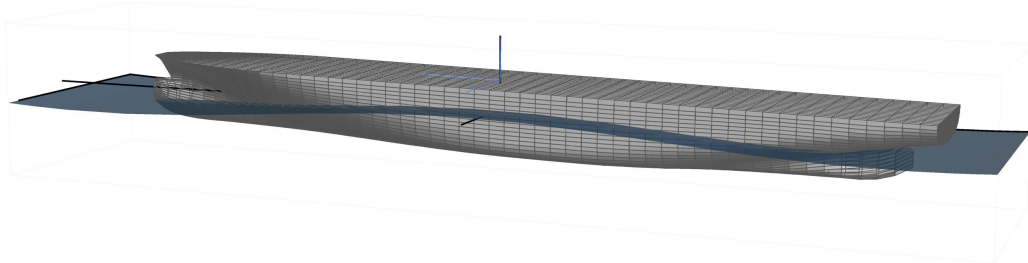
Looking at the graphs, it is clear that the Mathematica discretizations (models 5, 6, and 7) are in perfect agreement with the results obtained by Aveva. The same is true for the other loading conditions (see Appendix A). The models from Rhino, fail to calculate the righting arm, especially at larger roll angles. As already mentioned, due to the non-structural shape of the deck elements, the centroids are not evenly distributed over the entire deck surface. This provides incorrect information during calculations, as the program does not find a deck element submerged, even though in reality the edge of the deck may be immersed. This leads to the impression that the capsizing angle is larger or that the ship has in general a higher restoring ability.

In conclusion, this chapter has presented the way of developing the code for calculating the hydrostatic values and consequently the ship's equilibrium in the three degrees of freedom (regarding heave, roll, and pitch motion). Also by using the code, the righting arm is calculated at each position, time, and rolling angle of the ship. For the correct calculation of the required values, the appropriate geometry of the ship had to be used, creating a mesh with the adequate discretization and number of elements. For this reason, two different models were made, each with three different number of elements.

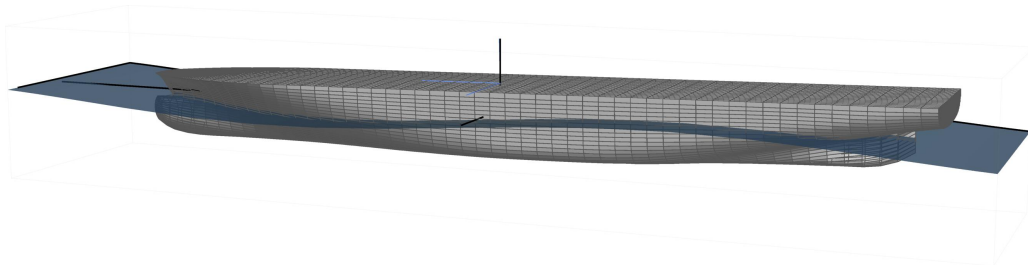
The hydrostatic values calculated by Mathematica were checked with Aveva's model and the ship's Trim & Stability Booklet, for each discretization (section 4.3.1). Further verification was also done for the GZ curves in still water (section 4.3.2) and in regular wave (section 4.3.3) for some typical loading conditions.

The comparisons show that the more structured discretization was quite accurate even for model no. 5, which has fewer elements. Model no. 5 had larger deviations for LCB and displacement calculations, while it was accurate on the computation of the GZ curve.

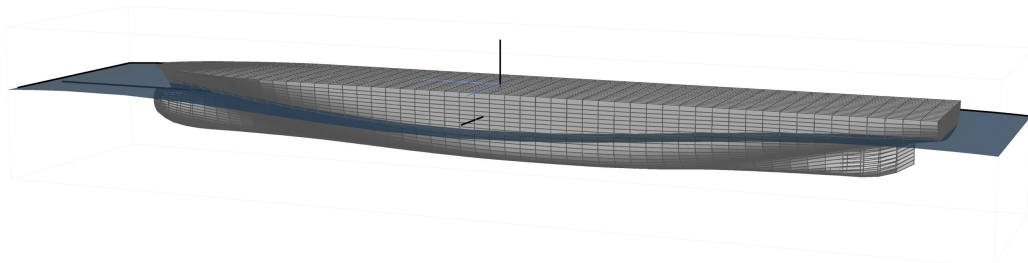
Models 6, and 7, have very close results to each other in all comparisons, with very satisfactory accuracy. For this reason, from now on, either model 6 or 7 are the options for the discretization of the hull, as far as the calculations are concerned.



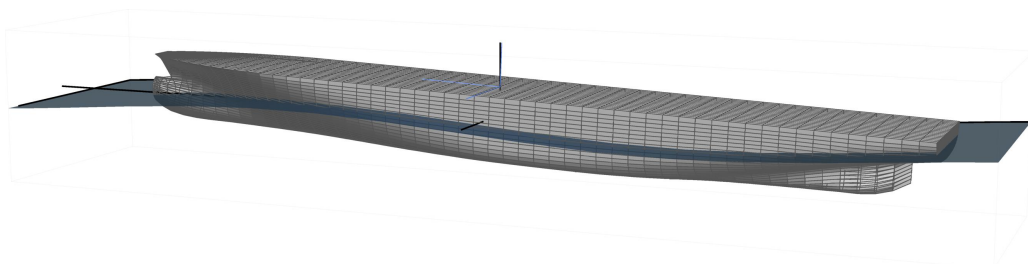
(a) Wave phase  $\epsilon = 0\pi$ ,  
or else with 0 m crest distance from Pivot Point



(b) Wave phase  $\epsilon = 0.5\pi$ ,  
or else with -59.59 m crest distance from Pivot Point



(c) Wave phase  $\epsilon = 1\pi$ ,  
or else with 119.175 m crest distance from Pivot Point



(d) Wave phase  $\epsilon = 1.5\pi$   
, or else with 59.59 m crest distance from Pivot Point

Figure 4.9: Positioning of a ship on a regular wave  
Model no. 6 with 4,382 element, positioned at different time instants by changing the wave phase

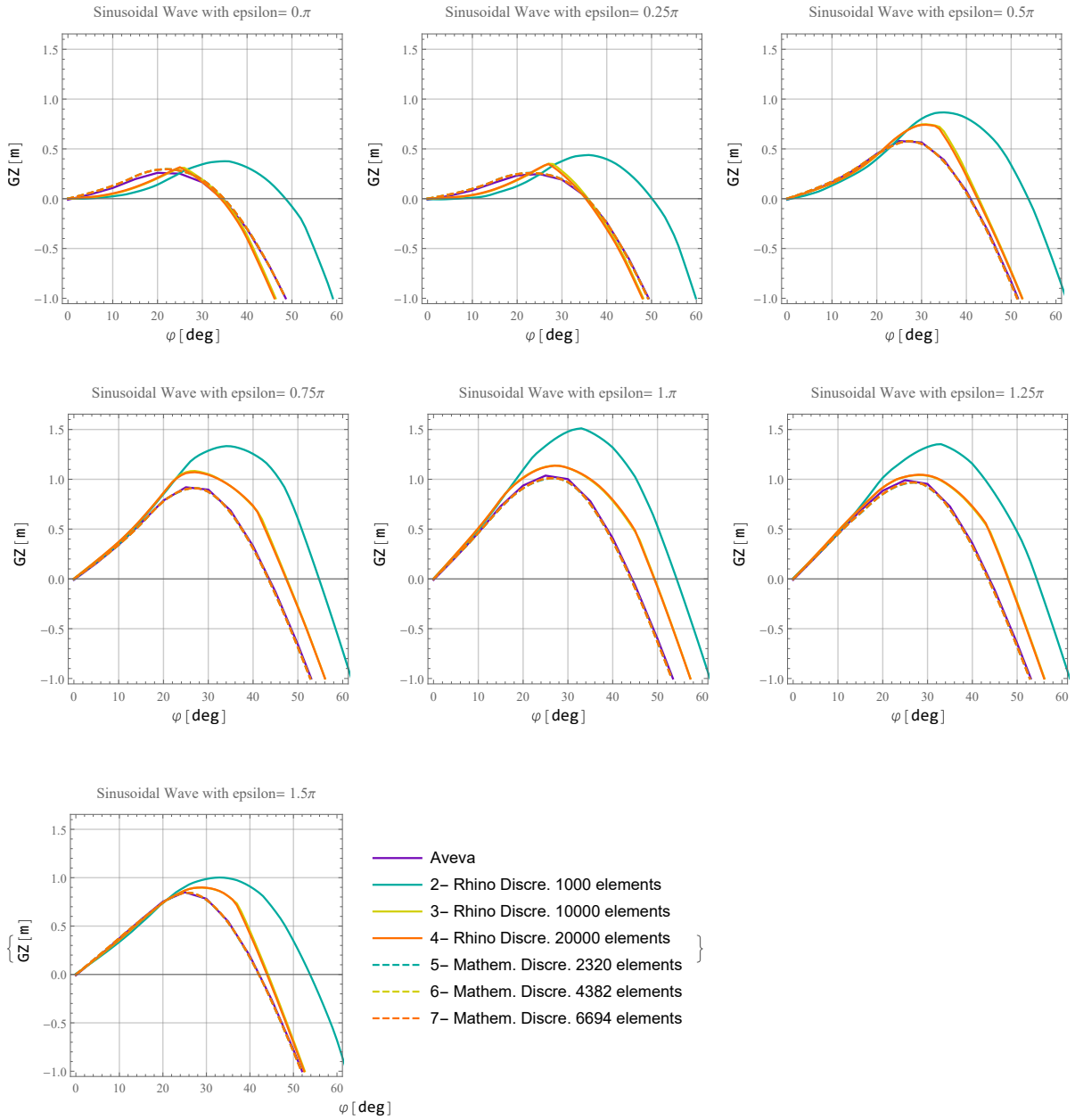


Figure 4.10: Validation with Aveva model of GZ curve in sinusoidal Wave for LC 18

# Chapter 5

## Differential Equation Model

In this chapter the form of the differential equation is presented. The model used, is a pseudo-static model which uses the equilibrium in two degrees of freedom, to calculate the righting arm in every time instant, during the solving of the rolling differential equation. Section 5.1 explains the assumptions made in the model and how it differs from the Mathiue's model. Then the terms of the differential are presented and how they are approximated. Next, in section 5.2, the application of the model for regular waves is presented. Runs for selected case studies were conducted. One of them is identical to the case study chosen by Ms. Dousia [26] to produce one of the stability chart in her diploma thesis. Finally, two stability diagrams will be presented, obtained after the simulations for specific cases.

### 5.1 Differential Roll Equation in Longitudinal waves

Ship motions are described as an object with respect to six degrees of freedom in translation and rotation as shown in figure 4.1. As already stated, the translation motions include surge, sway and heave and the rotation movements include roll (heel), pitch (trim) and yaw. In the actual operation condition, ship motions have a complicated relationship.

However, ship motions can be split into two categories. The first category consists of pitch, heave and roll influenced by sea waves and the second category consists of surge, sway and yaw produced mainly by propeller force, rudder, current and wind [53]. In this section, the method for finding the roll resonance and building the differential equation for longitudinal waves will be introduced.

The procedure for calculating the ship's roll response is based on modelling the roll motion dynamically using a single degree of freedom. At the same time, the coupling with heave and pitch motion is taken into account by means of hydrostatic calculations without considering dynamic effects. So the model developed is not one of 3DOF, but is pseudo-static, as far as the approximation of the righting arm is concerned.

In the general differential equation, developed in section 3.2.2, the righting arm is a function of time, position of the ship, and the inclination angle. In order to accurately describe the shape of the GZ curve, it is common use for the curve to be approximated as a polynomial power series with odd powers. As a result, the differential equation describing the rolling motion in longitudinal waves becomes non-linear (equation 3.2.8).



It is common practice, to assume a linear relation of the restoring term and the rolling angle. Further for regular waves, the GM varies approximately sinusoidally between two extreme values. This consideration leads to the the well-known Mathieu's equation (3.2.11), which is implemented in many occasions as an attempt to simplify the procedure of the GZ-curve calculation.

In this analysis, however, the pseudo-static model is used instead of the linear Mathieu's model. In this way we can transition from the linear to the non-linear model and compare the results between these two methods of calculating the ship's roll resonance. Afterwards, once the model for solving the differential equation is developed, the modelling of the irregular longitudinal waves can be included (see Chapter 6).

For calculating the ship's roll resonance, all the terms of the equations (3.2.8) need to be calculated. These terms are, the damping term, the natural roll frequency and the transverse moment of inertia. Considering that the ship has a constant forward speed, the value of  $\overline{GZ}$  needs to be computed by taking into account the relative position of the ship and the wave, as the ship moves forward.

### 5.1.1 Damping term

While describing the equation of roll motion there are many ways for the damping term to be expressed. To capture the nonlinear behavior of roll damping, higher order equations are used. Often a equivalent damping coefficient can be computed, in order to compare these models to linear damping coefficients. By calculating an equivalent damping coefficient, a linearized damping term is obtained.

However, for the present application the damping term of the differential rolling equation is chosen to be linear rather than linearized, thus having a linear relationship with the angular velocity. In addition,  $\zeta$  is the damping ratio's value and is obtained from the differential analysis as introduced in chapter 3.2.2. It usually takes values between 0.05 and 0.2.

### 5.1.2 Natural roll frequency and transverse moment of inertia

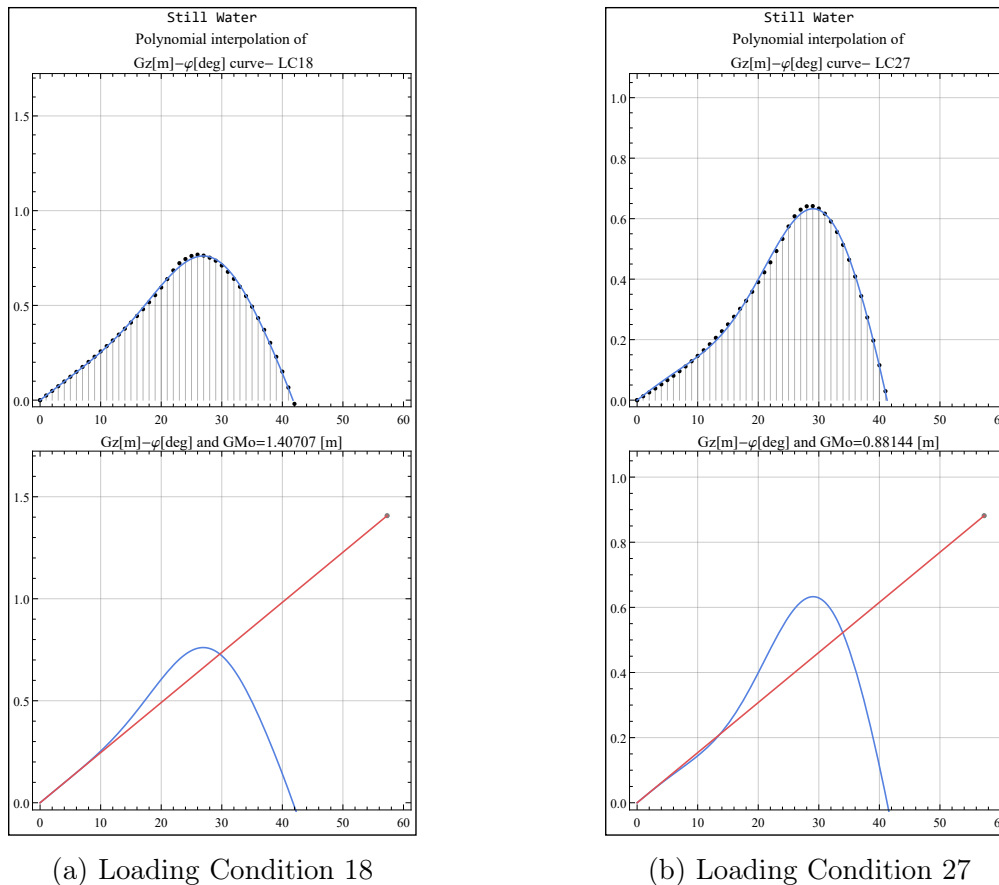
The natural rolling frequency is given by the formula (3.2.6). The main difficulty of this formula, is the evaluation of the moment of inertia that includes the mass moment of inertia and the added hydrodynamic moment of inertia due to the acceleration of the fluid by the oscillating ship. For this application the added moment of inertia is considered approximately constant with frequency and, therefore the total inertia is constant. The natural frequency of the ship, mainly depends on the loading condition and the distribution of the weight on the ship. Since no information is provided on the transverse moment of inertia or the natural rolling period of the ship, the approximate method, provided by the IMO is used [12]. According to the IMO, when the period of rolling motion cannot be measured, the following approach is indicated to be used.

$$T_0 = \frac{2CB}{\sqrt{GM_0}} \quad (5.1.1)$$

The coefficient  $C$  can be calculated as

$$C = 0.373 + 0.023 \frac{B}{T} - 0.043 \frac{L}{100} \quad (5.1.2)$$



Figure 5.1: Polynomial fitting of data for approximation of  $GM_0$ 

where  $B$ ,  $T$ , and  $L$  are the breadth, the mean draft, and the length of the ship at the waterline respectively.

The  $GM_0$ , is the initial metacentric height in still water and refers to a specific loading condition. It can be calculated by computing the gradient of the righting arm  $GZ(\phi)$  curve for inclination angle  $\phi = 0$ . The data for the production of the GZ curve in still water, can be calculated the same way as in chapter 4.3.2. Further, the function of the curve can be found by fitting the points to a eleventh-order polynomial power series [41], with the following form.

$$GZ(\phi) = C_1 \phi^1 + C_3 \phi^3 + C_5 \phi^5 + C_7 \phi^7 + C_9 \phi^9 + C_{11} \phi^{11} \quad (5.1.3)$$

After finding the function of the GZ curve, the value of the initial metacentric height is approximated by relation (3.1.13). Applying this procedure for the different loading conditions, the values of the natural rolling period, are obtained. It should be noted that these values may differ from the corresponding values listed in the ship's Trim & Stability Booklet. However, as it is already discussed in Chapter 4, the validity of the code is now taken for granted. The code calculates the righting arm with reasonable accuracy, with the introduction of the appropriate discretized hull. The results of the above process are shown in figure 5.1, for the loading conditions 18 and 27.

Once the natural period  $T_0$ , and therefore the frequency  $\omega_0$ , has been calculated, an approximation of transverse moment of inertia can be made from relation 3.2.6 for every

given loading condition.

### 5.1.3 Righting arm

The calculation of the GZ is the most important factor, and the main focus of this diploma thesis. The righting arm at any given time depends on the position of the ship and the angle of the intersection. As described in the previous chapter (section 4.1: [Calculation of Hydrostatic equilibrium in Mathematica](#)), for a certain rolling angle, the function *Equilibrium 35* is used, for the solution of the ship's position  $(\zeta, \theta)$  to be found. After knowing the position vector  $(r_s^e, q_s^e)$ , but with the equilibrium being applied only in the direction of the heave and pitch motion, the righting arm for the specific ship position can be computed. The sea state is entered into the program through the elevation of the free surface<sup>1</sup>, and the equilibrium of the two degrees of freedom (by heave and pitch motion) is calculated accordingly. The righting arm used is the one that results from equilibrium and is not approximated in a linear way (Mathieu's model) or by a higher degree polynomial function. For this reason the equilibrium is described as pseudo-static.

Three ways were studied, in which the GZ curve could be introduced into the program in the differential equation, to find the ship's roll resonance (see Appendix B.1). After experimenting with these methods, trying to find which one is the most suitable and the most time efficient, the model finally used is that of the equation (5.1.4). A function was created for this purpose<sup>2</sup>, which directly calculates the righting arm. This function uses as input the inclination angle and the absolute time of the simulation. In addition, the position of the ship is indirectly entered into the equation through the ship's speed, if any. This function is introduced directly into the differential function. So, the rolling angle satisfying the system, is approximated with the appropriate iterations (as an internal process of the differential solver). The differential is solved directly for all simulation time, with the time step either selected by the solver automatically or manually set by the user. The differential equation, in the program, has the following form, which is the closest to the form introduced in chapter 3.2.2.

$$\ddot{\phi} + 2\zeta \omega_0 \dot{\phi} + \frac{m g \overline{GZ}(x, t, \phi)}{I_x} = 0 \quad (5.1.4)$$

The approach is considered more accurate, because the function of GZ calculation is imbedded directly into the differential equation. As a result, after some iterations the angle, thus the response of the ship in roll motion, that satisfies all the equations, is approximated. For each instant, the response angle is found to satisfy the system.

### 5.1.4 Numerical Integration of the Roll equation

The above form of the differential equation is solved in Mathematica, with the *NDSolve* numerical solver<sup>3</sup>. The above differential equation, can be solved by numerical solvers, as they are no exact analytical solutions. *NDSolve* is a default Mathematica function,

<sup>1</sup>//BuoyUp2Lite/Needs/Mathematica/BuoyUp/FreeSurface.m

<sup>2</sup>//BuoyUp2Lite/Needs/Mathematica/BuoyUp/NDSolve4.m

<sup>3</sup>//BuoyUp2Lite/Needs/Mathematica/BuoyUp/NDSolve4.m

which adapts its step size so that the estimated error in the solution is just within the tolerances specified by `PrecisionGoal` and `AccuracyGoal`<sup>4</sup>. *NDSolve* typically solves differential equations by going through several different stages, depending on the type of equations. With the option `Method`, each stage is handled by the chosen method. The actual stages used and their order are determined by *NDSolve*, based on the problem to solve.

Originally the default form of *NDSolve* was used. However, later (see Chapter 6), when the information about the free surface of irregular wave was introduced during the solution of the differential equation, the times became prohibitive for the solution of each case. For this reason the functions for the hydrostatic calculations were rewritten in C/C++ programming language by Doctoral Candidate Ioannis Kontolefas. The interaction of C/C++ with the Wolfram Language is enabled through the Wolfram Symbolic Transfer Protocol (WSTP). In addition to the introduction of functions in C++, in order to speed up the hydrostatic calculations, another solver was implemented for the numerical integration of the rolling equation (WSTP-RK4<sup>5</sup>). With this solver, not only are the equations for hydrostatic calculations from C++ used, but it further uses "*ExplicitRungeKutta*" as the method of solving the equation. That means it is a solver using explicit Runge-Kutta methods of 4th degree. Also the option "*StartingStepSize*" is used, that specifies the initial step size used in trying to generate results.

With this addition the computing time has been reduced considerably. These functions, further developed at this stage, were then used to numerically solve the differential equation in Chapter 6. The numerical stability of the differential and the numerical part in general, are not directly related to the aim of the diploma thesis, as the physical problem is studied. Inevitably, attention had to be paid to this point as well, in order to reduce the computation times. The Appendix B.2 shows some calculations and comparisons between the ship's responses by using the default numerical solver and the *WSTP-RK4* with different initial solving steps, to confirm the accuracy of the solver.

Referring to the diagrams in Appendix B.2, we conclude that solver *WSTP-RK4* does not perform worse than the Default solver. On the contrary, the computation time, with starting time step equal to 2 sec, is reduced by a factor of 20. The results of all the cases are identical to each other most of the time. The only scenarios in which this is not the case is when the ship has large response angles (30 degrees and above). In these cases, some solvers predict capsizing and others do not. Of course, in a real case the ship would have capsized, either way. Therefore, all these cases will be considered later as capsizing cases, so the use of the *WSTP-RK4* solver will not change the results.

## 5.2 Application of developed model in Regular Waves

In this section, the practices mentioned in 5.1 are applied. The differential equation of roll is solved for regular following waves, for a chosen time span. Several simulations are conducted, for the Stability Chart to be produced. In 5.2.1 the parameters chosen to generate the two stability diagrams will be presented. The first one has parameters as identical as possible to the one generated by Ms. Dousia, in her diploma thesis. For the

---

<sup>4</sup>In this application the `PrecisionGoal` and `AccuracyGoal` are set equal to six.

<sup>5</sup>//BuoyUp2Lite/Needs/Mathematica/BuoyUp/NDSolve4.m

second chart, the parameters are for the same loading condition, but a different sea state. In section 5.2.2, the two diagrams, are presented, together with some conclusions drawn from them.

### 5.2.1 Parameters for the Stability charts

For the production of the stability charts in regular waves, the proper conditions and parameters should be defined. If possible, these parameters were chosen the same as those used by Dousia, to produce the corresponding charts. Some of the main parameters that affect the ship's response are the loading condition, the damping ratio, the initial conditions of the differential equation, as well as the wave steepness and encounter frequency.

The stability chart for parametric roll resonance corresponds to a specific wavelength  $\lambda$ . From the wavelength, the wavenumber  $k$ , and the wave frequency  $\omega_w$ , can be calculated. In order to produce the data of the diagram, we need to make the simulations for a range of the ratio  $a = \frac{4\omega_0^2}{\omega_e^2}$  and wave steepness  $H/\lambda$ . The ratio  $a$  is commonly used because, according to Mathieu's equation solutions, there is an unstable behavior when this ratio is appropriately 1 (principle resonance), 4 (fundamental resonance), and so on according to equation (3.2.12).

The wave encounter frequency depends on three factors; the speed of the ship, the radial wave frequency, and the direction of the wave. The wave encounter frequency is defined as follows.

$$\omega_e = \omega_w - k V_s \cos(\mu) = \omega_w - \frac{\omega_w^2}{g} V_s \cos(\mu) \quad (5.2.1)$$

, where  $\omega_w$  refers to the wave's radial frequency,  $V_s$  is the constant speed of the ship, and  $\mu$  is the encounter angle between the wave and the ship. Therefore, as long as it concerns longitudinal waves along with the ship, the angle  $\mu$  takes the following values.

- $\mu = 0 \text{ deg}$ : for following waves, i.e. the waves and the ship travel in the same direction.
- $\mu = 180 \text{ deg}$ : for head waves, i.e. the waves and the ship travel in the opposite direction.

From the above equation for the calculation of the encounter frequency, it is safe to say that the encounter frequency ( $\omega_e$ ) is greater than the wave frequency ( $\omega_w$ ) in head seas. In addition, the opposite applies for the following seas, as the encounter frequency is less than the wave frequency. In this study, it is avoided to use the developed model for head seas. The model is pseudo-static, so as the head seas have a big radial encounter frequency (thus low encounter period), it is uncertain whether the model works properly, as the changes are more rapid.

For the simulations, loading condition 18 was chosen, which is one of the cases considered by Dousia, in her work. It is a loading condition with relatively moderate stability. The characteristics resulting from this condition are shown in Table 5.1. Some other characteristics, such as parameters for the differential equation and wave characteristics, are also presented in the same table.

Table 5.1: Data necessary to derive the Stability Chart for two types of regular following waves for LC 18

Characteristics of loading condition		
Displacement	[tons]	76078.1
Mean Draught	[m]	12.52
KG	[m]	16.21
LCG form AP	[m]	114.99
Initial conditions of the differential equation		
$\phi(0)$	[rad]	$\pi/180$
$\dot{\phi}(0)$	[rad/sec]	0
Parameters used in the differential equation		
Damping ration $\zeta$	-	0.05
$I_x$	[tons m <sup>2</sup> ]	$1.20899 \cdot 10^7$
$GM_0$	[m]	1.40707
$T_0$	[sec]	21.3227
Simulation time	[sec]	600
Wave Characteristics		
Type of wave		A B
Range of height $H = 2a$	[m]	[0.5 ÷ 15] [0.5 ÷ 9]
Wave length	[m]	$1.25 L_{oa} = 312.5$ 188.85
Wavenumber k	[1/m]	0.020106 0.03327
Wave Period	[sec]	14.1513 11
Wave direction	[deg]	0 0
Stability Chart Plot Range Data		
Ratio $a$	-	[2.17 ÷ 5.77] [1.4 ÷ 5.9]
Range of wave steepness	-	[0.0016 ÷ 0.05] [0.00265 ÷ 0.04766]

The wave characteristics were entered as data for the Mathematica function<sup>6</sup> to calculate the free surface elevation at each location. The form of the free surface elevation was described by equation (3.3.3). Also, the drift of the ship on the longitudinal axis was taken into consideration, due to the fact that the ship travels some distance in a given time due to its forward speed.

A range of ship's speeds was also chosen so that the calculations can be done for a specific encounter frequency, hence a ratio  $a = \frac{4\omega_0^2}{\omega_e^2}$ . Therefore, in this set of simulations, the speed of the ship changes and not the wave frequency, which is constant because we consider a constant wavelength (or equivalent constant wave period). With constant wave frequency equal to  $\omega_w = \sqrt{kg}$ , the corresponding range of speeds of the ship is approximately:

$$V_s = 4.273 \div 19.205 [knots]$$

For the production of the diagrams in regular waves, two sea states were chosen. The first is the same as the one chosen by Dousia, in her diploma thesis (Type wave A). The second one was selected as one of the possible sea state from a scatter diagram of North Atlantic operation (Type wave B) as shown in figure 6.1.

For this set of simulations, the form of differential equation introduced in Chapter 5.1 was used, with the parameters described in table 5.1. The simulations were performed in 600 seconds in total. From these, the roll response for the first 100 seconds, were not taken into account, as it is considered to fall under the transient effect. Therefore for each pair of data ( $a, H/\lambda$ ) the maximum response observed after 100 seconds is captured. The maximums for each data pair are finally plotted in a Contour Plot creating the Stability Chart.

## 5.2.2 Stability Charts

The characteristics of the Stability Charts generated for regular following waves as shown in Table 5.1. In diagram 5.2, it is obvious that parametric roll appears with fundamental resonance. The minimum required value of wave height is at  $H/\lambda = 0.02 \Rightarrow H = 6.25 [m]$ .

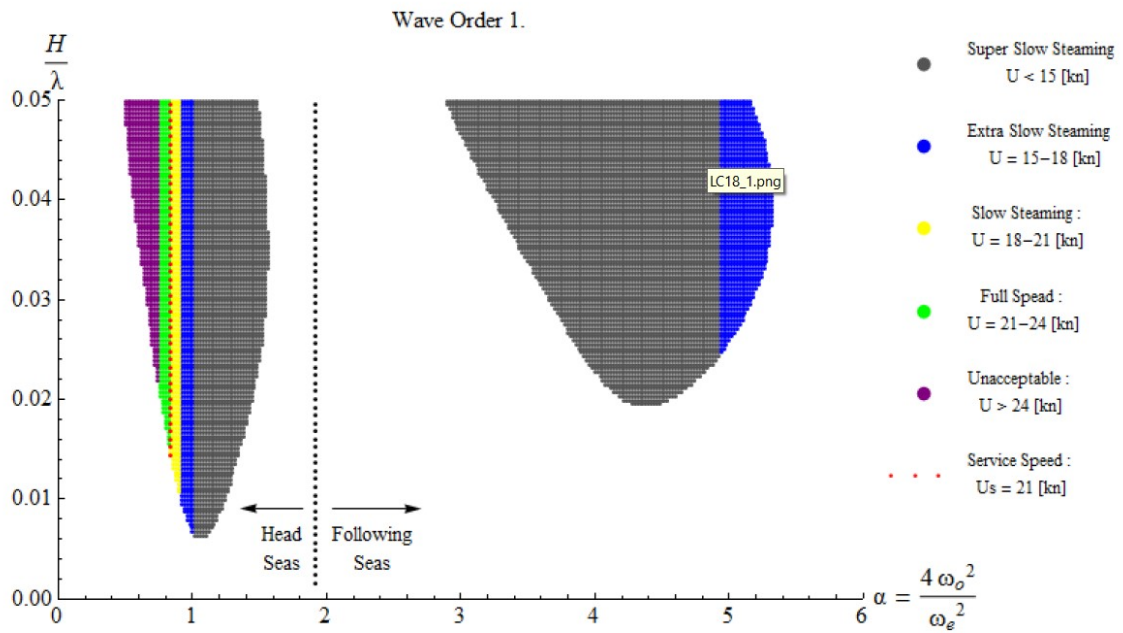
The minimum height, where parametric roll occurs, is the same as that shown in diagram 5.2a with the calculations done by Dousia. However the ratio  $a$  in figure 5.2b, which corresponds to the minimum wave steepness, is slightly smaller than in figure 5.2a (4.14 and 4.4 respectively). Apart from that, the charts seem to have the same form. The shape is also expected and is relatively similar to the one presented in the literature.

Parametric instability initially occurs for  $H/\lambda = 0.02$ , with a maximum response angle of 5 or 10 degrees. However as the wave steepness increases the response angle also increases rapidly. This effect is most pronounced on the left side of the instability region, i.e. for ratio  $a$  in the range of 3.4 to 3.9. This region starts at  $H/\lambda = 0.025 \Rightarrow H = 7.81m$  and spreads gradually, so that, at higher amplitudes there are intense responses everywhere.

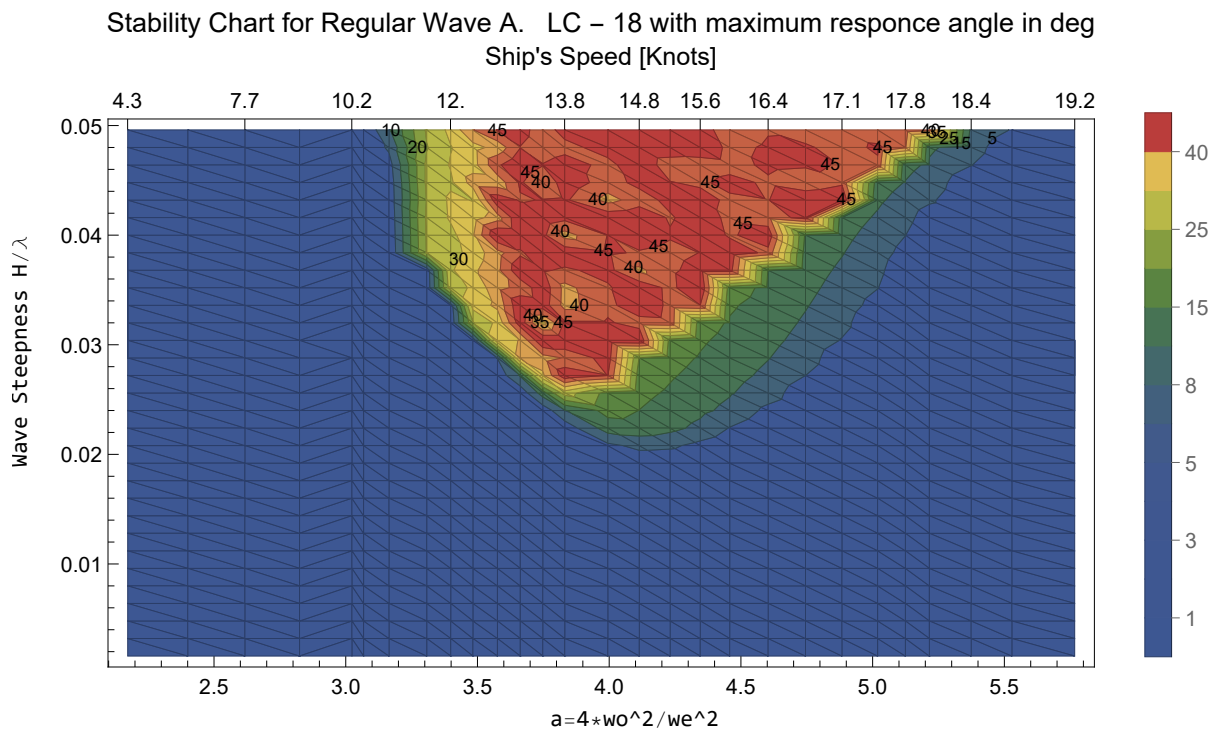
The ship's speed corresponding to the cases with instability have a range between 12 and 17 knots. These speeds are representative of the ship in case it is traveling with Slow Steaming.

---

<sup>6</sup>//BuoyUp2Lite/Needs/Mathematica/BuoyUp/FreeSurface.m



(a) Dousia's stability chart [26]



(b) Stability Chart with data produced by the model developed in this diploma thesis

Figure 5.2: Comparison of Stability Charts for regular following wave (Type A) for LC -18

The cases have constant wave period with wavelength equal to  $1.25 L_{oa}$ , but with various ship's forward speed



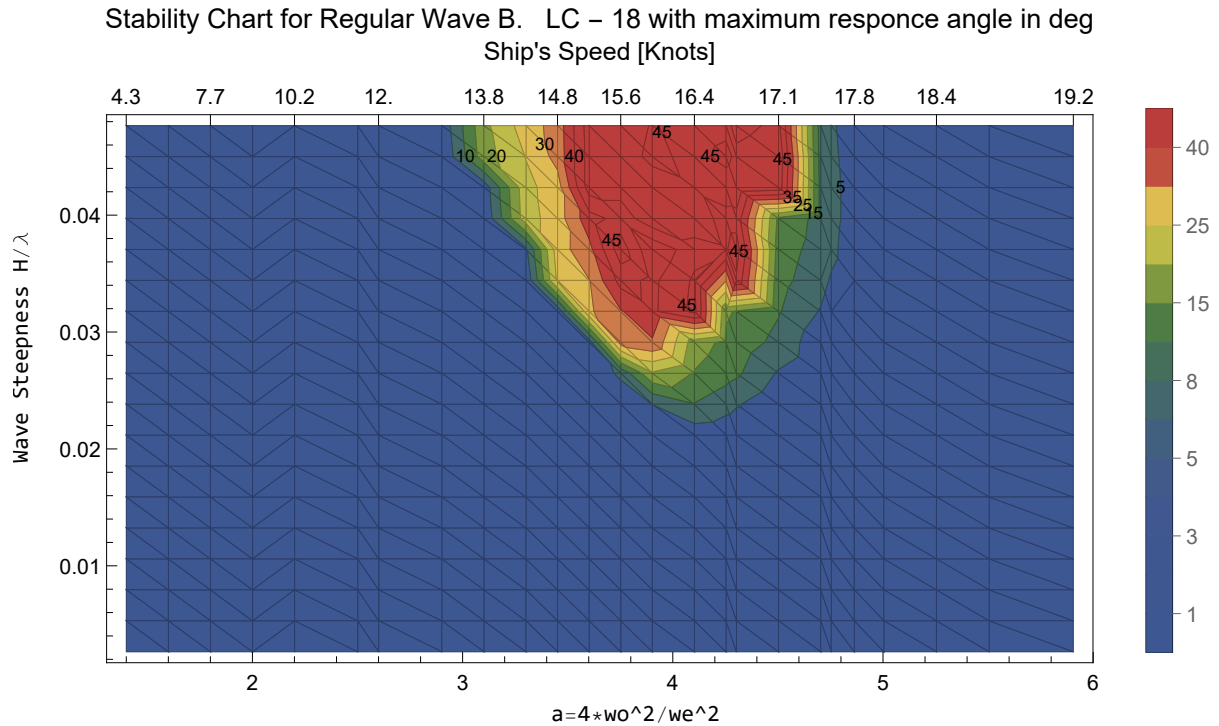


Figure 5.3: Stability Chart for regular following wave (Type B) for LC-18

In the diagram 5.3, the instability region appears close to  $a = 4$  again, although it is more restricted than the instability region in figure 5.2. The minimum required value of wave height is for  $H/\lambda = 0.02 \Rightarrow H = 3.7 \text{ m}$ , which corresponds to  $a = 4.1$ , thus a ship speed of about 16.4 knots. Again we can see that very quickly for  $H/\lambda > 0.028$ , the maximum responses of the ship take large values, dangerous to capsize the ship.



# Chapter 6

## Modelling Irregular waves

This chapter describes how random waves are modeled. In section 6.1, the logic behind the choice of the spectrum and its characteristics are explained. In addition, the way in which, the elevation of the free surface is constructed from the spectrum, is described. Finally, in section 6.2, the parameters to be used and the assumptions to be made for the construction of the stability charts for the random waves are presented.

### 6.1 Spectrum Characteristics and Discretization

The study conducted in this diploma thesis examines the ship's response to irregular waves. The analysis refers to unidirectional random waves, which result from a sum of regular partial waves. The free surface elevation for a specific time instant and longitudinal position is calculated with the use of the equation (3.3.9) introduced in Chapter 3 : [Irregular Waves](#).

Each term of the sum is described as a regular wave with a defined amplitude, and wave frequency (or else wavenumber  $k$ ). Every sum component has a different wave phase, thus is shifted accordingly, and this leads to a waveform as shown in the figure 3.10b. The phases for the components are chosen randomly and have the characteristics described in section [Irregular Waves](#) of Chapter 3. A specific sea state is represented by a wave spectrum and its characteristics. Each wavelet has a certain frequency, corresponding to a wave amplitude, thus transferring particular energy. This connection between wave frequency and amplitude is given by the formula (3.3.7). Therefore, the type of spectrum and its discretization (i.e. the number of sum terms that need to be used), should be determined to describe the free surface of the irregular waves.

The following applies to parametric instability as far as the sea state is concerned [42]:

1. Swells are the most dangerous waves for parametric roll.
2. Wind-generated waves are less dangerous than swells but can become equally dangerous if the ship's encounter period acquires values that create instability relative to the ship's own period.

In this study, the JONSWAP spectrum is chosen to be used. The JONSWAP spectrum was established during a joint research project, the "JOint North Sea WAve Project".

This spectrum model was proposed to describe deployed spectra, representing the development of wave energy as a result of the force of the wind. During wave development there is a high concentration of energy around the dominant frequency, resulting in a narrower spectrum than the Pierson-Moskowitz (PM) spectrum. Thus it is a peak-enhanced Pierson-Moskowitz spectrum with the following form

$$S_{\eta_w}(\omega) = (1 - 0.287 \ln(\gamma)) \frac{5}{16} H_s^2 \frac{\omega_p^4}{\omega^4} \exp\left(-\frac{5}{4} \left(\frac{\omega_p}{\omega}\right)^4\right) \gamma^{\exp(-0.5 \left(\frac{\omega - \omega_p}{\sigma \omega_p}\right)^2)} \quad (6.1.1)$$

where  $\sigma = \begin{cases} \sigma_a & , \omega \leq \omega_p \\ \sigma_b & , \omega > \omega_p \end{cases}$  are the sigma parameters which are a relative measure of the width of the spectrum's peak. The typical values for these parameters (especially for the North Atlantic) are  $\sigma_a = 0.07$ , and  $\sigma_b = 0.09$  [54].

The peak enhancement factor (gamma) is representing the ratio of the maximum spectral density to that of the corresponding Pierson-Moskowitz spectrum. It is usually regarded to have an upper limit of about 7 and a lower limit of 1 [55]. Average values for the Jonswap experimental data are  $\gamma = 3.3$ . For  $\gamma = 1$ , the Jonswap wave spectrum reduces to the PM wave spectrum [56]. Thus, the average value given above for these parameters are used for the present study.

For the values of the peak period and the significant wave height for each sea state, the North Atlantic scatter diagram is used [56]. A scatter diagram defines the probability of occurrence of the different sea states. Each sea state is defined by the significant wave height,  $H_s$ , in m, and the zero up-crossing period,  $T_z$  (or peak period  $T_p$ ) in sec. The North Atlantic scatter diagram is shown in figure 6.1.

$T_p$ (s)	3.5	4.5	5.5	6.5	7.5	8.5	9.5	10.5	11.5	12.5	13.5	14.5	15.5	16.5	17.5	18.5	Sum
$H_s$ (m)																	
0.5	1.3	133.7	865.6	1186.0	634.2	186.3	36.9	5.6	0.7	0.1	0.0	0.0	0.0	0.0	0.0	0.0	3050
1.5	0.0	29.3	986.0	4976.0	7738.0	5569.7	2375.7	703.5	160.7	30.5	5.1	0.8	0.1	0.0	0.0	0.0	22575
2.5	0.0	2.2	197.5	2158.8	6230.0	7449.5	4860.4	2066.0	644.5	160.2	33.7	6.3	1.1	0.2	0.0	0.0	23810
3.5	0.0	0.0	34.9	695.5	3226.5	5675.0	5099.1	2838.0	1114.1	337.7	84.3	18.2	3.5	0.6	0.1	0.0	19128
4.5	0.0	0.0	6.0	196.1	1354.3	3288.5	3857.5	2685.5	1275.2	455.1	130.9	31.9	6.9	1.3	0.2	0.0	13289
5.5	0.0	0.0	1.0	51.0	498.4	1602.9	2372.7	2008.3	1126.0	463.6	150.9	41.0	9.7	2.1	0.4	0.1	8328
6.5	0.0	0.0	0.2	12.6	167.0	690.3	1257.9	1268.6	825.9	386.8	140.8	42.2	10.9	2.5	0.5	0.1	4806
7.5	0.0	0.0	0.0	3.0	52.1	270.1	594.4	703.2	524.9	276.7	111.7	36.7	10.2	2.5	0.6	0.1	2586
8.5	0.0	0.0	0.0	0.7	15.4	97.9	255.9	350.6	296.9	174.6	77.6	27.7	8.4	2.2	0.5	0.1	1309
9.5	0.0	0.0	0.0	0.2	4.3	33.2	101.9	159.9	152.2	99.2	48.3	18.7	6.1	1.7	0.4	0.1	626
10.5	0.0	0.0	0.0	0.0	1.2	10.7	37.9	67.5	71.7	51.5	27.3	11.4	4.0	1.2	0.3	0.1	285
11.5	0.0	0.0	0.0	0.0	0.3	3.3	13.3	26.6	31.4	24.7	14.2	6.4	2.4	0.7	0.2	0.1	124
12.5	0.0	0.0	0.0	0.0	0.1	1.0	4.4	9.9	12.8	11.0	6.8	3.3	1.3	0.4	0.1	0.0	51
13.5	0.0	0.0	0.0	0.0	0.0	0.3	1.4	3.5	5.0	4.6	3.1	1.6	0.7	0.2	0.1	0.0	21
14.5	0.0	0.0	0.0	0.0	0.0	0.1	0.4	1.2	1.8	1.8	1.3	0.7	0.3	0.1	0.0	0.0	8
15.5	0.0	0.0	0.0	0.0	0.0	0.0	0.1	0.4	0.6	0.7	0.5	0.3	0.1	0.1	0.0	0.0	3
16.5	0.0	0.0	0.0	0.0	0.0	0.0	0.0	0.1	0.2	0.2	0.2	0.1	0.1	0.0	0.0	0.0	1
Sum	1	165	2091	9280	19922	24879	20870	12898	6245	2479	837	247	66	16	3	1	100000

Figure 6.1: Scatter diagram for North Atlantic operation with  $H_s$  in m and  $T_p$  in s

After determining the energy spectrum, it is possible to find the time history of the free surface elevation by adding a large number of components, i.e. cosine waves (see equation (3.3.9)). In principle, an infinite number of regular wave components is required. In fact, it is sufficient to select the appropriate number of components for each sea state. For this purpose, a characteristic interval of frequencies should be initially divided into small intervals  $[\omega_i, \omega_i + \delta\omega_i]$ . For each interval, the value of the spectrum corresponding, let us say, to the frequency  $\omega_i$ ,  $S_{\eta_w}(\omega_i)$ , is selected. Then the area under a segment of the curve

equals the energy of that frequency component wave, so the amplitude of the wavelet can be calculated by the equation (3.3.7) as follows.

$$a_i = \sqrt{2 S_{\eta_w}(\omega_i) \delta\omega} \quad (6.1.2)$$

Considering that frequency intervals are sufficiently small, each segment can be approximated by a rectangle, and then the sum of all the areas of the rectangles will equal the energy of the sea state. However, a limited number of  $N \approx 50$  should be used, since generally, the components with small ordinate values can be ignored [49].

In addition, to create an irregular wave energy time history, the phase angle for each component ( $\epsilon$  or else  $\Xi_n(\beta)$  as shown in equation (3.3.9)) should be determined. The wave elevation is a sum of many random components (since phase  $\epsilon$  is a random number, components are random numbers too). Usually, most of the contribution comes from the frequencies around the peak of the spectrum, and usually, there are enough of them, so we can say that we consider the sum of a large number of approximately equal random components [42]. For this study, these phases are chosen randomly by a *RandomReal* generator by Mathematica between the range of  $[0, 2\pi)$ . With the use of *RandomReal*, real numbers are chosen with a uniform probability distribution in the desired range. For every case, we generate as many random numbers (a list of randomly generated phases) as the number of components needed. For the calculation, sixteen different groups (or else seeds) of random phases are used for each case<sup>1</sup>.

The next step is to choose the frequencies and the intervals, of which the values of the spectrum are calculated, thus the number of components. The number of components is affected by the frequency spacing. It is known from simulation practice that if equal frequency spacing is used, the time history reconstructed nearly repeats itself. This effect is called the "self-repeating effect", and in order to diminish this effect, it is suggested to use unequal spacing for the frequency set. This phenomenon is further explained and studied in Appendix C.1, by following the approach of Belenky [57]. For this application, the spacing of the frequencies was chosen as equal. However, to prevent the self-repeating effect the distance was set equal to [42]:

$$\delta\omega = \frac{2\pi}{T_{sim}} \quad (6.1.3)$$

where  $T_{sim}$  is the total duration for which the simulation is performed to find the ship's response. As the total simulation time is chosen as 600 sec, then the step of the spectrum discretization is equal to  $\delta\omega = 2\pi/600 = 0.01047 \text{ rad/sec}$ . With this method (equal steps for the discretization of the spectrum), of course, a sufficient number of components are selected, which provide meaningful statistical information.

Subsequently, taking the above discretization step as given, the number of elements is calculated. This number changes as the characteristics of the spectrum ( $H_s, T_p$ ) change its form. Therefore for each case, the actual area under the spectrum curve was calculated. Then an initial frequency ( $\omega_{in}$ ) is chosen so that very small values of the spectrum are excluded. Then for each resulting segment for each interval  $[\omega_i, \omega_i + \delta\omega]$ , the area for

<sup>1</sup>With the use of *SeedRandom[x]* of Mathematica, we make sure you get the same sequence of pseudorandom numbers on different occasions. In this application, we used seeds 1 to 16.

each rectangle ( $E_i = S_{\eta_w}(\omega_i) \delta\omega$ ) is calculated. An iterative procedure is then followed, starting with the initial frequency ( $\omega_{in}$ ), and with step,  $\delta\omega$ , so that, the partial areas are calculated and summed up each time. This process stops when the total area obtained by summing the individual rectangles is equal to the actual area under the spectrum curve with an error of 5%. This ensures an accurate approximation of the area under the spectrum curve, hence the energy of the sea state. Still with the appropriate choice of  $\omega_{in}$ , very small values of the spectrum are excluded, which would both require more computational time and would not have a significant effect on the shape of the free surface. The  $\omega_{in}$ , for the simulations below, is chosen to be  $\omega_{in} = w_p - 0.5 w_p$ .

With the method described above, the number of components used in every case is found. This means that for every set of  $(H_s, T_p)$ , the number of components computed, have to be summed at every time step of the simulation, for the free surface elevation to be calculated. Some examples of the sea states (from figure 6.1) and their spectrum discretization, which are also used for the simulations, are shown below.

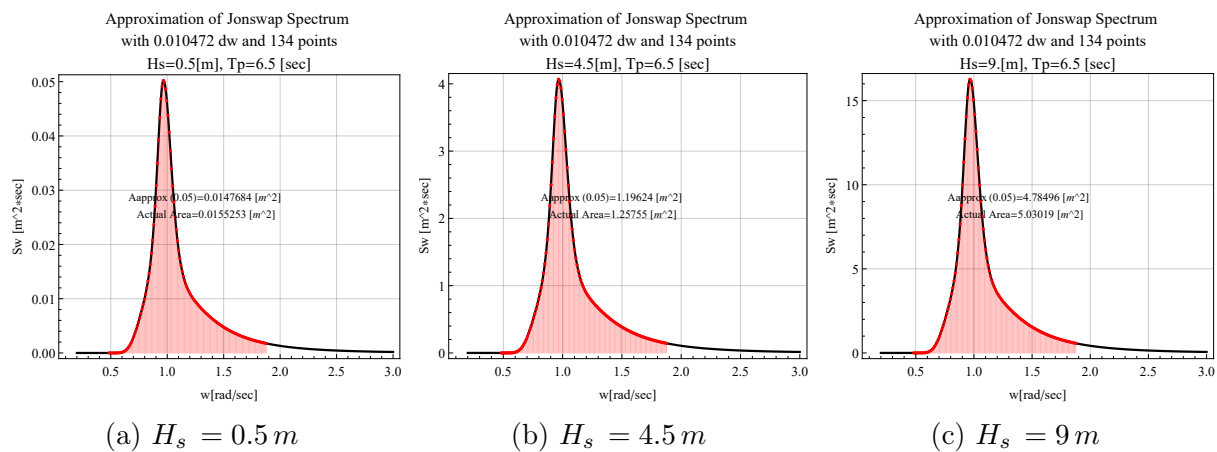


Figure 6.2: Jonswap spectrum discretization for  $T_p = 6.5$  sec

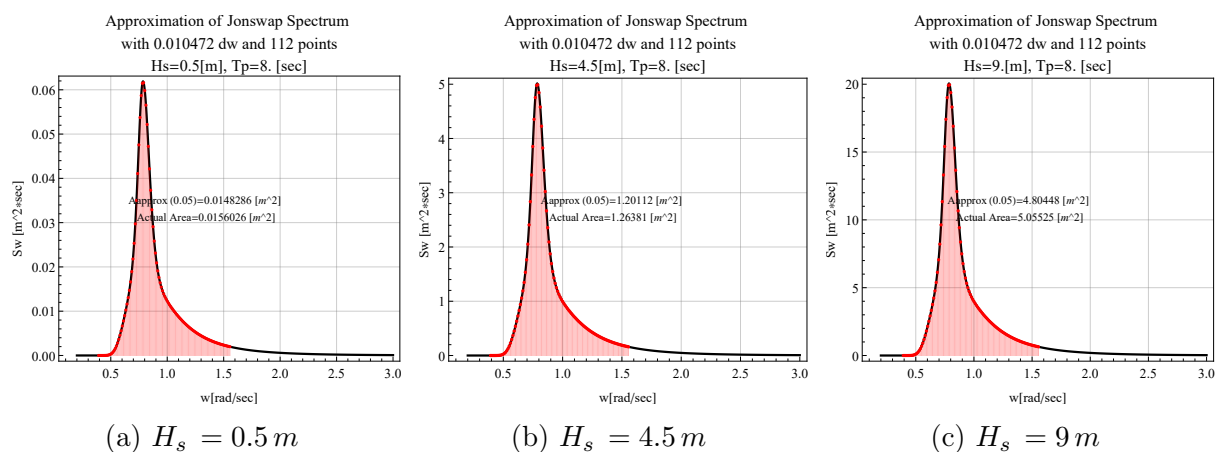


Figure 6.3: Jonswap spectrum discretization for  $T_p = 8.$  sec

As can be seen from the above figures, the number of points that make up the sum to produce the free surface elevation is not always the same. For bigger  $T_p = 14$  sec, thus

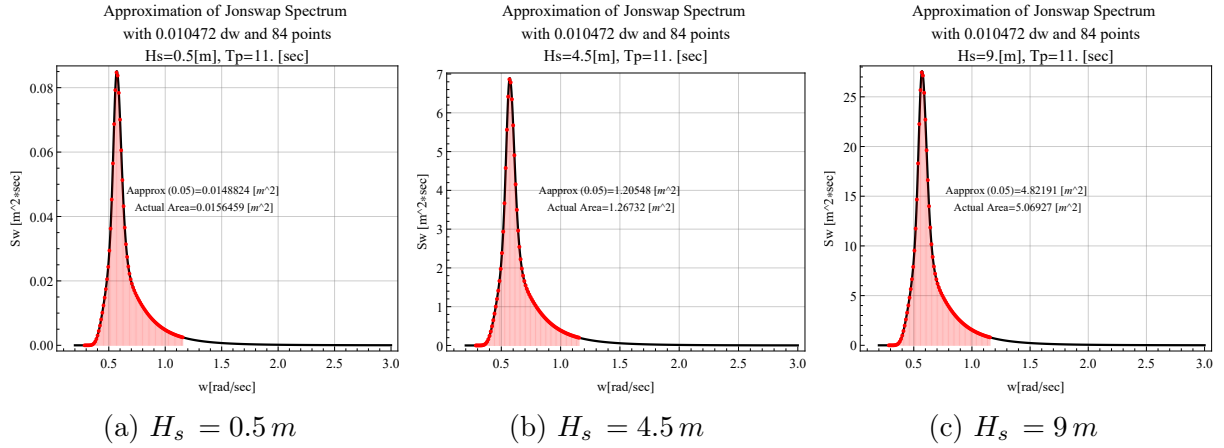


Figure 6.4: Jonswap spectrum discretization for  $T_p = 11. sec$

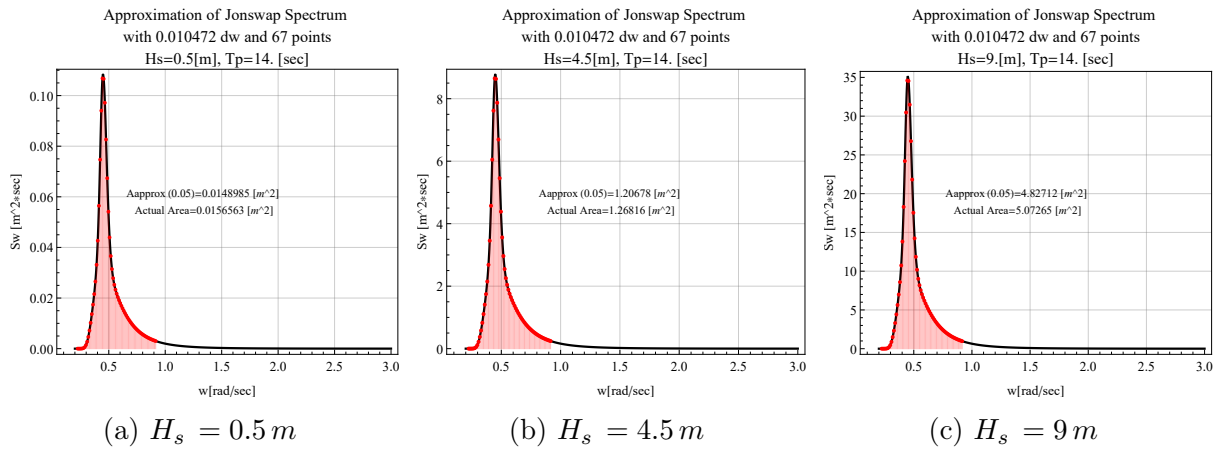


Figure 6.5: Jonswap spectrum discretization for  $T_p = 14. sec$

for smaller peak frequency, fewer points are needed, for the spectrum to be described. The opposite is true for spectra with a higher peak frequency ( $T_p = 6.5 sec$ ).

With the above analysis, we described how the free surface information for irregular longitudinal waves are obtained by the energy spectrum.. For each sea state (i.e. each case to be studied), sixteen different randomly generated lists of angle phases are used. In this way, the ship's response is calculated for sixteen different random realizations of the water surface for the same sea state. To ensure that these lists are not randomly generated with the same numbers, sixteen seeds are used (Seed 1, Seed 2,..., and Seed 16).

## 6.2 Parameters of Stability Charts

In this section, the parameters for the production of the Stability Charts in irregular waves, are defined. Mainly, the methodology is the same as that described in section 5.2.1 for regular waves.

The loading condition 18 was studied, as in the regular waves. This is a condition with

moderate stability as it has a relatively high center of gravity. Loading conditions 27 and 15 were chosen not to be considered, as their stability in regular waves is questionable. As shown in the diagrams in Appendix A, the righting arm is drastically reduced when the ship meets the crest of the wave amidship. This is evidence that the ship may be suffering from Pure Loss of Stability. For these reasons, condition 18 was chosen which is an intermediate condition.

The characteristics, therefore, regarding the loading condition and the parameters used in the differential equation remain the same, as shown in Table 5.1. For random waves, the wave characteristics change. Now instead of wave period and steepness, we refer to peak period and significant height respectively. Still, since there is no fixed wave period, the ratio  $a = \frac{4\omega_0^2}{\omega_{ep}^2}$  is calculated in the same way, but instead the peak period is used to calculate the "encounter" frequency corresponding to the peak radial frequency, as shown below.

$$\omega_{ep} = \omega_p - k V_s \cos(\mu) = \omega_p - \frac{\omega_p^2}{g} V_s \cos(\mu) \quad (6.2.1)$$

Furthermore, for the calculations, the discretization of the hull with 4,382 elements is used. As shown by the analysis done in chapter 4, the more structured discretizations with 4,382, and 6,694 were the ones that provided the most accurate results. In addition, to reduce the computational time, the discretization with the fewest elements of the two is used, as the calculations of the hydrostatics and the GZ are much faster.

The energy of waves can take certain values and, therefore, for a sea state, the energy corresponding to a wave height can be distributed at certain frequencies. Therefore, according to the scatter diagram, there are specific pairs  $(T_p, H_s)$  or else  $(a, H_s)$ , which represent sea states. Therefore the areas for which Stability Charts will be produced are restricted by these values.

As the encounter frequency depends on the wave frequency and the speed of the ship, two categories of diagrams are produced. Several diagrams are obtained in order to get a better insight into the occurrence of parametric instability in random waves. First, the runs are performed for each case, keeping the ship's speed constant and changing the sea states (i.e.  $T_p$ ). In the second approach simulations are made by changing the ship's speed for the pairs  $(T_p, H_s)$ , but keeping the peak period constant. In addition, in Appendix C.2, the tables with the cases used and their computation time are documented.

# Chapter 7

## Results and Discussion

For the different cases of sea states and forward ship's speeds, the Stability Charts are presented below. The diagrams show the areas of instability in parametric roll, in random one-directional following longitudinal waves. Each case  $(T_p, H_s)$  is the result of the ship's response to 16 different runs of the experiment (by changing the seed that generates the list of random angle phases). In other words, 16 different ship responses are calculated for the same sea state. The 16 realizations of the experiment in every case, do not in any way provide a sufficient sample space for statistical analysis. However, if in a case  $(T_p, H_s)$ , instability occurs in a sufficient number of seeds, this means that it is a region with a higher probability of instability. The maximum response angle of the ship is also an important factor, that should be taken into consideration.

For each time history of the ship's response, and for every seed, the maximum response angle is found, from 100 seconds onwards (the first 100 are not taken into account as they are considered to belong to the transition region). A threshold for exceeding the response angle is then defined, and compared to the maximum response angle observed in each case. Then in each case, and for each of the 16 seeds, it is recorded whether or not the maximum response angle exceeded the set limit. At the end in each case  $(T_p, H_s)$ , the number of seeds whose maximum response angle, exceeded the threshold value, is assigned. These results are presented below in the form of Contour Plots, and for several threshold values.

### 7.1 Forward ship's speed $V_s = 6.5$ knots constant

In this situation the ship's speed was kept constant and the peak period was alternated in each case. The data used have the range indicated in the table C.1, in the appendix C.2.

There seems to be an area of instability of a smaller scale. There are many seeds for which there is instability but with a small ship roll angle (charts with a threshold of 2 and 5 deg). This region occurs for peak periods between 11, 11.5 and 12 sec ( the a ratio is 1.6 to 1.8 respectively), for minimum  $H_s$  of 5.5 m. If we consider some correspondences with the stability diagrams, according to the literature, it appears that the principal resonance is shifted to the right, (for larger a), and upwards (instability occurs for relatively large  $H_s$ ).



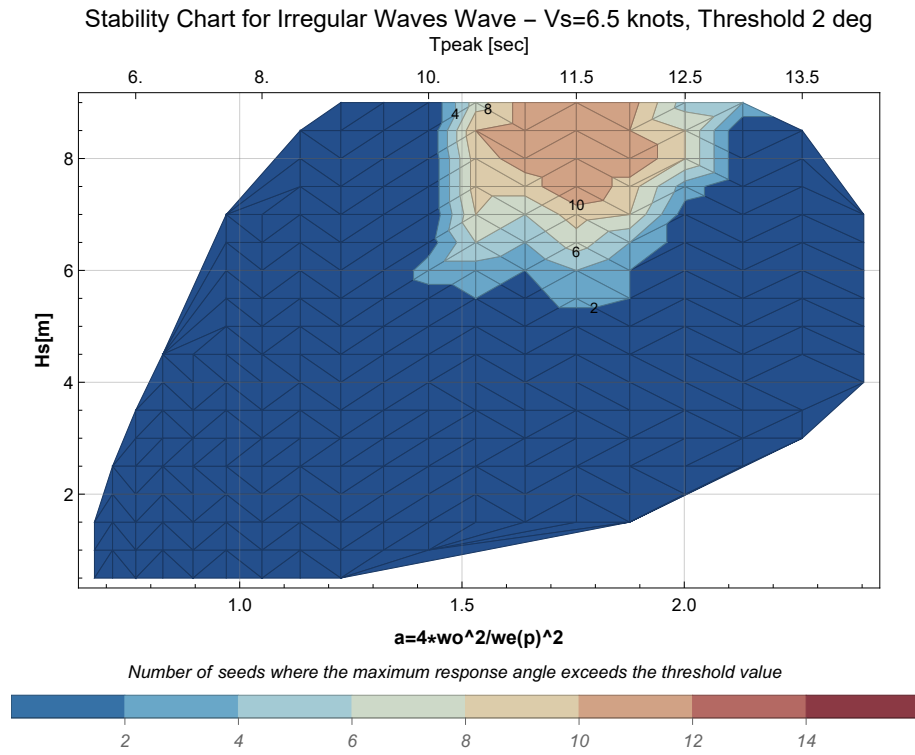


Figure 7.1: Stability Chart for constant  $V_s = 6.5$  knots and threshold  $=2$  deg

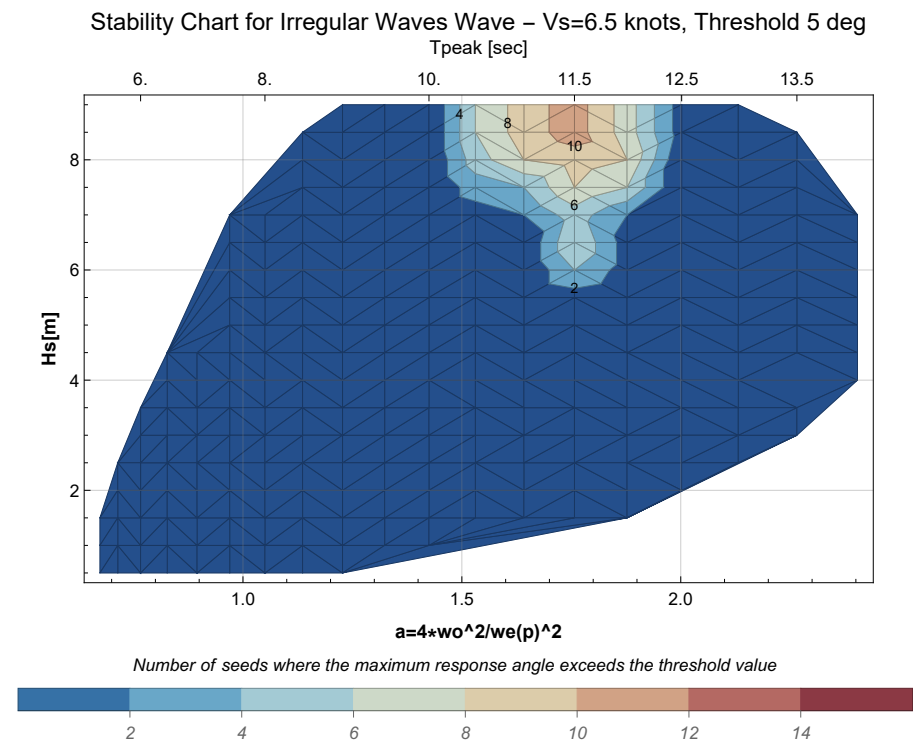


Figure 7.2: Stability Chart for constant  $V_s = 6.5$  knots and threshold  $=5$  deg



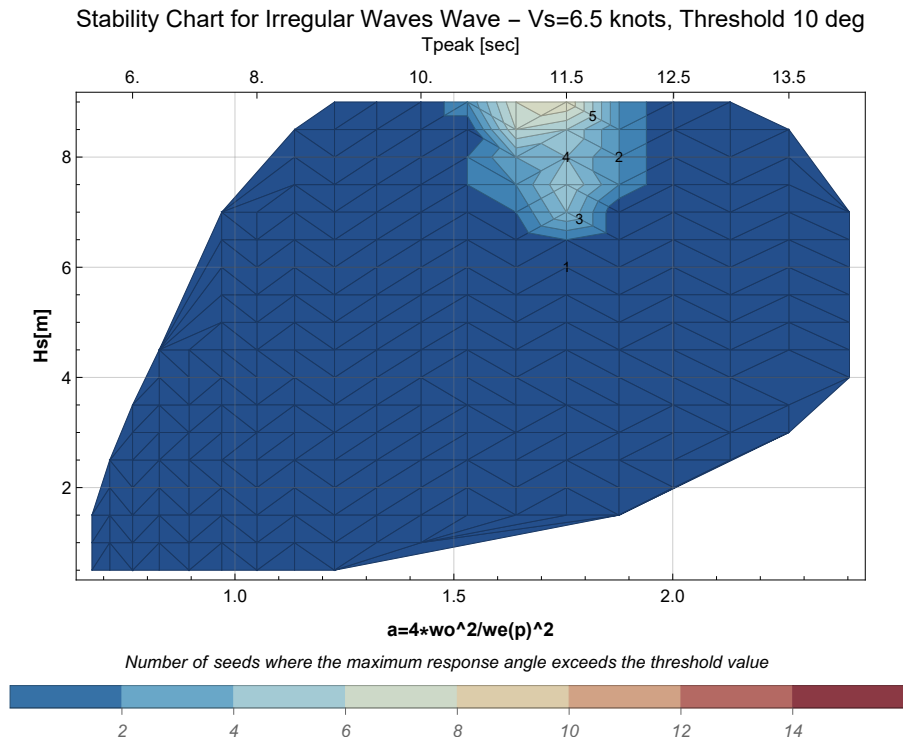


Figure 7.3: Stability Chart for constant  $V_s = 6.5$  knots and threshold =10 deg

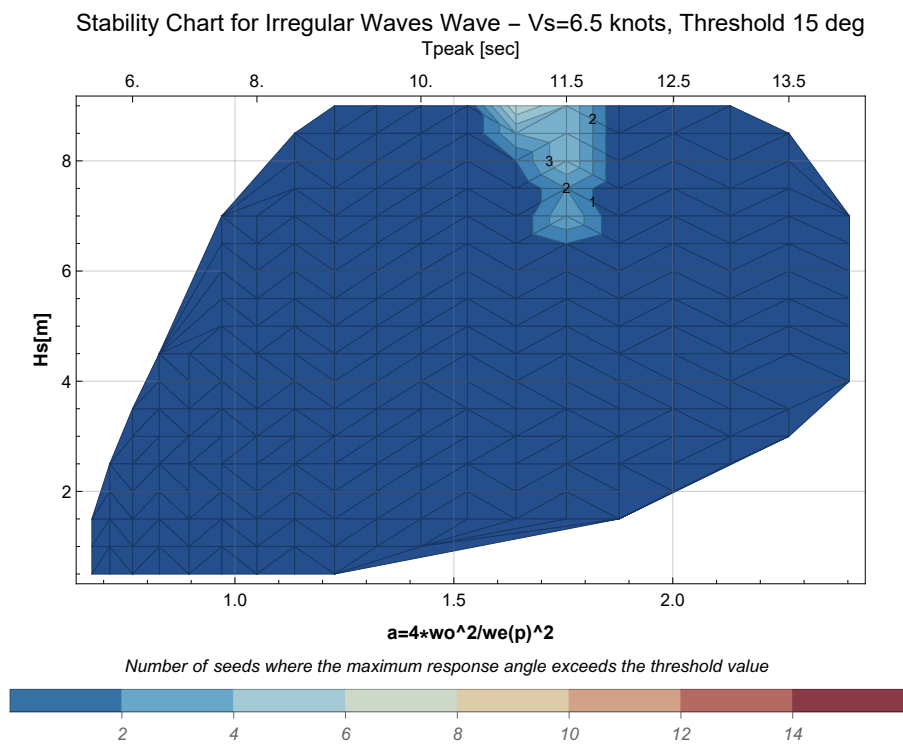


Figure 7.4: Stability Chart for constant  $V_s = 6.5$  knots and threshold =15 deg

For larger thresholds (10 and 15 deg), this area decreases significantly around the peak period 11 and 11.5 sec, but with an incidence rate of 4-5 seeds out of 16. For the threshold value greater than 15 deg, there is a number of seeds which, as presented in figure C.5, show very large response (above 30 degrees of rolling angle). These are obviously dangerous cases of capsizing, but they are far fewer than we would expect for regular waves.

## 7.2 Forward ship's speed $V_s = 12.5$ knots constant

In this situation the ship's speed was kept constant to 12.5 knots and the peak period was alternated in each case. The data used have the range indicated in the table C.2, in the appendix C.2.

For small threshold (1 deg), two regions are observed, one near  $a=2$  and the other for  $a=3$ . However, the first area is not present in the other diagrams where the threshold value was increased. These are not cases of parametric instability, as illustrated in figures C.10 and C.11. They are an extension of the transition region, which for these cases extends beyond 100 seconds.

Finally, for the region with ratio  $a$  around 3, pronounced parametric instability appears with a minimum  $H_s = 7$  m (figure 7.6) and then with a minimum  $H_s = 7.5$  m (figure 7.7). This case, with the ship's speed at 12.5 knots, has more pronounced responses, which in a large percentage leads to capsizing of the ship for significant wave height of 8 meters and above.

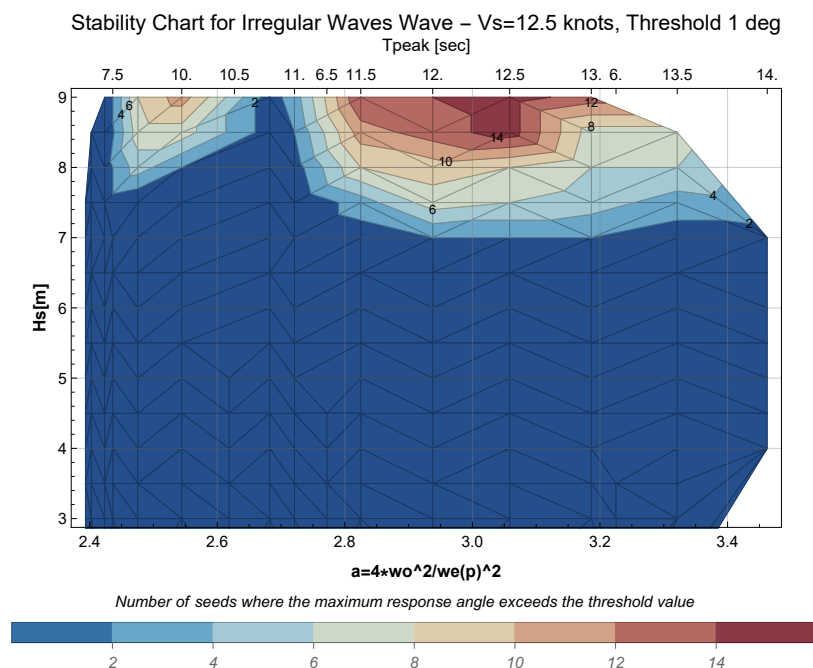


Figure 7.5: Stability Chart for constant  $V_s = 12.5$  knots and threshold = 1 deg

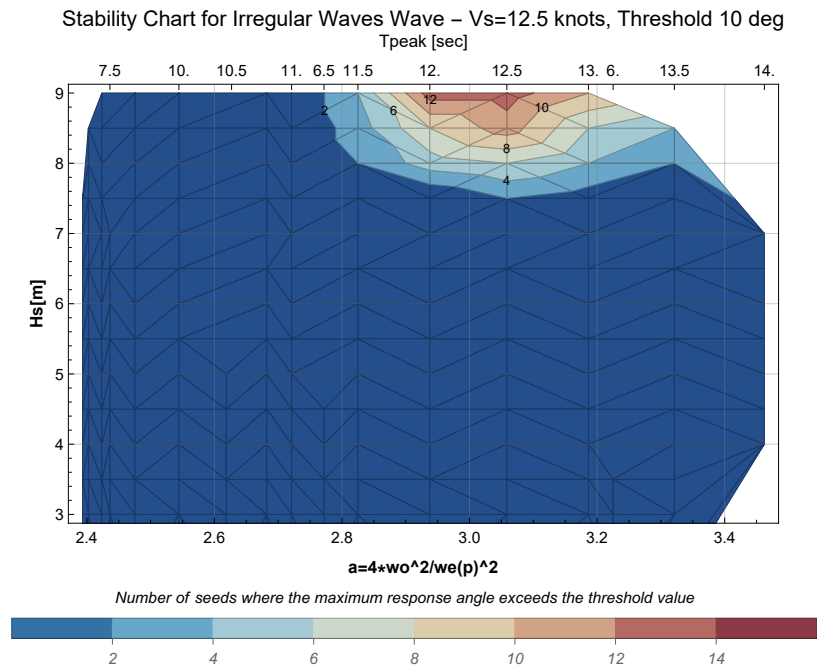


Figure 7.6: Stability Chart for constant  $V_s = 12.5$  knots and threshold =10 deg

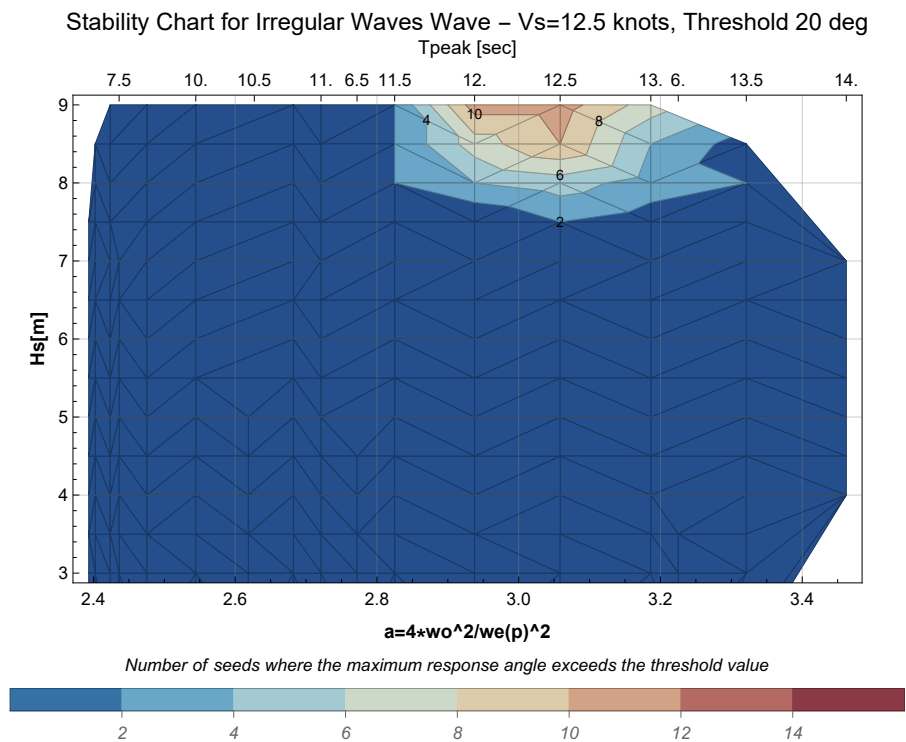


Figure 7.7: Stability Chart for constant  $V_s = 12.5$  knots and threshold =20 deg

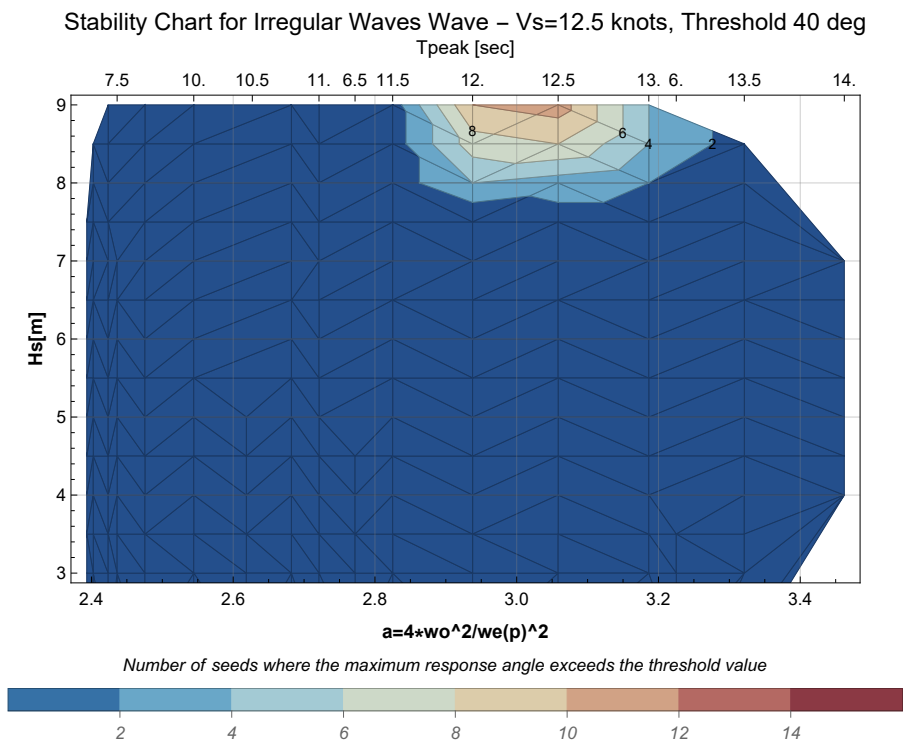


Figure 7.8: Stability Chart for constant  $V_s = 12.5$  knots and threshold =40 deg

### 7.3 Peak period $T_p = 11$ sec constant

In this situation the peak period was kept constant to 11 sec and the ship's speed was changing in each case. The data used have the range indicated in the table C.3b, in the appendix C.2.

There are 2 regions of instability, very close together for a ratio  $a$  of 1.6 to 2.8 approximately. These areas correspond to small ship speed, between 4 and 10 knots. Again, if we assume that this region corresponds to the theoretical principal resonance, it is shifted to the right, just like in the case with the constant speed at 6.5 knots.

Moreover, we can see that no other region of instability appears, at bigger ratio values of  $a$ . In contrast, the regular wave with a wave period of 11 sec had created the instability region in the fundamental region (figure 5.3), which does not appear in the stability chart for the irregular waves. Of course, no direct comparison of the diagrams could be made, because the free surface elevation, resulting from the energy spectrum with a peak period of 11 sec, is obtained as the sum of several wavelets from different frequencies.

It is also observed that many of the seeds show instability with relatively low significant height. In contrast to the above case, instability occurs (and it is not just the transient effect) for  $H_s$  of 5 m, as shown in figure C.12. Of course, this instability is of small scale and usually does not exceed 5 to 6 degrees of rolling angle. Hence afterwards in diagram 7.10, the instability range is significantly reduced.

Finally, for larger limits, the area of instability becomes significantly smaller. There are some seeds, which create instability with large angles (shown in the diagrams C.7),

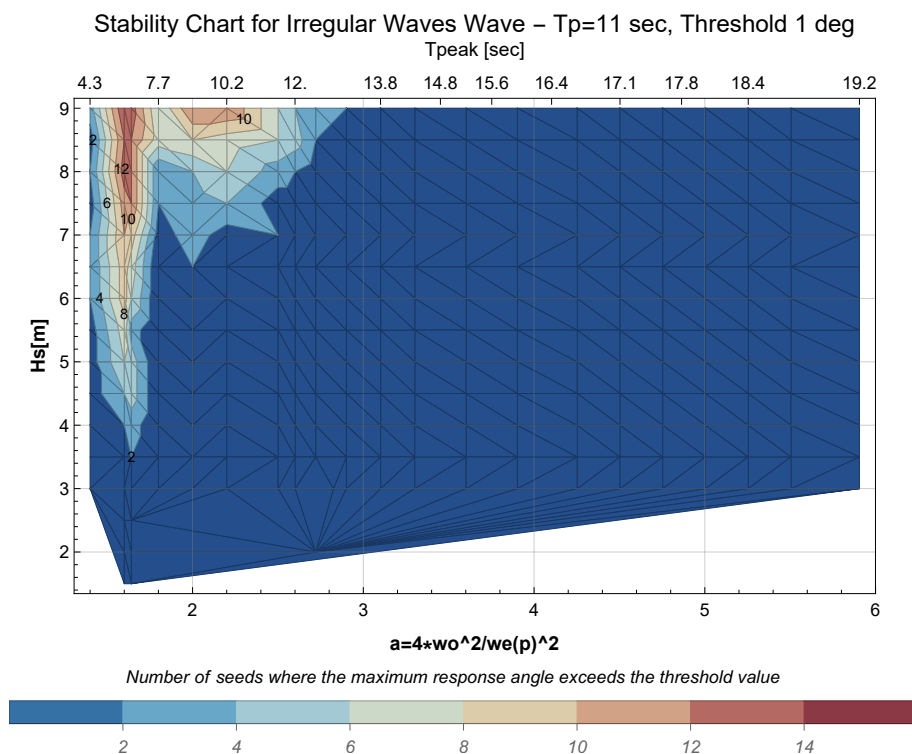


Figure 7.9: Stability Chart for constant  $T_p = 11$  sec and threshold = 1 deg

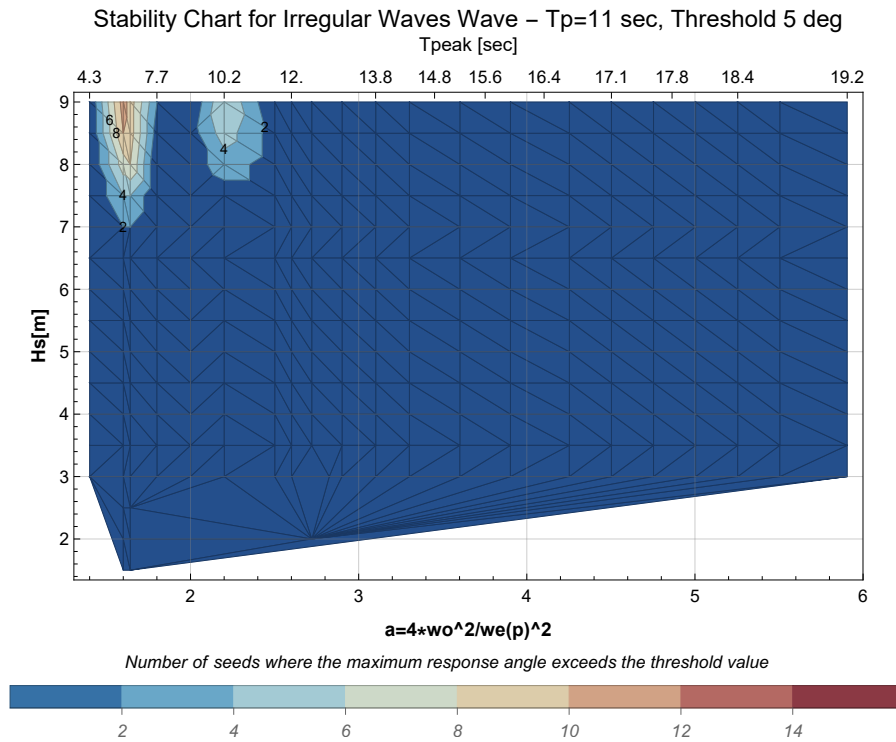


Figure 7.10: Stability Chart for constant  $T_p = 11$  sec and threshold =5 deg

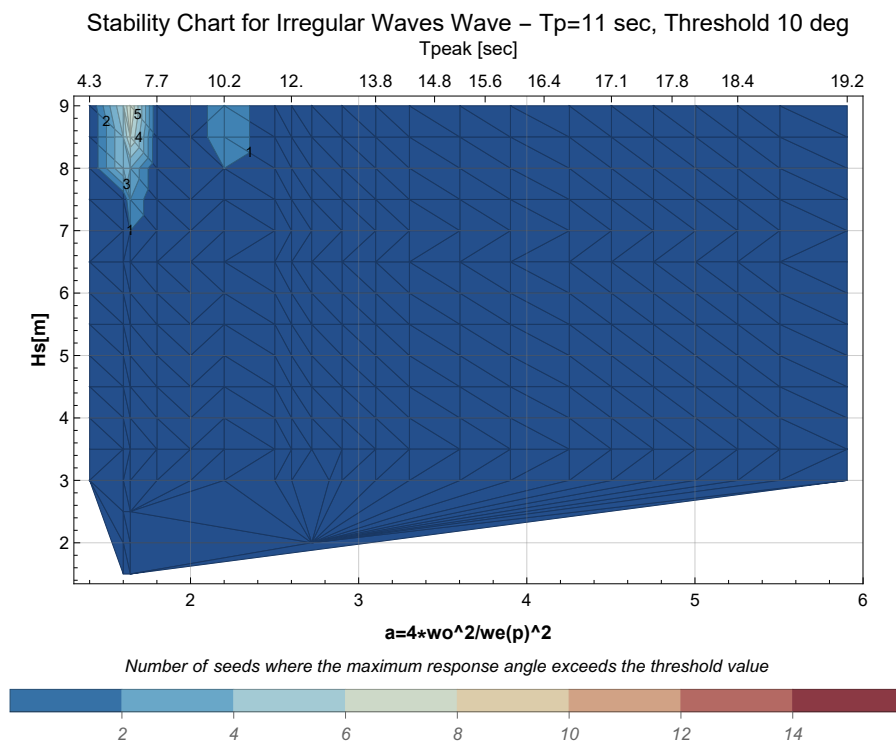


Figure 7.11: Stability Chart for constant  $T_p = 11$  sec and threshold =10 deg

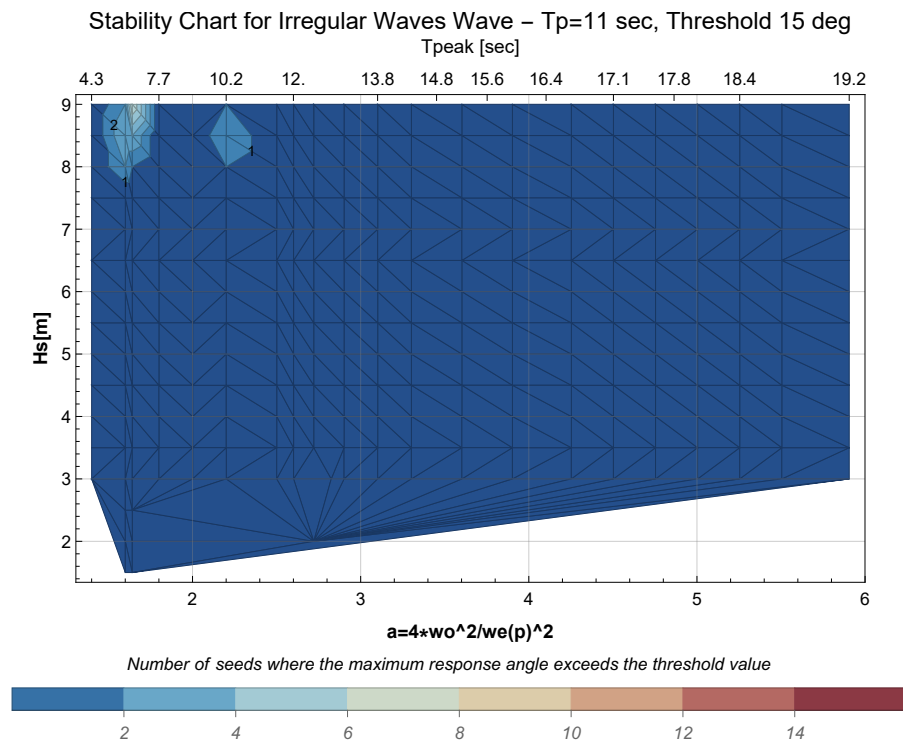


Figure 7.12: Stability Chart for constant  $T_p = 11$  sec and threshold =15 deg

but the number of these seeds is small (5 out of 16 or less).

## 7.4 Peak period $T_p = 8.5$ sec constant

In this situation the peak period was kept constant to 8.5 sec and the ship's speed was changing in each case. The data used have the range indicated in the table C.3c. For these simulations, it is easy to assume that there is no instability at any of the speeds tested for the sea state with a peak period of 8.5 seconds, as shown in figure 7.13.

## 7.5 Forward ship's speed $V_s = 0$ knots constant

In this situation the ship's speed was kept constant to 0 knots and the peak period was alternated in each case. The data used have the range indicated in the table C.3a. The simulations were initially made for the large significant height, and were only carried out up to  $H_s = 3.5$  m, as presented in figure 7.14. In this case, no instability occurred either. There are, of course, some seeds that show some response greater than 1 deg even after 100 sec. As shown in figure C.9, the response angle is small and can be considered to be part of the transient effect.



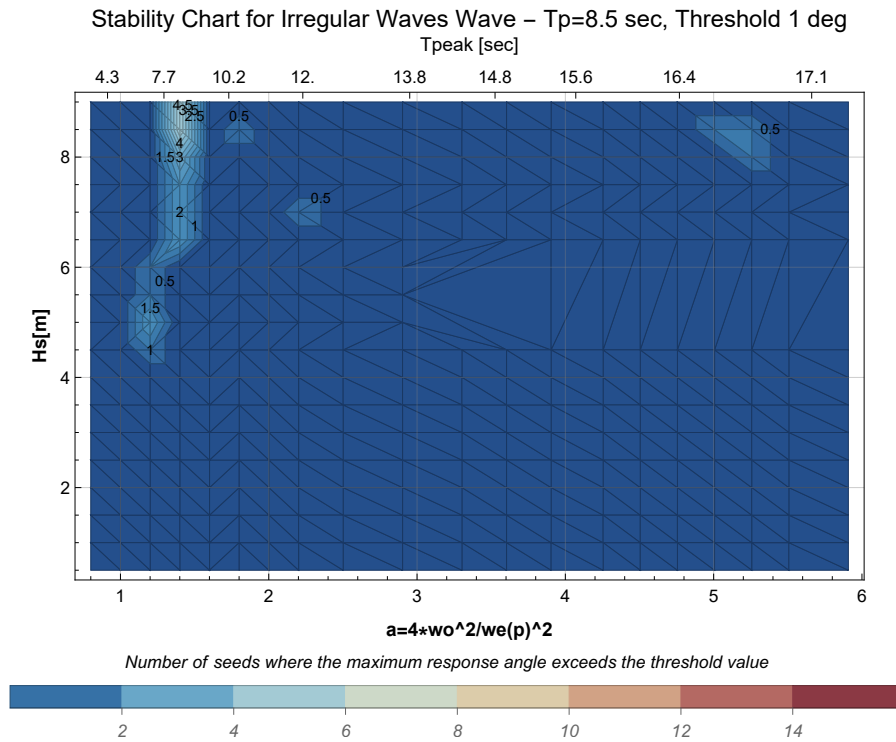


Figure 7.13: Stability Chart for constant  $T_p = 8.5$  sec and threshold =1 deg

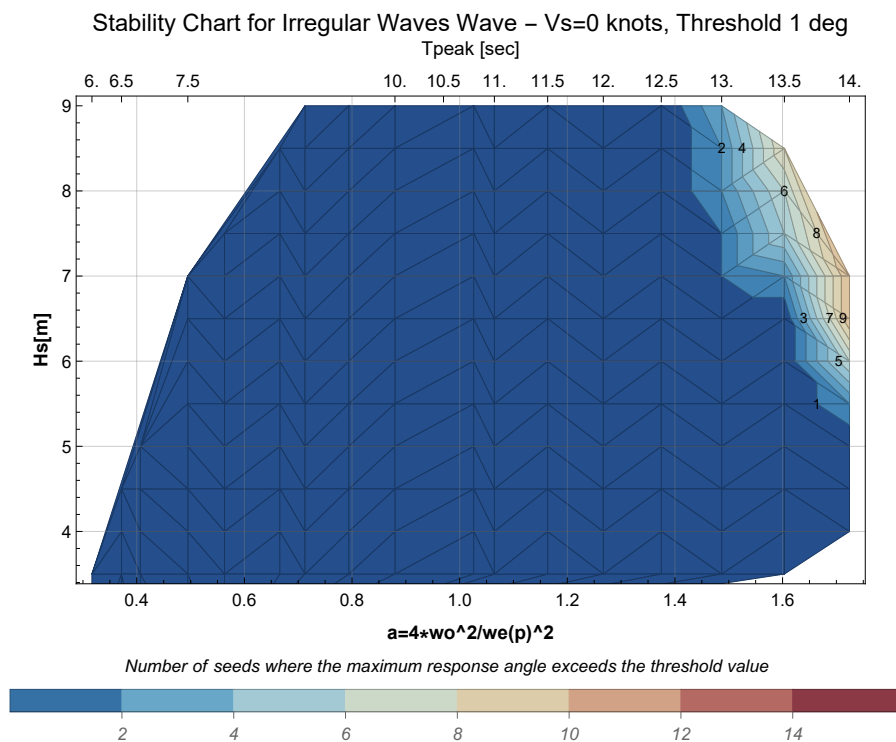


Figure 7.14: Stability Chart for constant  $V_s = 0$  knots and threshold =1 deg

## 7.6 Discussion

From the above diagrams, becomes apparent that we cannot be certain in which cases instability will occur or not. In many cases instability occurred in areas close to  $a$  from 1.5 to 2 (case for constant  $V_s = 6.5$  knots or case with constant  $T_p = 11$  sec), or close to  $a = 3$  (case for constant  $V_s = 12.5$  knots). In the case with a ratio  $a$ , of near 2 the instability started from a lower significant height ( $H_s=5.5-6$  m), compared to the unstable regions close to  $a=3$  ( $H_s=7$  and above). In any case, the number of seeds showing instability with large response angles (from 10-15 threshold and above), was relatively small (less than half of the seeds).

In addition, the ship speeds at which instability occurred were relatively low, not exceeding 12.5 knots. The presence or absence of instability, therefore, depends both on the speed and on the sea state, but it is not always necessary that there will be instability for specific values of  $a$  ratio. This is illustrated by the fact that the case with a constant peak period of 8.5 sec, did not generate any instability, even though a wide range of velocities, and hence  $a$  ratios, were considered.

The instability does not occur for every seed, even for considerable significant heights, and is more limited than in regular waves and occurs in smaller regions. However, parametric instability is still present even in random waves and in some cases so strong that it can lead to capsizing.

# Chapter 8

## Conclusion and Future Work

### 8.1 Conclusions

In this diploma thesis, an attempt was made to develop a model in order to find the ship's response to random waves. For this purpose, a numerical model was created in the Mathematica environment to calculate the exact value of righting arm in any given time instant. The righting arm is calculated in relation to the position of the ship in the wave, or in other words the free surface elevation. The model used, is a pseudo-static model which uses the equilibrium in two degrees of freedom, to calculate the righting arm in every time instant, during the solving of the rolling differential equation. Then, the response of the ship was found by solving the 1-DOF rolling differential equation with the nonlinear restoring term containing the calculated righting arm.

In the thesis first, the accuracy of the numerical model was confirmed hydrostatically, and hydrodynamically (for a regular cosine wave) through the calculation of the GZ curve in Aveva. Through this process, trials were carried out to ensure the appropriate discretization of the hull, which is introduced into the model for the calculations.

After the model was developed, stability diagrams were constructed for two cases of regular waves (one of which had been studied by Ms. Dousia in her thesis). Only one case of Dousia's study was examined, and was found to have several similarities, with the one studied in this thesis. The instability region for parametric roll as well as the extremes were quite close to those calculated by the model in this thesis. An important difference between the two models is that by using this model, the maximum angle of response of the ship could be found, and whether or not it would lead to capsize. Dousia's model expresses the restoring term by the change in metacentric height relative to the ship's position and relates it linearly to the rolling angle. On the contrary, the present developed model is considered non-linear because in the GZ equation, the angle with respect to the ship's position and time is included.

Subsequently, the random wave was introduced into the code. In the thesis only longitudinal following waves are studied. The free-surface elevation is calculated with the random phase model, as a sum of regular waves, with phases, generated randomly. Energy spectra were used to generate the waveforms, which describe the distribution of the energy and therefore the wave heights at the harmonic frequencies.

Last but not least, the simulations were made to find the ship's response to different sea states. Only one loading condition of the ship was examined. To give a broader pic-

ture, several simulations with different parameters were performed and the corresponding stability diagrams were produced.

Finally, we end up to the following conclusions:

- The discretization of the hull is an important factor, as it determines the calculation time and at the same time the accuracy of the model during the hydrostatic calculations. A more structured grid, which does not necessarily aim to capture the geometry perfectly, is preferred, as it has no strange geometries and there is a uniform numerical discretization of the ship's hull.
- The development of a numerical model is a complex process, requiring the control of many parameters. The modeling is done so that the computation time is not prohibitive, but at the same time, the accuracy of the model is not reduced (examples are the discretization of the hull, the solution time step, and how the calculation of the restoring term is introduced in the differential equation).
- In the initial test for the regular waves (done only for one loading condition), the stability diagram produced, had very close form to the one generated with the linear model created by Ms. Dousia. There was, however, additional information about the maximum angles of the ship's response when parametric roll occurs.
- In random waves, because the random phase model was used, several runs are required for each case (so that, lists of phase angles are generated randomly each time). In the diploma thesis, calculations were made for 16 different realizations of the same experiment (or otherwise referred, in this thesis as, seeds). If more seeds were included, there would be a better picture of whether or not a region is more likely to experience parametric instability. However, with the existing data, we can make some worthwhile observations.
- From the data we have, it appears that the phenomenon of parametric roll is present even in random waves. The free surface of the random waves does not always follow the periodic alternation between crest and trough, as it does in regular waves. However, parametric roll does occur, although not to such a large extent.
- Parametric roll in irregular waves occurs in smaller regions than in regular waves. While dangerous responses are not always developed with large rolling angles. For quite high significant height ( $H_s > 8\text{ m}$ , which is not so rare situation to occur, as shown in table 6.1), there are seeds, where the ship capsizes. The number of these seeds is always less than 50% of the seeds (usually they have a rate of 3 – 4/16).
- In addition, we can say that there are no clear regions of principal and fundamental response, in the sense that exists for regular waves. For random waves, when parametric instability is detected, these regions are shifted close to regions with ratio  $a$  from 1.6 to 2.4 and 3 respectively. While in some cases no instability occurs at all, in any of the values of the ratio  $a$ .
- Finally, for the specific loading condition considered, parametric instability occurred for lower ship speeds (approximately 4 and 12.5 knots). While for the cases tested in regular waves, instability occurred for ship speeds of 14 and 16 knots.

## 8.2 Future Work

At this point, the presentation of the results and findings of the diploma thesis is completed. Some of the author's suggestions for extending the study work carried out are the following:

- Discretization of the spectrum, with unequal frequency steps. In this way, it may be possible to reduce the computing time. With this method, it could be possible to run simulations for a longer period of time without a significant increase in computational cost.
- The examination of different types of spectra. In particular, spectra could be considered for swell seas, which according to the literature may be more dangerous sea states for parametric roll.
- The damping term can be described by non-linear damping coefficients, to capture the nonlinear behavior of roll damping, with higher-order equations. Alternatively, an equivalent damping coefficient can be computed for the specific ship and its LC.
- Considering more loading situations, as the instability of the ship also depends on the LC of the ship.
- Modify the model to allow coupling in all six degrees of freedom and find out whether there is indeed an effect or whether coupling by heave and pitch only is adequate.

# References

- [3] J. R. Paulling, “Parametric rolling of ships - then and now”, *Contemporary Ideas on Ship Stability and Capsizing in Waves*, 2011.
- [5] “Maritime accident report svendborg mærsk heavy weather damage on 14 february 2014”, Tech. Rep., September 2014.
- [6] “Accident report into the loss of 137 containers from the container ship cma cgm g. washington in the north pacific ocean on 20 january 2018”, Tech. Rep., JANUARY 2020.
- [7] “Maersk essen marine accident reposrt on loss of cargo”, Tech. Rep., 2022.
- [8] Y. Goda, *Random seas and design of Maritime structures*. World Scientific Publishing Co. Pte. Ltd., 2000, vol. 15.
- [9] *Recommendation on intact stability for passanger and cargo ships inder 100 meters in length*, vol. Resolution A. 167 (ES.IV), IMCO (current IMO), 28 November 1968.
- [10] I. M. Organization. “Ship design and stability”. (2022), [Online]. Available: <https://www.imo.org/en/OurWork/Safety/Pages/ShipDesignAndStability-default.aspx>.
- [11] *Adoption of the International Code on Intact Stability*, vol. Resolution MSC . 267(85), IS CODE, The Maritime Safety Commitee, Convention of the International Maritime Organization, 2008.
- [12] *Guidance th the master for avoiding dangerous situations in following and quartering seas*, vol. Resolution MSC.1/Circ. 707, Annex, The Maritime Safety Commitee, Convention of the International Maritime Organization, 1995.
- [13] *Interim Guidlines on the Second Generation Intact Stability Criteria*, vol. Resolution MSC.1/Circ. 1627, IS CODE, The Maritime Safety Commitee, Convention of the International Maritime Organization, 2020.
- [14] W. Froude, “On the rolling of the ships”, *Second session of thr Institute of Naval Architects*, pp. 180–229, March 1861. [Online]. Available: [https://www.rina.org.uk/On\\_the\\_Rolling\\_of\\_Ships.html](https://www.rina.org.uk/On_the_Rolling_of_Ships.html).
- [15] K. Spyrou, “Designing against parametric instability in following seas”, *Ocean Engineering*, vol. 27, Issue 02, pp. 625–653, June 2000.
- [16] Κωνσταντίνος Σπύρου, Καθηγητής Ε.Μ.Π., *Σημειώσεις Μαθήματος 9ου εξαμήνου σπουδών- Ευστάθεια Διατοχισμού και Υπόβαθρο Κανονισμών*. Σύνδεσμος ελληνικών ακαδημαϊκών βιβλιοθηκών, Ε.Μ.Π., 2011.

- [17] J. Paulling and R. Rosenberg, "On unstable ship motions resulting from nonlinear coupling", *Journal of Ship Research*, vol. 3, Issue 02, June 1959.
- [18] O. Grim, "Stabilität und sicherheit im seegang", Tech. Rep., 1952, pp. 10–21.
- [19] J. R. Paulling, Kastner, Sigismund, Schaffran, and Stephen, "Experimental studies of capsizing of intact ships in heavy seas", Tech. Rep., November 1972.
- [20] N. Umeda, M. Hamamoto, Y. Takaishi, Y. Chiba, A. Matsuda, and K. Spyrou, "Model experiments of ship capsize in astern seas", Tech. Rep., January 1995.
- [21] E. Pesman and M. Taylan, "Effect of encounter angle on parametric roll motion in regular waves", *International Symposium on Naval Architecture and Maritime*, vol. 1, pp. 337–345, 2011.
- [22] M. A. S. Neves and C. A. Rodriguez, "On unstable ship motions resulting from strong non-linear coupling", *Ocean Engineering*, vol. 3, pp. 1853–1883, 2006.
- [23] G. Bulian, "Nonlinear parametric rolling in regular waves a general procedure for the analytical approximation of the gz curve and its use in time domain simulation", *Ocean Engineering*, vol. 32, pp. 309–330, 2005.
- [24] M. A. S. Neves, N. A. Perez, O. M. Lorca, and C. A. Rodriguez, "An investigation on head-sea parametric rolling for two fishing vessels", *Contemporary Ideas on Ship Stability and Capsizing in Waves*, pp. 231–252, 2011.
- [25] Y. Shin, V. Blenky, J. Paulling, K. Weems, and W. Lin, "Criteria for parametric roll of large containerships in longitudinal seas", ABS Technical Papers, Tech. Rep., 2004, pp. 117–147.
- [26] G. Dousia, "Numerical analysis of parametric roll resonance of a containership sailing in nonlinear, longitudinal seas", National Technical University of Athens, 2015.
- [27] V. Belenky, C. C. Bassler, and K. Spyrou, *Development of Second Generation Intact Stability Criteria*. NSWCCD-50-TR-2011/065, 2011.
- [28] G. Contento, A. Francescutto, and M. Piciullo, "On the effectiveness of constant coefficients roll motion equation", *Ocean Engineering*, pp. 597–618, 1996.
- [29] S. Surendran and J. V. R. Reddy, "Numerical simulation of ship stability for dynamic environment", *Ocean Engineering*, pp. 1305–1317, 2003.
- [30] M. Taylan, "The effect of nonlinear damping and restoring in ship rolling", *Faculty of Naval Architecture and Ocean Engineering, Technical University of Istanbul*, pp. 921–932, 2000.
- [31] J. V. Perunovic, "Influence of the gz calculation method on parametric roll prediction", *Ocean Engineering*, vol. 38(2011), pp. 295–393, 5 May 2010.
- [32] G. Bulian, A. Francescutto, and C. Lugni, "On the nonlinear modeling of the parametric rolling in regular and irregular waves", *International Conference on the Stability of Ships and Ocean Vehicles*, vol. 8th, pp. 305–323, 2003.
- [33] A. Biran, *Ship Hydrostatics and Stability*. Butterworth-Heinenmann, 2003.
- [34] P. J. Pritchard, *Fox and McDonald's introduction to Fluid Mechanics*, 8th ed. John Wiley and Sons, Inc., 2011.



- [35] Γιώργος Τζαμπίρας, *Υδροστατική και Ευστάθεια Πλοίου*. Σύνδεσμος ελληνικών ακαδημαϊκών βιβλιοθηκών, ΕΜΠ, 2015.
- [36] K. Rawson and E. Tupper, *Basic Ship Theory*, 5th. Butterworth-Heinemann, 2001.
- [37] I. Nam-Kyun and H. Choe, “A quantitative methodology for evaluating the ship stability using the index for marine ship intact stability assessment model”, *International Journal of Naval Architecture and Ocean Engineering* 13, pp. 246–256, 2021.
- [38] *Explanatory Notes to the International Code on Intact Stability*, vol. Resolution MSC.1/Circ. 1281, IS CODE, The Maritime Safety Committee, Convention of the International Maritime Organization, 2008.
- [39] B. O. el Moctar and M. Abdel-Maksoud, “Ship roll damping analysis”, Universität Duisburg-Essen, Tech. Rep., 2016.
- [40] A. D. Papanikolaou, E. Boulougouris, and D. Spanos, “On the specification of the roll radius of gyration for ro-ro passenger ships in view of the implementation of solas 95 res.14 equivalent model test method”, National Technical University of Athens, Department of Naval Architecture and Marine Engineering Laboratory of Ship Design, Tech. Rep., 1996.
- [41] W. Wawrzynski and P. Krata, “Method for ship’s rolling period prediction with regard to non-linearity of gz curve”, *Journal of Theoretical and Applied Mechanics*, pp. 1329–1343, 2016.
- [42] V. Belenky and N. B. Sevastianov, *Stability and safety of ships: Risk of capsizing*, 2 edition (30 jun. 2007). Society of Naval Architects and Marine Engineering (SNAME), 2003, ISBN: 0-939773-61-9.
- [43] A. Sjule, “Evaluation of vulnerability to parametric rolling”, Kth Royal Institute of Technology School of Engineering Sciences, 2016.
- [44] M. College, *Oceanography 101*. LibreTexts, 2022.
- [47] A. F. Molland, *The Maritime Engineering Reference Book*. Elsevier Ltd., 2008, ISBN: 978-0-7506-8987-8.
- [48] I. Young, *Wind-Generated Waves*. Ocean Wave Dynamics, 2010.
- [49] K. Judge. “Seakeeping and maneuvering”. (2019), [Online]. Available: <https://www.usna.edu/NAOE/academics/en455.php>.
- [50] M. K. Ochi and E. N. Hubble, “Six-parameter wave spectra”, *Proc 15th Coastal Engineering Conference*, pp. 301–328, 1976.
- [52] Y. Robin, T. Michalski, J. Chen, M. Poelker, and J. LeRose. “Yaw, pitch and roll rotations”. (2012), [Online]. Available: <https://hallaweb.jlab.org/experiment/g2p/survey/>.
- [53] A. M. Thu and H. H. W. Ei Ei Htwe, “Numerical investigation of ship’s incoupled roll, heave and pitch motion in irregular sea”, *International Journal of Mechanical And Production Engineering*, pp. 44–48, 2015.
- [54] A. K. Magnusson and E. B. Gregersen, *Spectral shape parameters in storm events from different data sources*, 2015.

- 
- [55] *Selected design wave by long term staochastic method*, Class Guidelines, ABS(American Bureau of Shipping), 2016.
  - [56] *Wave Loads*, vol. DNVGL-CG-0130, Class Guidelines, DNV-GL, 2018.
  - [57] V. Belenky, “On self-repeating effect in reconstruction of irregular waves”, *Contemporary Ideas on Ship Stability and Capsizing in Waves*, pp. 586–597, 2011.

# Image References

- [1] “Maritime accident report svendborg mærsk heavy weather damage on 14 february 2014”, Tech. Rep., September 2014.
- [2] “Accident report into the loss of 137 containers from the container ship cma cgm g. washington in the north pacific ocean on 20 january 2018”, Tech. Rep., January 2020.
- [4] “Maersk essen marine accident reposrt on loss of cargo”, Tech. Rep., 2022.
- [45] K. Surf and Sea. “How to read a surf report”. (2017), [Online]. Available: <https://learntosurfkona.com/featured/how-to-read-a-surf-report/>.
- [46] H. Naeserer, “The capillary waves’ contribution to wind-wave generation”, 2022.
- [51] D. Selimovic. “Open accessarticle improving the performance of dynamic ship positioning systems: A review of filtering and estimation techniques”. (2020), [Online]. Available: <https://www.mdpi.com/2077-1312/8/4/234/htm>.

# Appendix A

## Validation of GZ curve in wave with Aveva model

In this Appendix, diagrams depicting the validation with Aveva model, of the GZ curves in sinusoidal waves are presented. The diagrams show the change in the GZ curve, as the wave passes at various time instants. For each case, the Gz curves obtained from the six hull discretizations are presented so that they can be compared with each other. This section provides the complimentary to Section 4.3.3: [GZ curve in sinusoidal longitudinal wave](#) of Chapter's 4 figures for the rest Loading Conditions, LC 15, LC 27, LC 30, and LC 36.

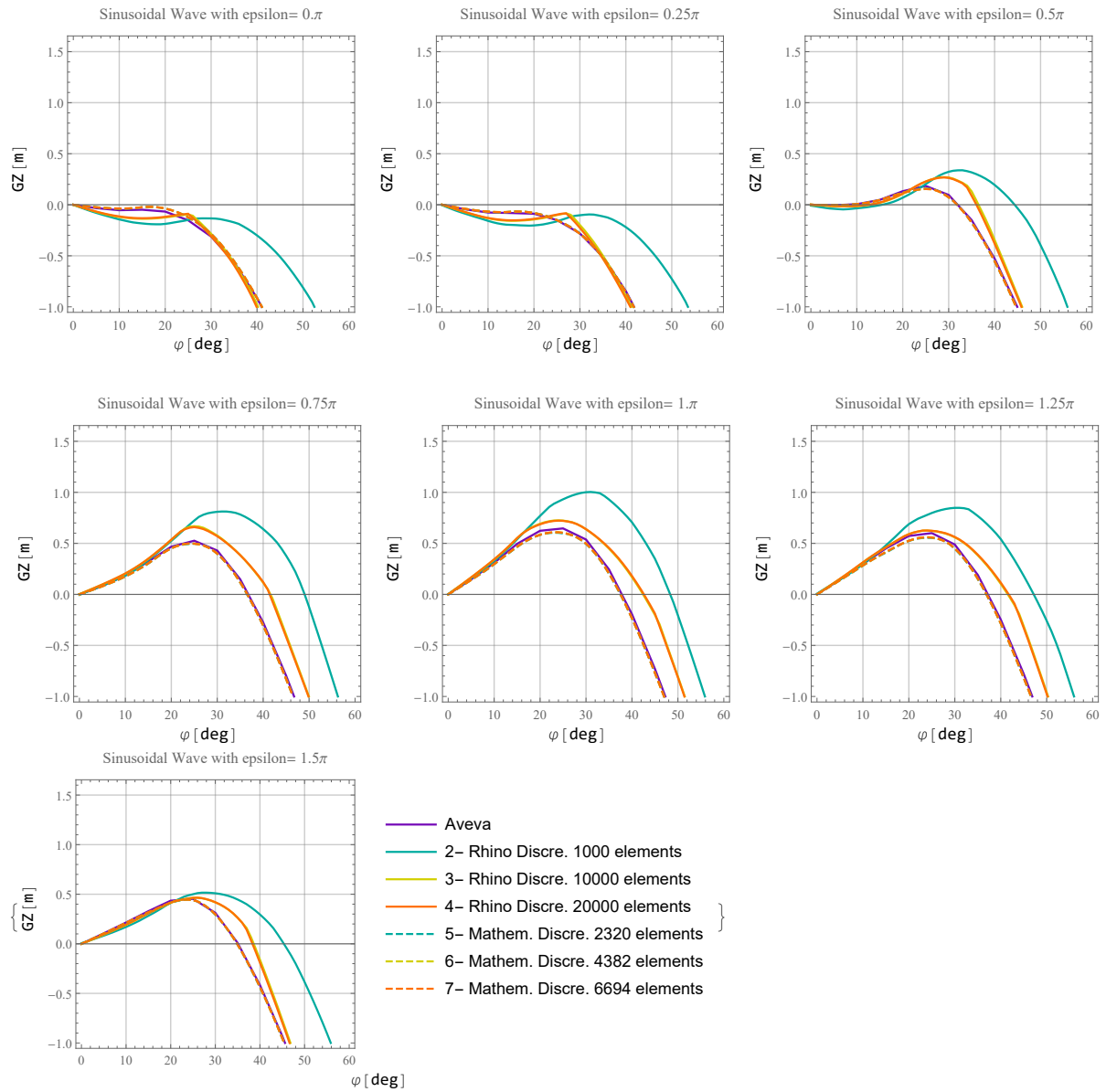


Figure A.1: Validation with Aveva model of GZ curve in sinusoidal Wave for LC 15

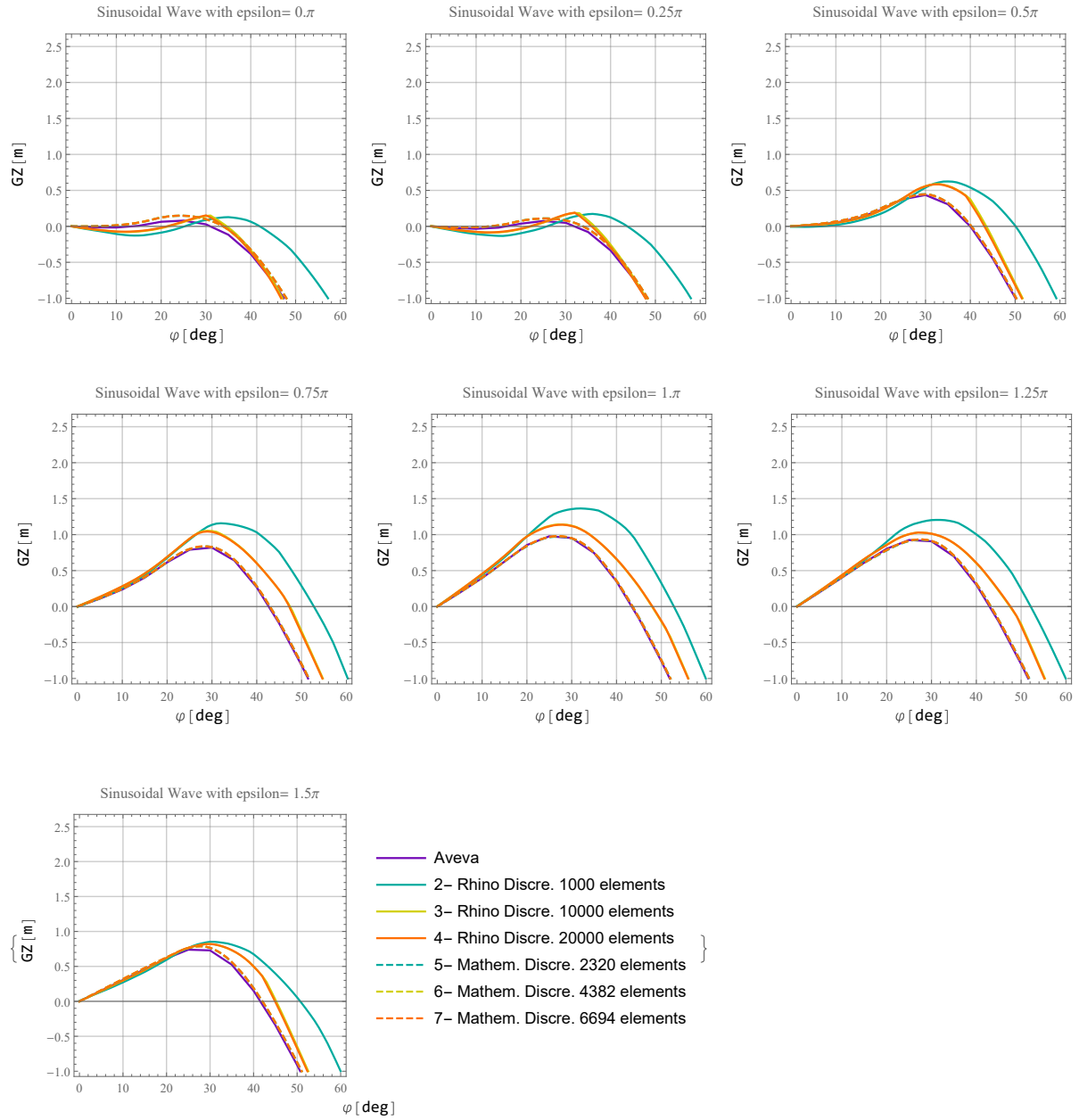


Figure A.2: Validation with Aveva model of GZ curve in sinusoidal Wave for LC 27

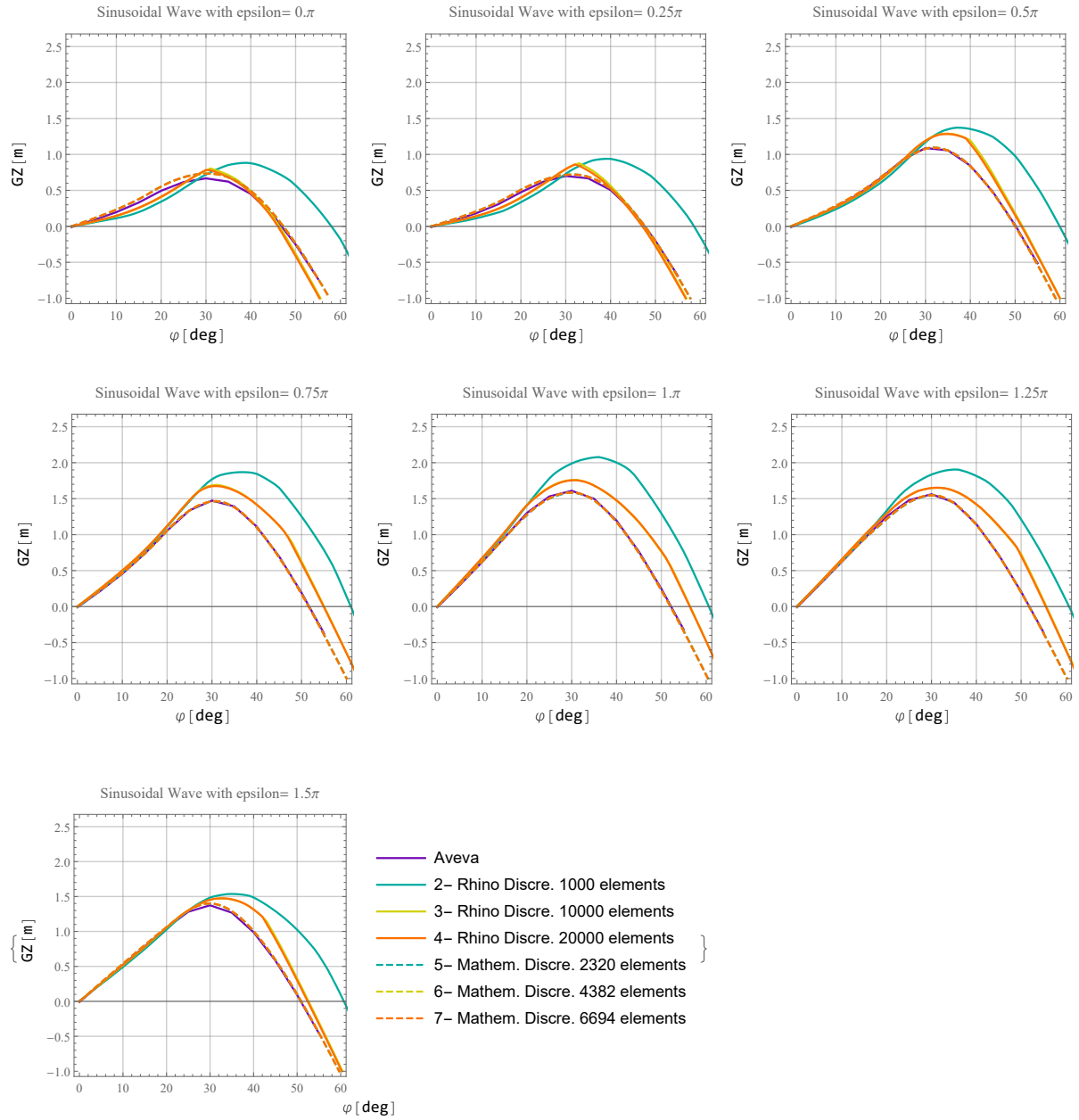


Figure A.3: Validation with Aveva model of GZ curve in sinusoidal Wave for LC 30



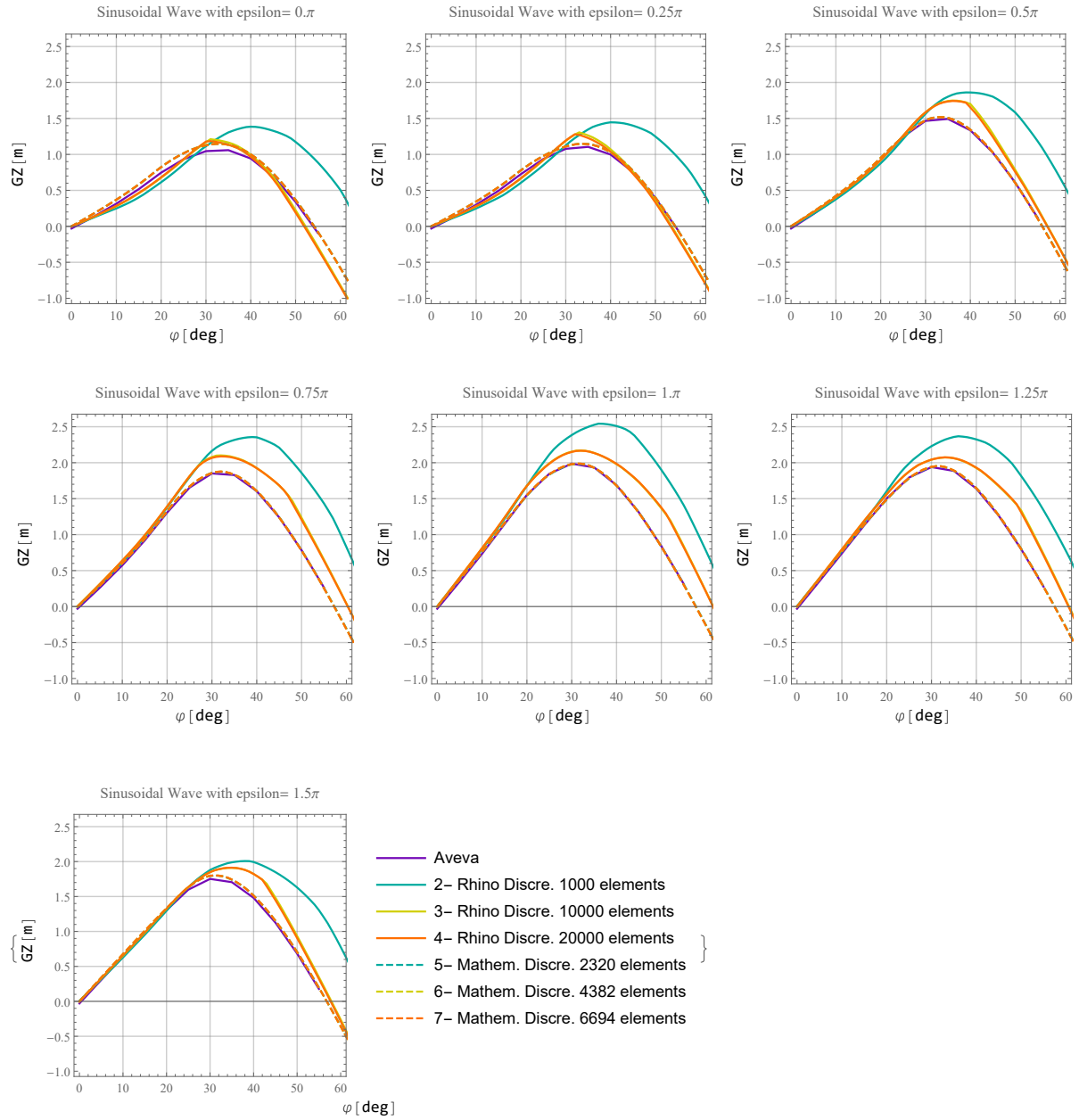


Figure A.4: Validation with Aveva model of GZ curve in sinusoidal Wave for LC 36

# Appendix B

## Equation of Roll

### B.1 Study for the three approaches of solving the differential equation

This Appendix provides material for the brief analysis performed for the form of the righting arm, in the restoring term of the rolling differential equation. Three cases were examined as explained in Section 5.1.3: [Righting arm](#) of Chapter 5.

**Case 1:** In the first approach, the total time of simulation is divided into many time instants with a time step that is selected (*step*). At the beginning the *step* was set to 1 or 1.5 sec, but then it was reduced to 0.25 sec for greater accuracy. At any given time instant, the ship is balanced at the vertical translation (heave) and the rotation about the transverse plane (pitch). Also the ship is placed in the appropriate longitudinal position relative to the wave (for when the ship has forward speed). Then with the appropriate function the curve GZ is calculated for this specific position of the ship on the wave for a range of inclination angles. Then the values of this curve are fitted to a polynomial power series as in equation (5.1.3) to find the coefficients for the function  $GZ(\phi)$ . By introducing the GZ curve function, the differential equation has the following form.

$$\ddot{\phi} + 2\zeta \omega_0 \dot{\phi} + \frac{\Delta g \overline{GZ}(\phi)}{I_x} = 0 \quad (\text{B.1.1})$$

Finally, the above differential equation is solved, for the time interval  $[0, \textit{step}]$ , and the response of the ship is found, for this specific time instant. With the inclination angle obtained from the differential equation, the new position of the ship can be defined. By calculating the new equilibrium of the ship on heave and pitch motion, the same procedure is followed until the next time step. The differential equation is solved, for the time interval  $[\textit{step}, 2 \textit{step}]$ .

**Case 2:** In the second approach, again time is divided and the differential equation is solved for a specific time period, as in the first approach. The only difference is that, the entire GZ curve is not calculated for a range of angles. In the restoring term only a value of the righting arm is used. This corresponds to the value of the righting arm that the ship had for the response angle estimated in the previous calculation cycle. The

differential equation, in the program, has the following form.

$$\ddot{\phi} + 2\zeta \omega_0 \dot{\phi} + \frac{\Delta g \overline{GZ}}{I_x} = 0 \quad (\text{B.1.2})$$

**Case 3:** In the third approach, a function<sup>1</sup> was created that directly calculates the righting arm. This function uses as input the inclination angle and the absolute time of the simulation. The differential is solved directly for all simulation time, with the time step either selected by the solver automatically or manually. The differential equation, in the program, has the following form as 5.1.4, which is the closest to the form introduced in chapter 3.2.2.

It should be noted that, just because in the differential equations of cases 1 and 2, the righting arm do not appear to be time-dependent, it does not mean that this dependence does not exist. In these cases the differential equation is solved in many short time intervals. As at each time period the initial conditions have changed, the ship's position is redefined and the equilibrium is recalculated. The data from the previous time interval are then used to calculate the next time instant. Therefore, the time dependence still exists, it is just not apparent. Moreover, the time step is set small, hence it is assumed that between the intervals, no major changer occur in the system. Initially for the first case, calculations were made for both 1 and 0.25 sec time step. Then only the 0.25 sec time step was used for the comparison.

Table B.1: Parameters for solving the differential equation with the three approaches

Characteristics of loading condition		
Displacement	[tons]	68192
Mean Draught	[m]	11.52
KG	[m]	15.62
LCG	[m]	116.41
Initial conditions of the differential equation		
$\phi(0)$	[rad]	$\pi/180$
$\dot{\phi}(0)$	[rad/sec]	0
Parameters used in the differential equation		
$\zeta$	-	0.05
$I_x$	[tons m <sup>2</sup> ]	$5.98374 \cdot 10^7$
$GM_0$	[m]	2.05
$T_0$	[sec]	41.5
Wave Characteristics		
$a$	[m]	3
Wave length	[m]	$L_{pp} = 238.35$
Wave direction	[deg]	0

The test for the three cases was performed for a general loading condition with the characteristics shown in table B.1. From the beginning, the third case was considered the

<sup>1</sup>Function GzEq35 in Directory //BuoyUp2Lite/Needs/Mathematica/BuoyUp/NDSolve4.m

most appropriate approach to the problem, for the reasons mentioned below. The other cases were studied in an attempt to reduce the computation time. For this reason, the ship's responses on regular waves, for these specific cases were compared with each other.

The third approach is considered to be more accurate, because the function of GZ calculation is imbedded directly into the differential equation. As a result, after some iterations the angle, thus the response of the ship in roll motion, that satisfies equation, is approximated. For each instant, the response angle is found to satisfy the system. In contrast to the other two cases, where the differential is solved for one time interval in order to find the response angle, and then this is used as the initial condition for the next time interval.

Even when cases 1 and 2, were studied with a reduced step, the results were not satisfactory. The time step between calculations, especially for case 2, was reduced considerably. But even with a small time step, the results for case 2 were not always close to those of case 3. When comparing the responses, sometimes there was a correspondence in the results, and in other cases there was not. So even though the second case requires less computing time, it is not preferred because it does not accurately calculate the ship's response.

Further, as far as the first case is concerned, it is the one that requires the most time to perform, because the whole GZ curve is calculated. Also, the polynomial interpolation of the GZ curve's data, to create the fitted function of the instantaneous GZ curve, may lead to a distortion of its form.

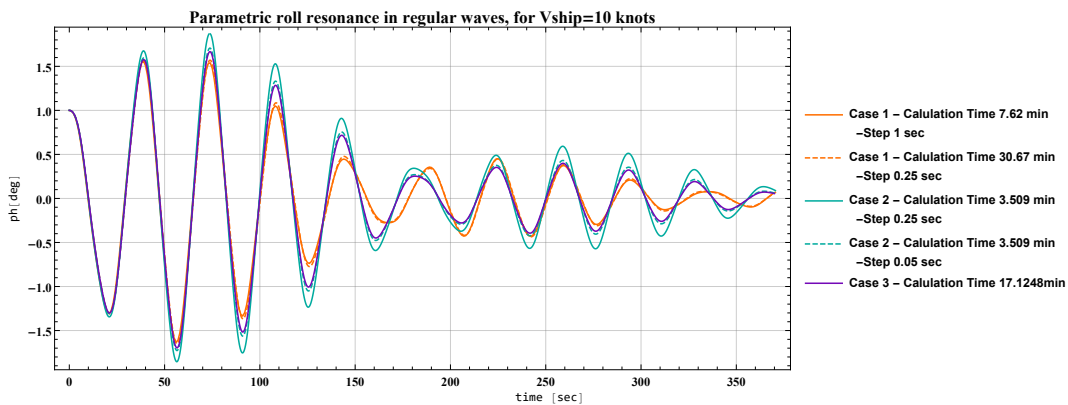


Figure B.1: Comparison of the three different cases with  $V_s = 10$  knots

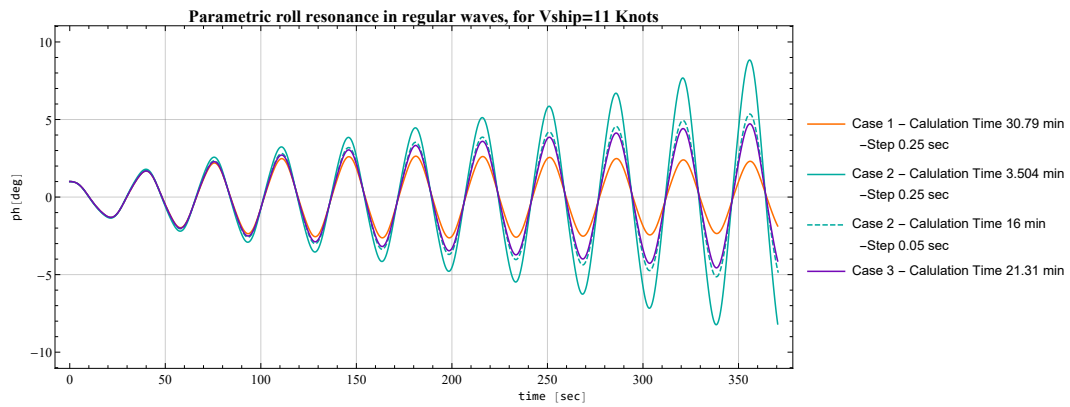


Figure B.2: Comparison of the three different cases with  $V_s = 11$  knots

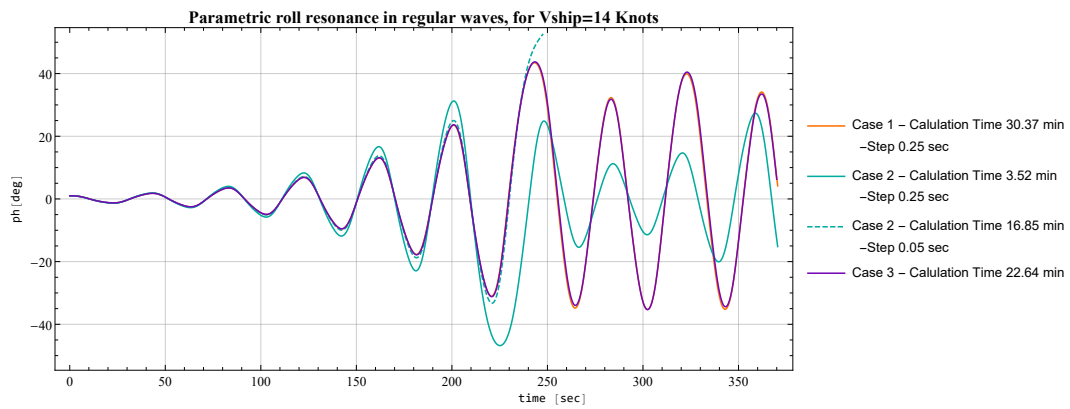


Figure B.3: Comparison of the three different cases with  $V_s = 14$  knots

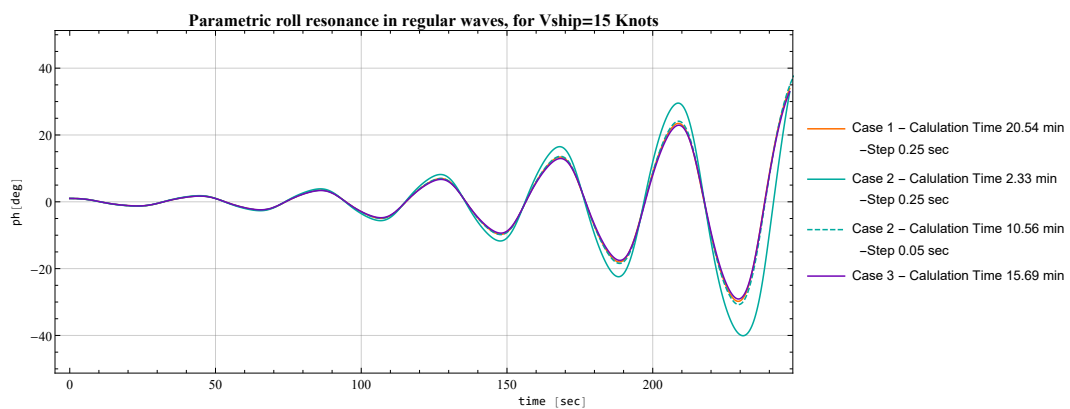


Figure B.4: Comparison of the three different cases with  $V_s = 15$  knots

## B.2 Roll resonance while reducing the initial time step of solver in Mathematica

This Appendix provides material for the brief analysis performed on the accuracy provided by the solver developed to reduce the computation time. As explained in Section 5.1.4: [Numerical Integration of the Roll equation](#), the numerical solver *WSTP-RK4*, was developed. The figures in this appendix compare the ship's responses resulting from the use of the default numerical solver and the *WSTP-RK4*. In the solver *WSTP-RK4* there is the option to select the starting time step. Thus, for a given condition, the same simulations were performed, but with different starting time steps (0.5, 1 and 2 sec). The calculation time is indicated in the legend of each diagram.

The simulations were performed for loading condition 15 with the characteristics listed in the following table. The ship's forward speed, was also chosen to be 12 or 13 knots. In addition this time the simulations were conducted for irregular waves, with specific spectrum characteristics and for 16 different seeds. The procedure for modelling irregular waves is explained in (see chapter 6).

Table B.2: Parameters for solving the differential equation with the three approaches

Characteristics of LC 15		
Displacement	[tons]	75973.8
Mean Draught	[m]	12.52
[ <i>KG</i> , <i>VCG</i> , <i>LCG</i> ]	[m]	[17.17, 0, 115.39]
Initial conditions of the differential equation		
$\phi(0)$	[rad]	$\pi/180$
$\dot{\phi}(0)$	[rad/sec]	0
Parameters used in the differential equation		
$\zeta$	-	0.075
$I_x$	[ <i>tons m</i> <sup>2</sup> ]	$1.20733 \cdot 10^7$
$GM_0$	[m]	0.494
$T_0$	[sec]	35.9863
Wave Characteristics		
$H_s$	[m]	2.5
$T_{peak}$	[sec]	[11.5, 12.5, 13.5]
Wave direction	[deg]	0

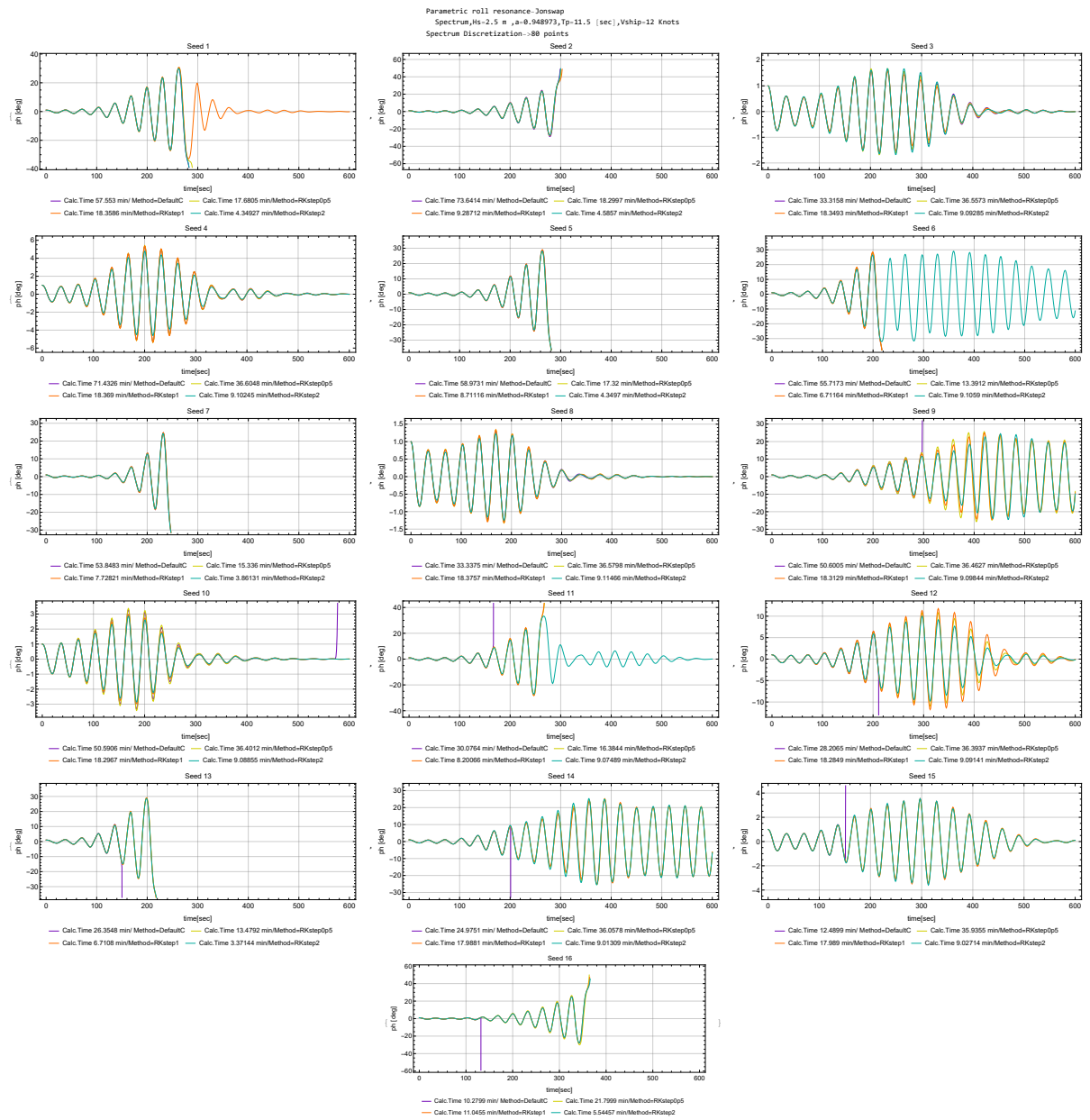


Figure B.5: Comparison of Parametric Roll Resonance in irregular waves ( $T_{peak} = 11.5$  sec,  $V_s = 12$  knots) with 4 differential solvers. The 16 different seeds of the random phase generator are presented and the 4 differential solvers (Default, Runge-Kutta step 0.5, 1, and 2 sec) are compared.

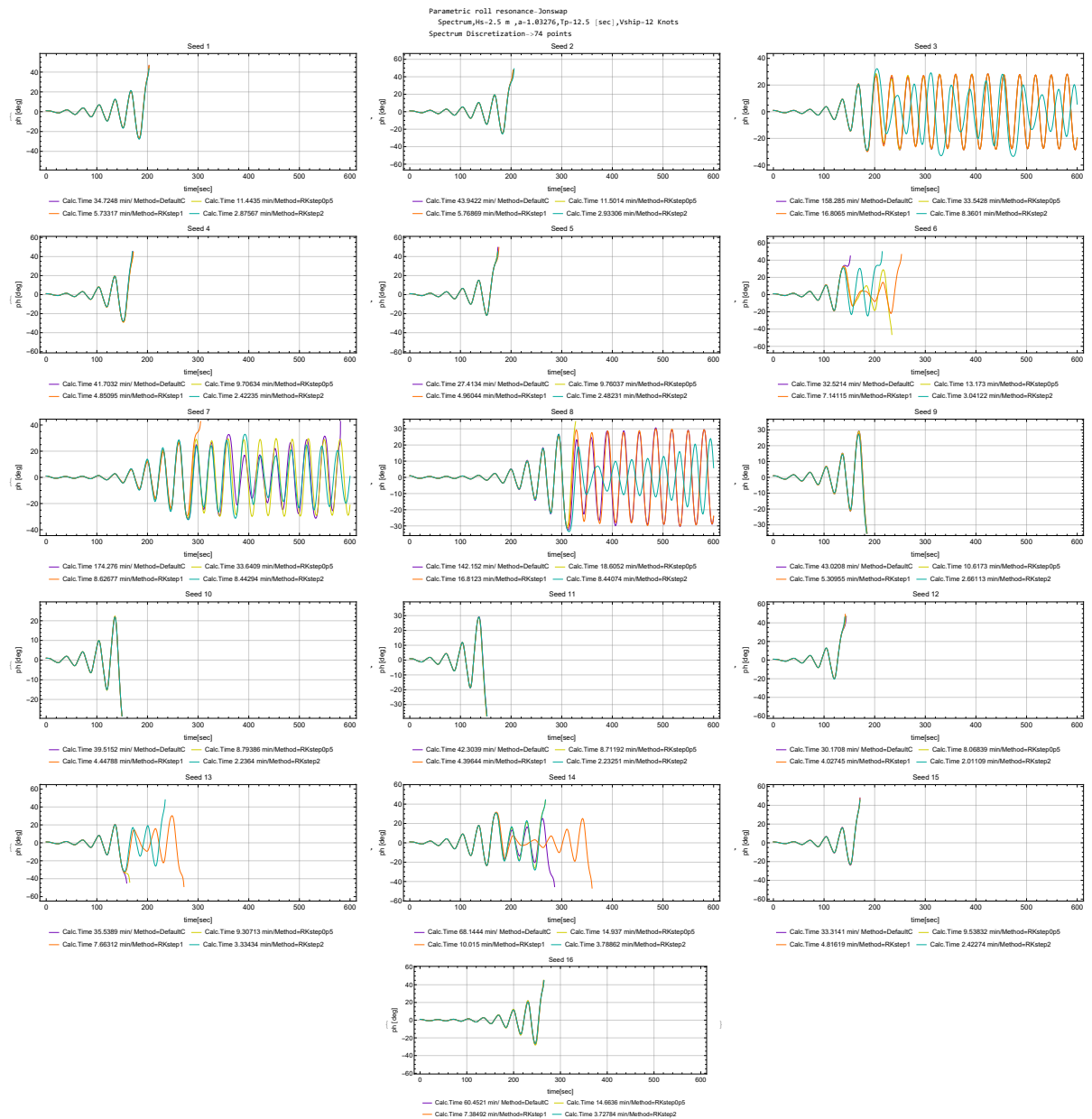


Figure B.6: Comparison of Parametric Roll Resonance in irregular waves ( $T_{peak} = 12.5$  sec,  $V_s = 12$  knots) with 4 differential solvers. The 16 different seeds of the random phase generator are presented and the 4 differential solvers (Default, Runge-Kutta step 0.5, 1, and 2 sec) are compared.



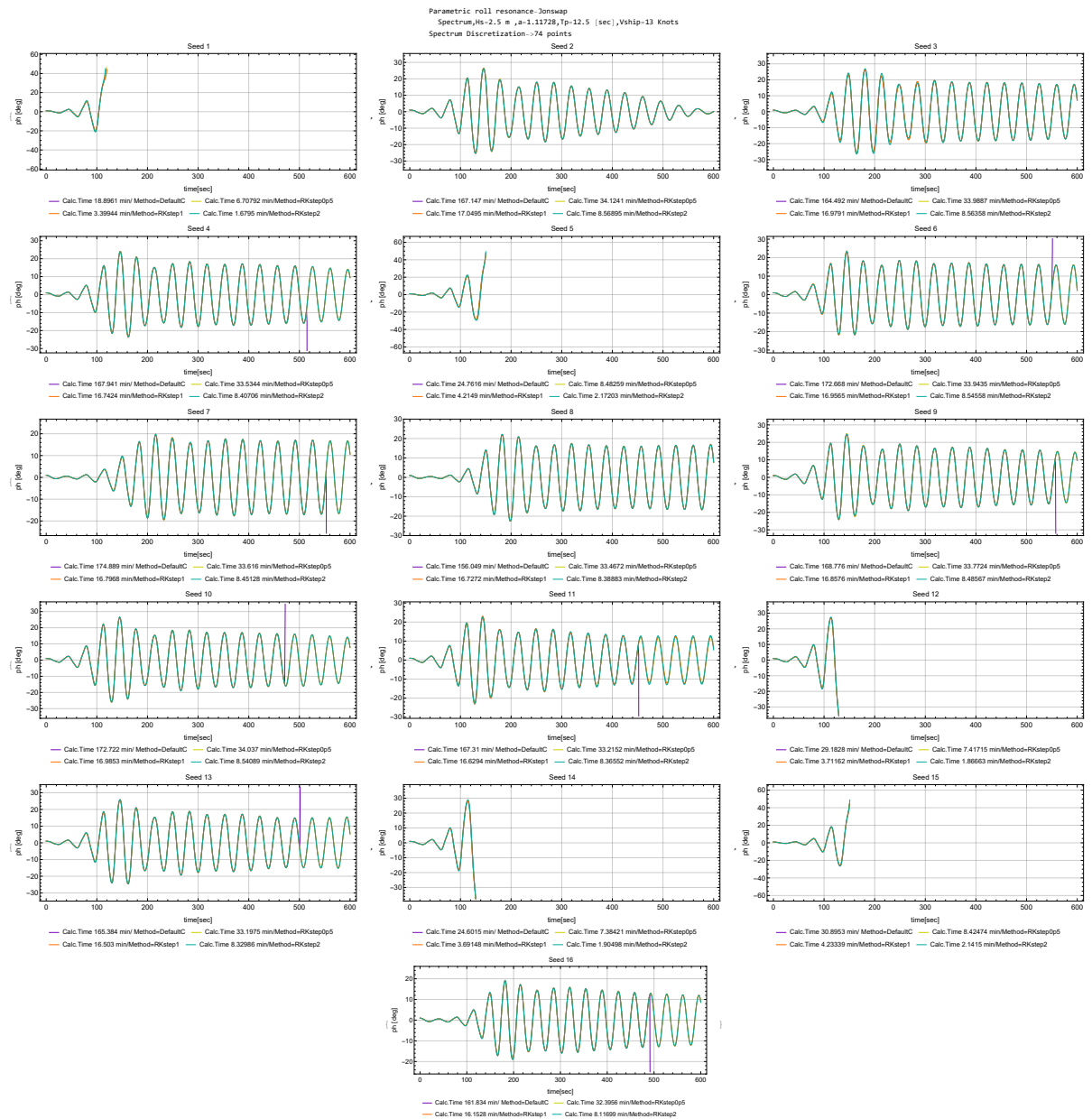


Figure B.7: Comparison of Parametric Roll Resonance in irregular waves ( $T_{peak} = 12.5$  sec,  $V_s = 13$  knots) with 4 differential solvers. The 16 different seeds of the random phase generator are presented and the 4 differential solvers (Default, Runge-Kutta step 0.5, 1, and 2 sec) are compared.

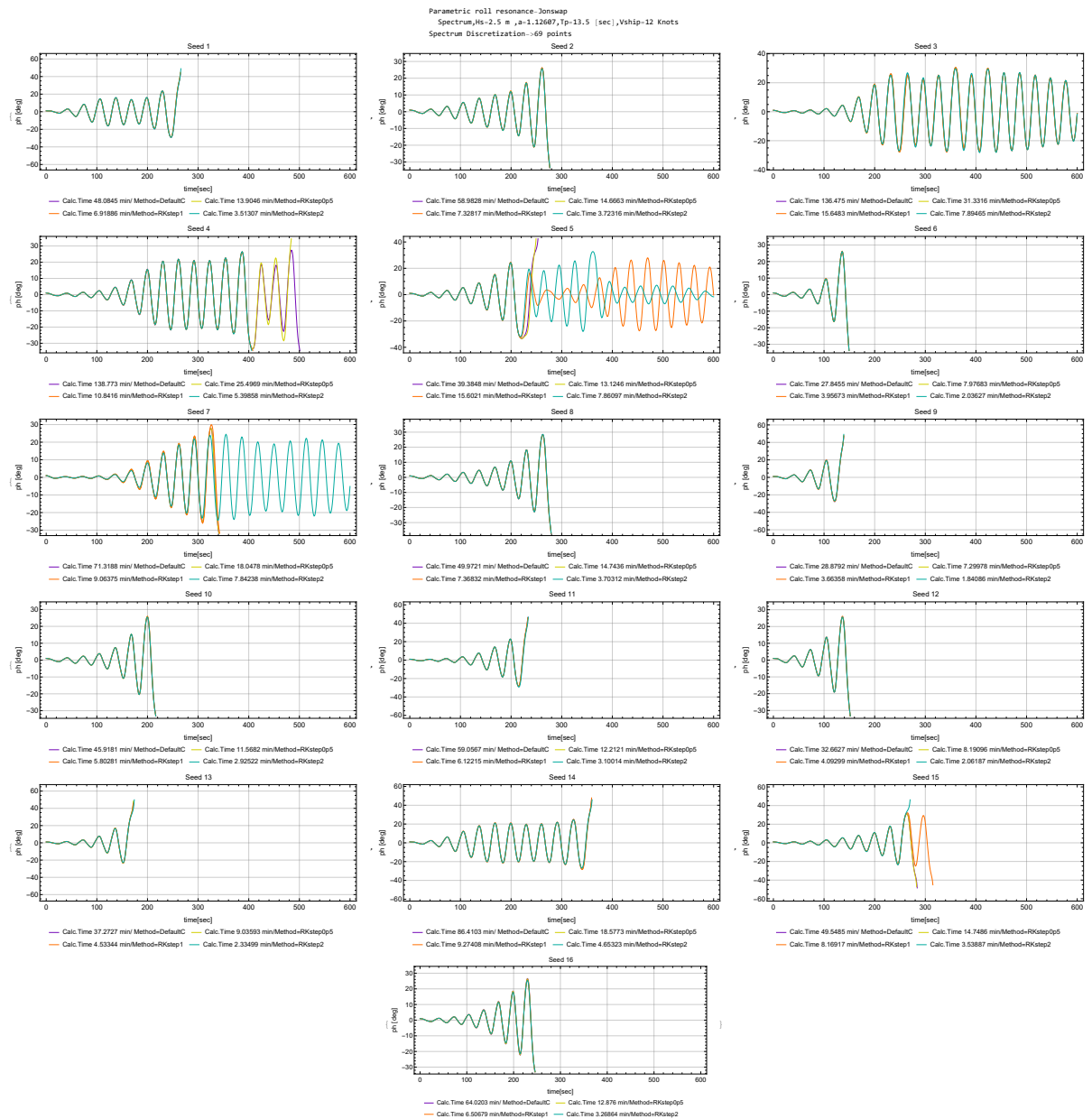


Figure B.8: Comparison of Parametric Roll Resonance in irregular waves ( $T_{peak} = 13.5$  sec,  $V_s = 12$  knots) with 4 differential solvers. The 16 different seeds of the random phase generator are presented and the 4 differential solvers (Default, Runge-Kutta step 0.5, 1, and 2 sec) are compared.

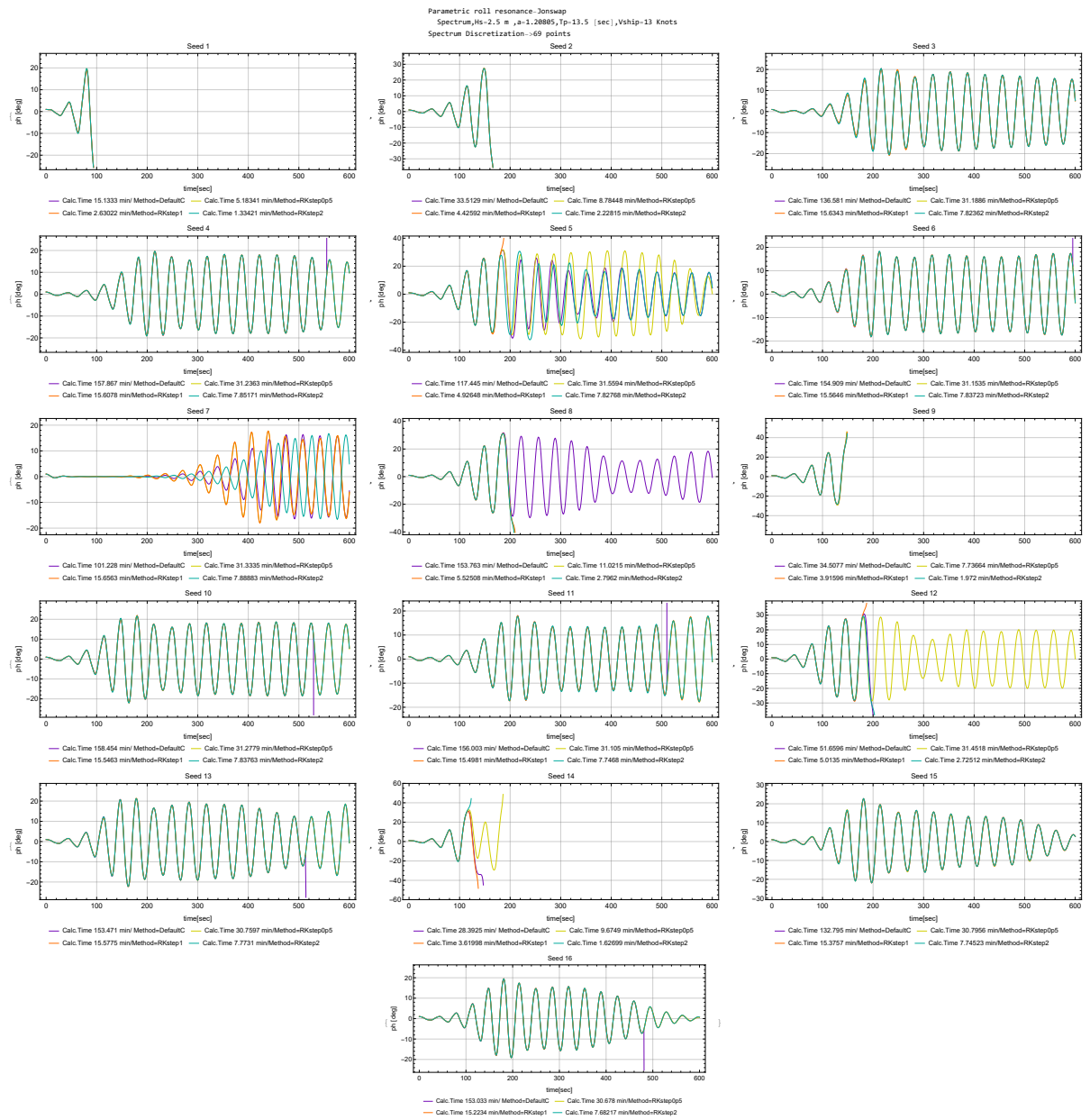


Figure B.9: Comparison of Parametric Roll Resonance in irregular waves ( $T_{peak} = 13.5$  sec,  $V_s = 13$  knots) with 4 differential solvers. The 16 different seeds of the random phase generator are presented and the 4 differential solvers (Default, Runge-Kutta step 0.5, 1, and 2 sec) are compared.

# Appendix C

## Irregular Waves

### C.1 Self-Repeating Effect

In this Appendix, we will give a brief introduction to the phenomenon of self-repeating, and explain how it was used to discretize the spectrum in order to produce the free surface of irregular waves. This section provides the supplementary material of the section 6.1: [Spectrum Characteristics and Discretization](#) of Chapter's 6.

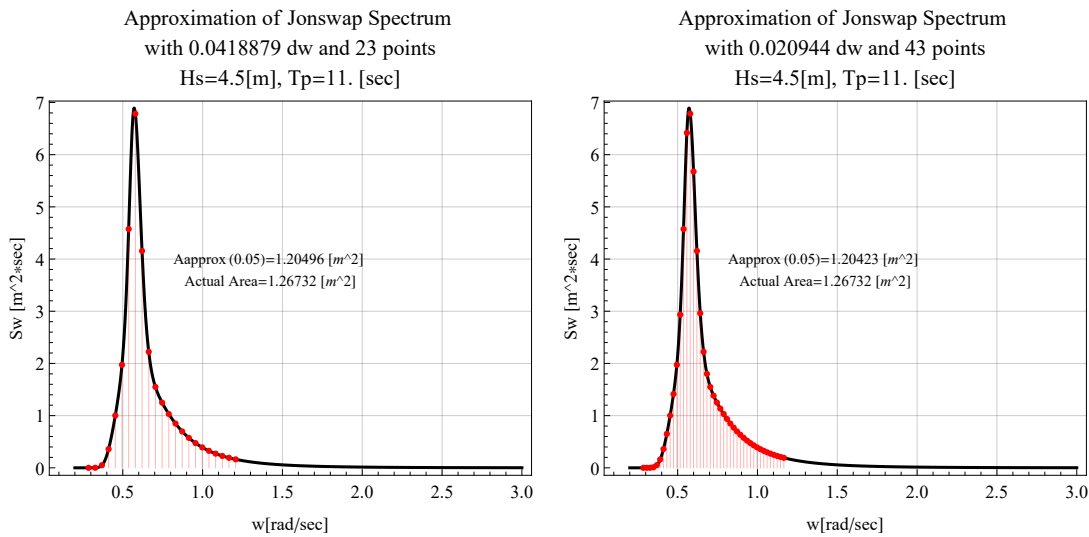


Figure C.1: Jonswap spectrum discretization for  $T_p = 11$ . sec and  $H_s = 4.5$  m with 23 and 43 components respectively

The self-repeating effect is a phenomenon that occurs, when a wave record is reconstructed from spectrum analysis, by using a constant frequency step. When plotting the autocorrelation function for such a record, this can be observed, as a repetitive pattern of high values appears. This means an unrealistically strong probabilistic dependence exists between certain time sections of the process. This effect can be avoided by choosing a non-constant frequency step. However, in the present application, we use a fixed step to discretize the energy spectrum. A brief analysis is performed, which shows how this can be implemented without showing the self-repeating effect.

Figure C.1 presents, the same sea spectrum (with the same characteristics). In both cases a fixed step, bigger than the step  $2\pi/600$  sec, is used (see figure 6.4). The fist has step equal to  $2\pi/300 = 0.020944 \text{ rad/sec}$ , and the second discretization has  $2\pi/150 = 0.04188 \text{ rad/sec}$ .

For these cases, as well as, for the discretization used in this diploma thesis (with step  $2\pi/300 \text{ rad/sec}$ ), the autocorrelation function will be obtained, following the below formula.

$$R(\tau_j) = \sum_{i=1}^N S_{\eta_{\omega_i}} \cos(\omega_i \tau_j); \quad \tau_j = \tau - s = \Delta t j \quad (\text{C.1.1})$$

The result of calculations of autocorrelation function is presented in figures C.3, and C.2. The autocorrelation functions in these figures have several characteristic features. From the plotting of the water elevation for certain time durations, high amplitude oscillations are followed by low-amplitude internals. The patterns are repeated at specific intervals, which are the periods when group similarities are encountered in the elevation of the sea. When the frequency step decreases, then these groups occur more often.

A closer look at the time history shown in figure C.2 reveals that two wave groups are looking suspiciously similar. For the discretization with 23 components, that the first wave group (for  $t = [0, 150]$ ) is very close to the third wave group ( $t = [450, 600]$ ). The second wave group resembles the first group taken but with the sign inverted (the second group is already plotted with the sign inverted). In figure C.2, we see also that are two bigger wave groups that are almost identical (without one of them being inverted). In figure C.3, the frequency step is larger, but identical wave groups are also detected. Finally, in figure C.4, the self-repeating effect does not exist, as the frequency step is reduced sufficiently so that the high amplitude oscillations in the autocorrelation function are shifted in time.

After this analysis, it is easy to say why we chose a fixed discretization step equal to  $2\pi/600 \text{ [rad/sec]}$ , since we know a priori that the simulations are performed for 600 sec. However, it should be noted that in order to avoid the self-repeating effect, a large number of frequencies must be used if a long period of simulation is needed. For instance, if we wanted to find the roll response for 1200 seconds, thus for 20 minutes, instead of 10, the step should be at least  $2\pi/1200 = 0.04188 \text{ rad/sec}$ . This would require 165 frequencies (twice as much). So 165 components would be needed to reconstruct a 20-minute wave record, and so on. It means that 165 components have to be summed at every time step of the simulation which significantly increases the computational cost of such a simulation.

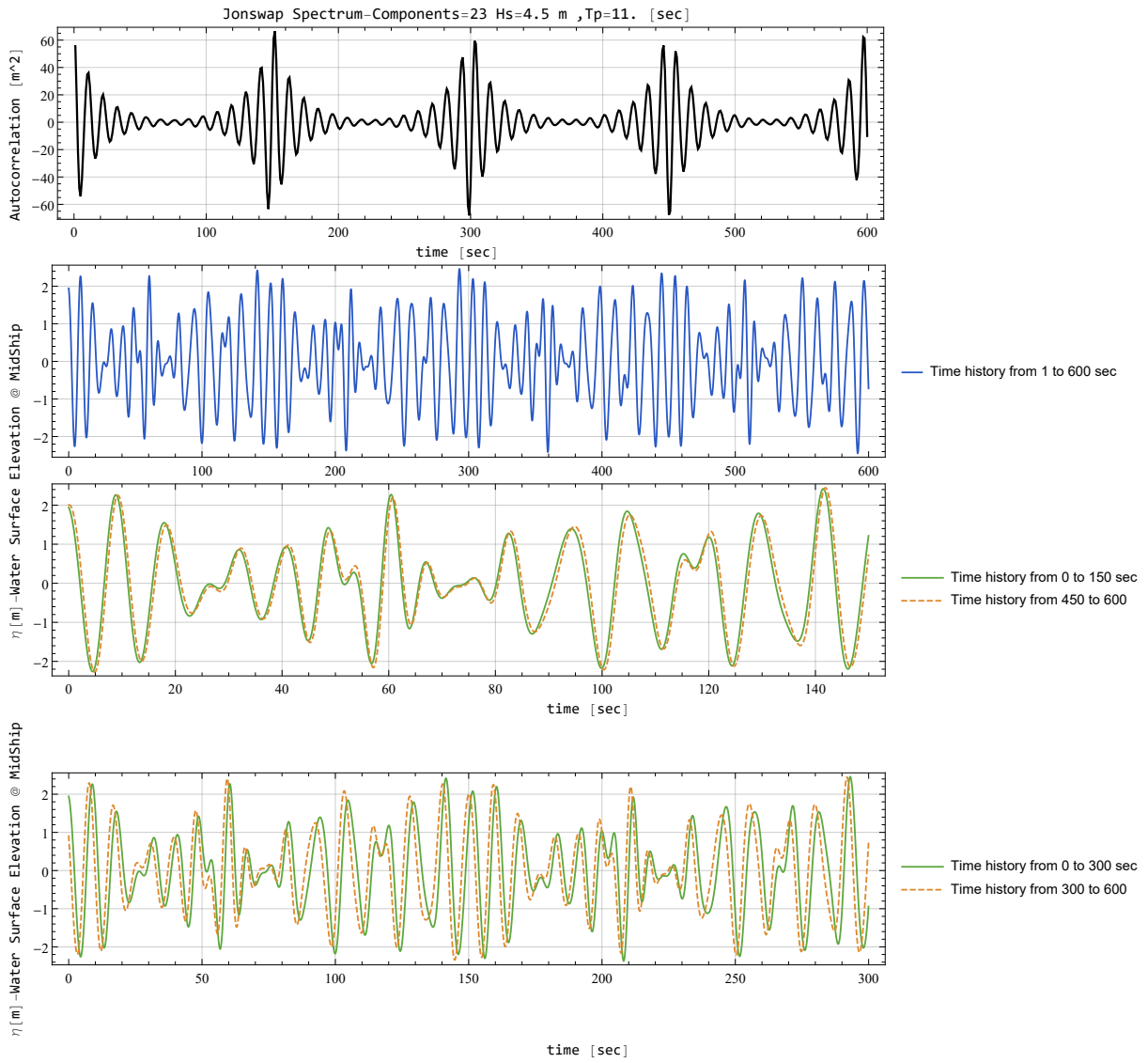


Figure C.2: Autocorrelation function and water surface elevation for spectrum discretization with  $N = 23$  components

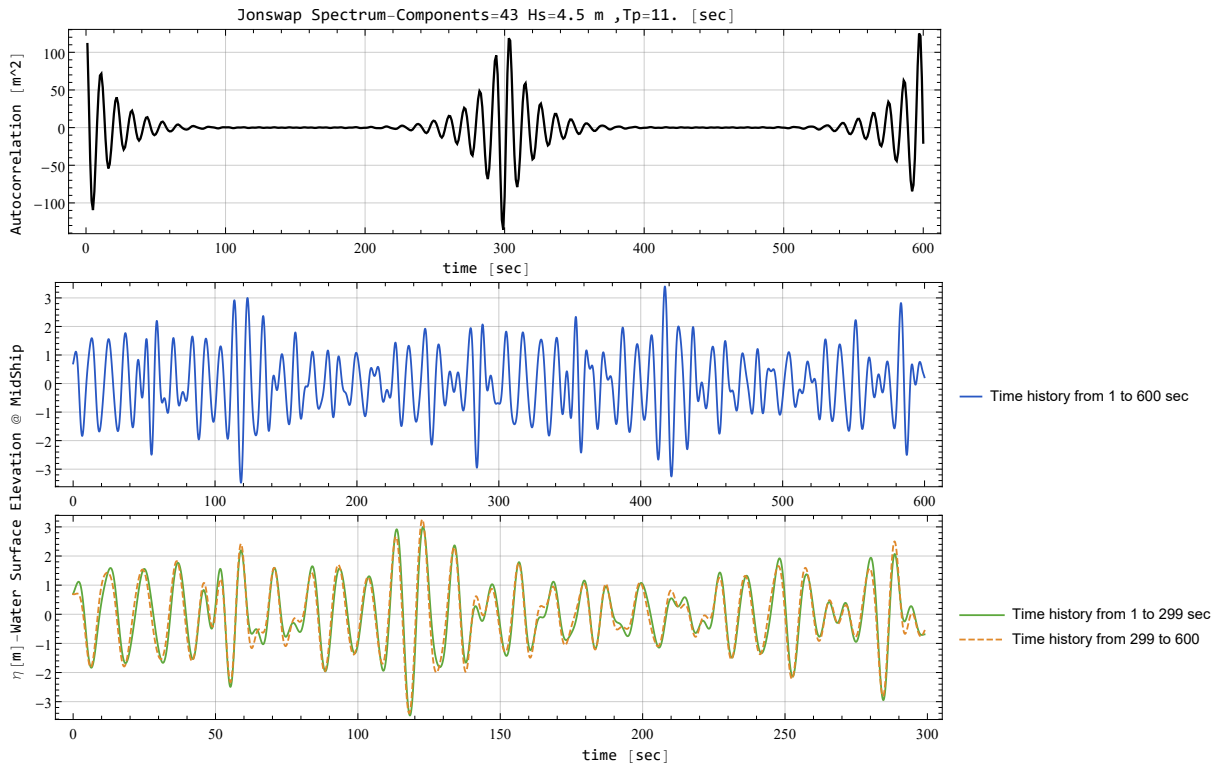


Figure C.3: Autocorrelation function and water surface elevation for spectrum discretization with  $N = 43$  components

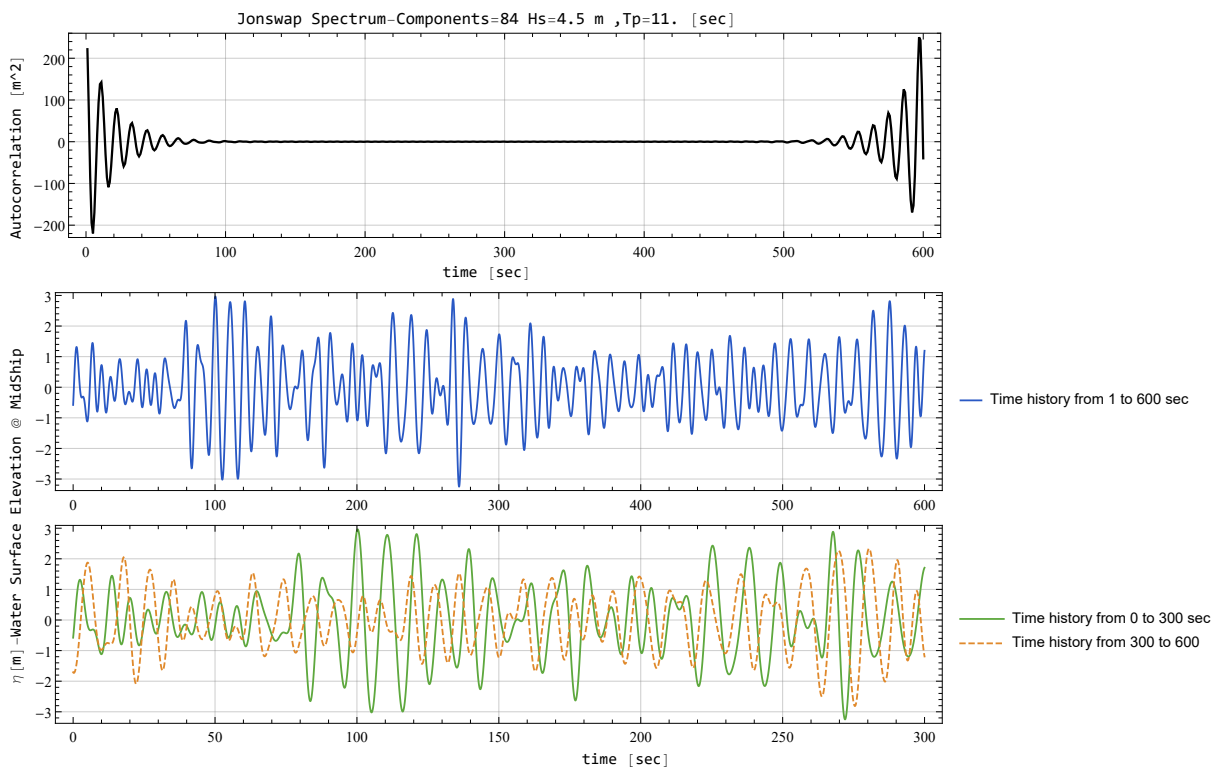


Figure C.4: Autocorrelation function and water surface elevation for spectrum discretization with  $N = 84$  components

## C.2 Data sets for Stability Charts and their Computation time

In this section there is additional material on the range of cases chosen to be used to produce the stability diagrams. The tables below show the pairings ( $T_p$ ,  $H_s$ ) for which the simulations were performed. The total time required for the calculation of all cases is also presented.

Table C.1: Range of data and total computation time-constant  $V_s = 6.5$  knots

$H_s$ [m]	Range of $T_p$ in sec	Cases x seeds
0.5	[5, 5.5, ..., 8.5, 9]	9 x 16
1.0	[5, 5.5, ..., 9.5, 10]	11 x 16
1.5	[5, 5.5, ..., 11.5, 12]	15 x 16
2.0	[5.5, 6, ..., 12, 12.5]	15 x 16
2.5	[5.5, 6, ..., 12.5, 13]	16 x 16
[3, 3.5]	[6, 6.5, ..., 13, 13.5]	16 x 2 x 16
[4, 4.5]	[6.5, 7, ..., 13.5, 14]	16 x 2 x 16
5.0	[7, 7.5, ..., 13.5, 14]	15 x 16
[5.5, 6, ..., 7]	[7.5, 8, ..., 13.5, 14]	14 x 4 x 16
7.5	[8, 8.5, ..., 13, 13.5]	12 x 16
[8, 8.5]	[8.5, 9, ..., 13, 13.5]	11 x 2 x 16
9	[9, 10.5, ..., 12.5, 13]	9 x 16
Total Time: 75.744 hrs=3.1 days// Total cases: 244 x 16 =3904		

Table C.2: Range of data and total computation time-constant  $V_s = 12.5$  knots

$H_s$ [m]	Range of $T_p$ in sec	Cases x seeds
0.5	[6, 6.5, 6.8, 7.5, 8, 8.7, 9]	7 x 16
1.0	[6, 6.5, 6.8, 7.5, 8, 8.7, 9, 9.5, 10]	9 x 16
2.0	[6, 6.5, 6.8, 7.5, 8, 8.7, 9, 9.5, 10, 10.8, 11, 11.5, 12, 12.5]	14 x 16
[3, 3.5]	[6, 6.5, 6.8, 7.5, 8, 8.7, 9, 9.5, 10, 10.8, 11, 11.5, 12, 12.5, 13, 13.5]	16 x 2 x 16
[4, 4.5]	[6.5, 6.8, 7.5, 8, 8.7, 9, 9.5, 10, 10.8, 11, 11.5, 12, 12.5, 13, 13.5, 14]	16 x 2 x 16
5.0	[6.8, 7.5, 8, 8.7, 9, 9.5, 10, 10.8, 11, 11.5, 12, 12.5, 13, 13.5, 14]	15 x 16
[5.5, 6, ..., 7]	[7.5, 8, 8.7, 9, 9.5, 10, 10.8, 11, 11.5, 12, 12.5, 13, 13.5, 14]	14 x 4 x 16
7.5	[8, 8.7, 9, 9.5, 10, 10.8, 11, 11.5, 12, 12.5, 13, 13.5]	12 x 16
[8, 8.5]	[8, 9, 9.5, 10, 10.8, 11, 11.5, 12, 12.5, 13, 13.5]	11 x 2 x 16
9	[9, 9.5, 10, 10.8, 11, 11.5, 12, 12.5, 13]	9 x 16
Total Time: 64.035 hrs=2.66 days// Total cases: 208 x 16 =3328		



Table C.3: Range of data and total computation time for the other 3 cases

(a) Constant  $V_s = 0$  knots

$H_s$ [m]	Range of $T_p$ in sec	Cases x seeds
2.5	[6, 6.5, 6.8, 7.5, 8]	5 x 16
3.5	[6, 6.5, 6.8, 7.5, 8, 8.7, 9, 9.5, 10, 10.8, 11, 11.5, 12, 12.5, 13, 13.5]	16 x 16
[4, 4.5]	[6.5, 6.8, 7.5, 8, 8.7, 9, 9.5, 10, 10.8, 11, 11.5, 12, 12.5, 13, 13.5, 14]	16 x 2 x 16
5.0	[6.8, 7.5, 8, 8.7, 9, 9.5, 10, 10.8, 11, 11.5, 12, 12.5, 13, 13.5, 14]	15 x 16
[5.5, 6, ..., 7]	[7.5, 8, 8.7, 9, 9.5, 10, 10.8, 11, 11.5, 12, 12.5, 13, 13.5, 14]	14 x 4 x 16
7.5	[8, 8.7, 9, 9.5, 10, 10.8, 11, 11.5, 12, 12.5, 13, 13.5]	12 x 16
[8, 8.5]	[8, 9, 9.5, 10, 10.8, 11, 11.5, 12, 12.5, 13, 13.5]	11 x 2 x 16
9	[9, 9.5, 10, 10.8, 11, 11.5, 12, 12.5, 13]	9 x 16
Total Time: 54.32 hrs=2.26 days// Total cases: 167 x 16 =2672		

(b) Constant  $T_p = 11$  sec

$H_s$ [m]	Range of $V_s$ in knots	Cases x seeds
[1.5, 2, 2.5]	[6.15, 6.5]	3 x 2 x 16
[3, 3.5, ..., 9]	[4.27, 6.15, 6.5, 7.71, 9.03, 10.16, 11.60, 12.02, 13.16, 14.42, 14.84, 15.23, 15.94, 16.37, 16.77, 17.148, 17.58, 17.98, 18.35, 18.69, 19.2]	21 x 13 x 16
Total Time: 90.84 hrs=3.78 days// Total cases: 279 x 16 =4464		

(c) Constant  $T_p = 8.5$  sec

$H_s$ [m]	Range of $V_s$ in knots	Cases x seeds
[1, 1.5, ..., 9]	[4.27, 6.15, 6.5, 7.71, 9.03, 10.16, 11.60, 12.02, 13.16, 14.42, 14.84, 15.23, 15.94, 16.37, 16.77, 17.148, 17.58, 17.98, 18.35, 18.69, 19.2]	21 x 18 x 16
Total Time: 110.96 hrs=5.04 days// Total cases: 378 x 16 =6048		

### C.3 Stability Charts for every seed

In this appendix the stability diagrams for random waves, are presented in a contour plots. For each case studied, the maximum response that occurred for each seed is plotted. This section provides the supplementary material of the section 7: [Results and Discussion](#) of Chapter's 6.



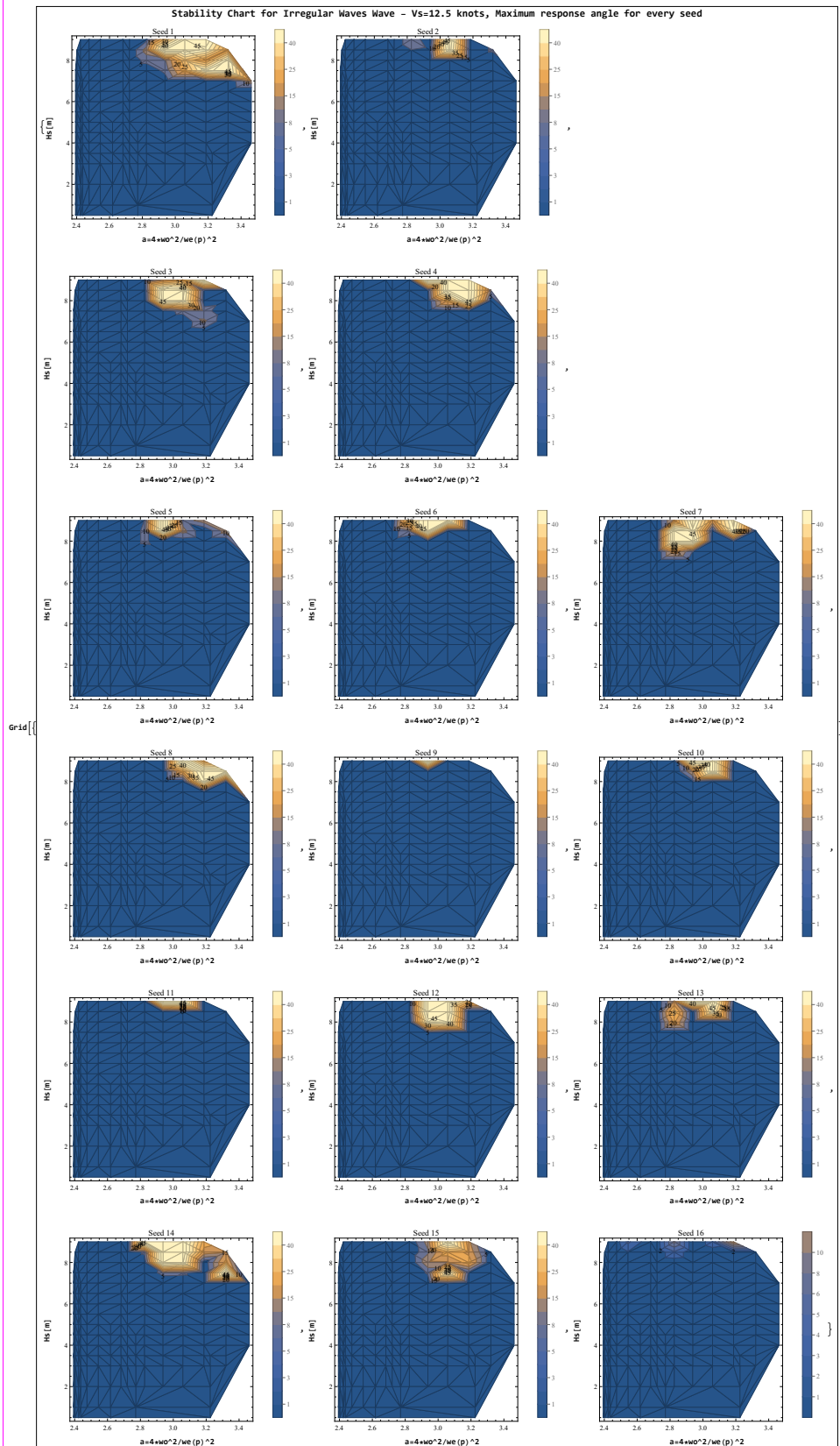


Figure C.6: Diagram for maximum angle response for every seed-constant  $V_s = 12.5$  knots

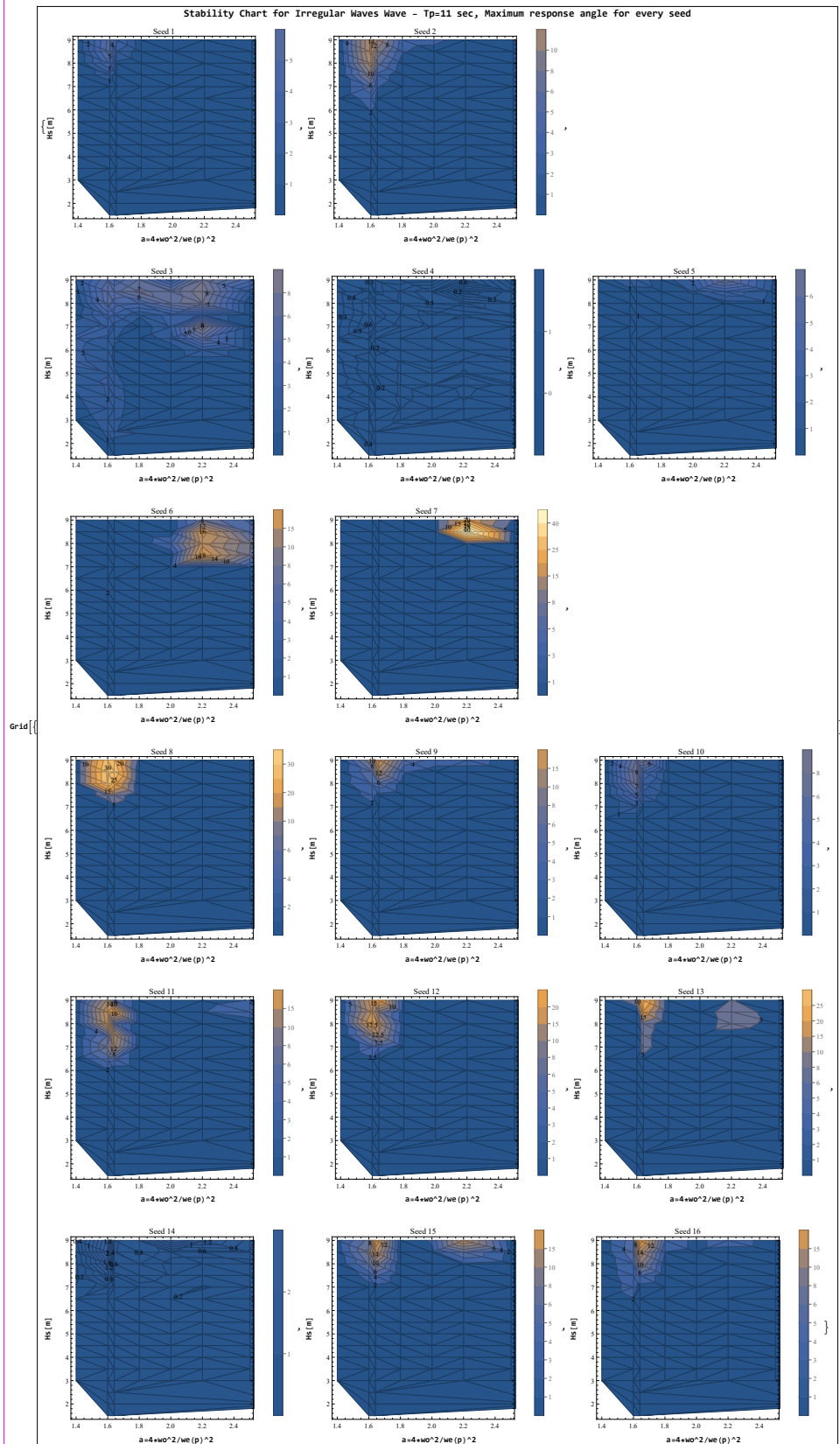


Figure C.7: Diagram for maximum angle response for every seed - constant  $T_p = 11$  sec

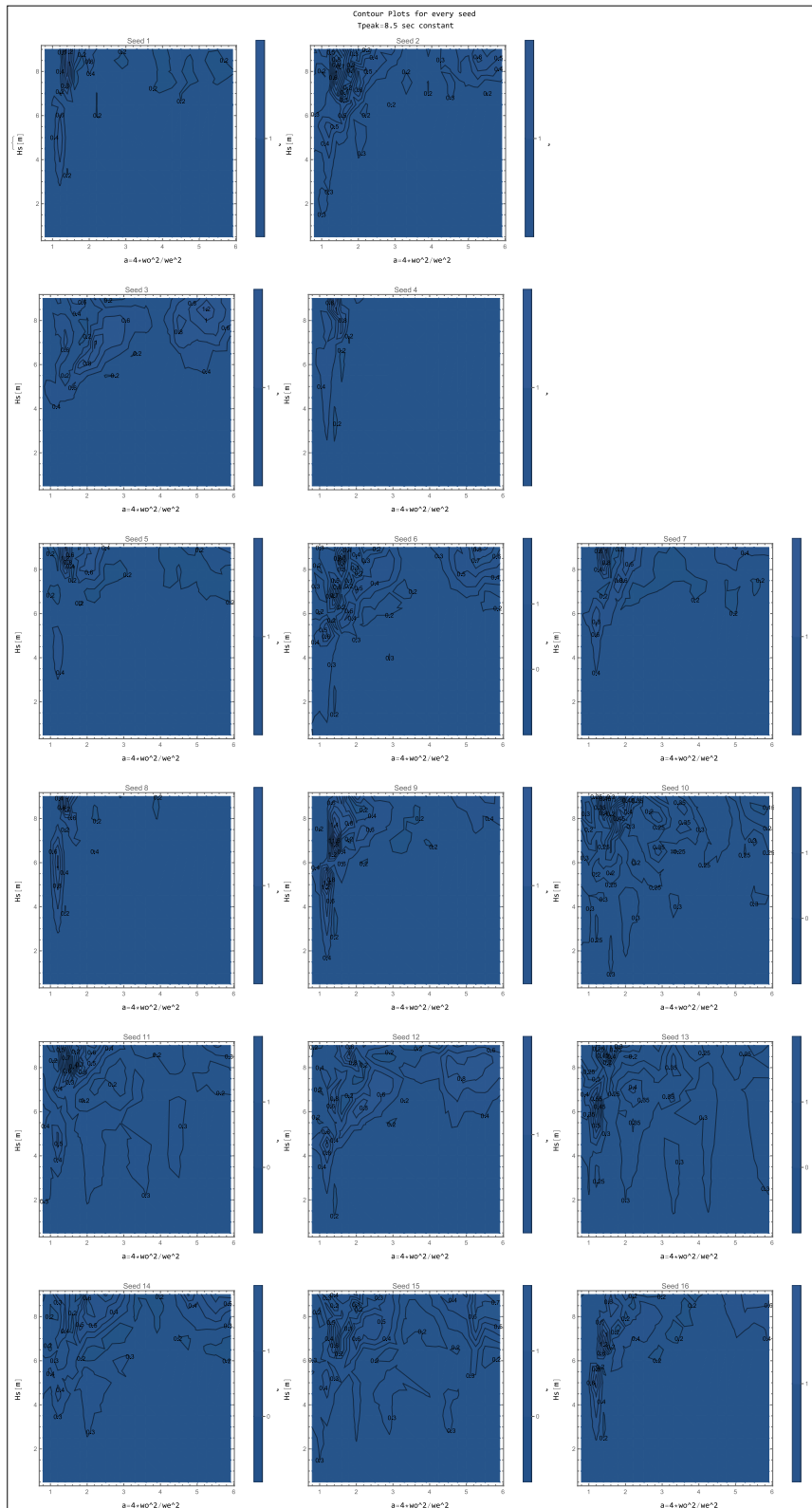


Figure C.8: Diagram for maximum angle response for every seed - constant  $T_p = 8.5$  sec

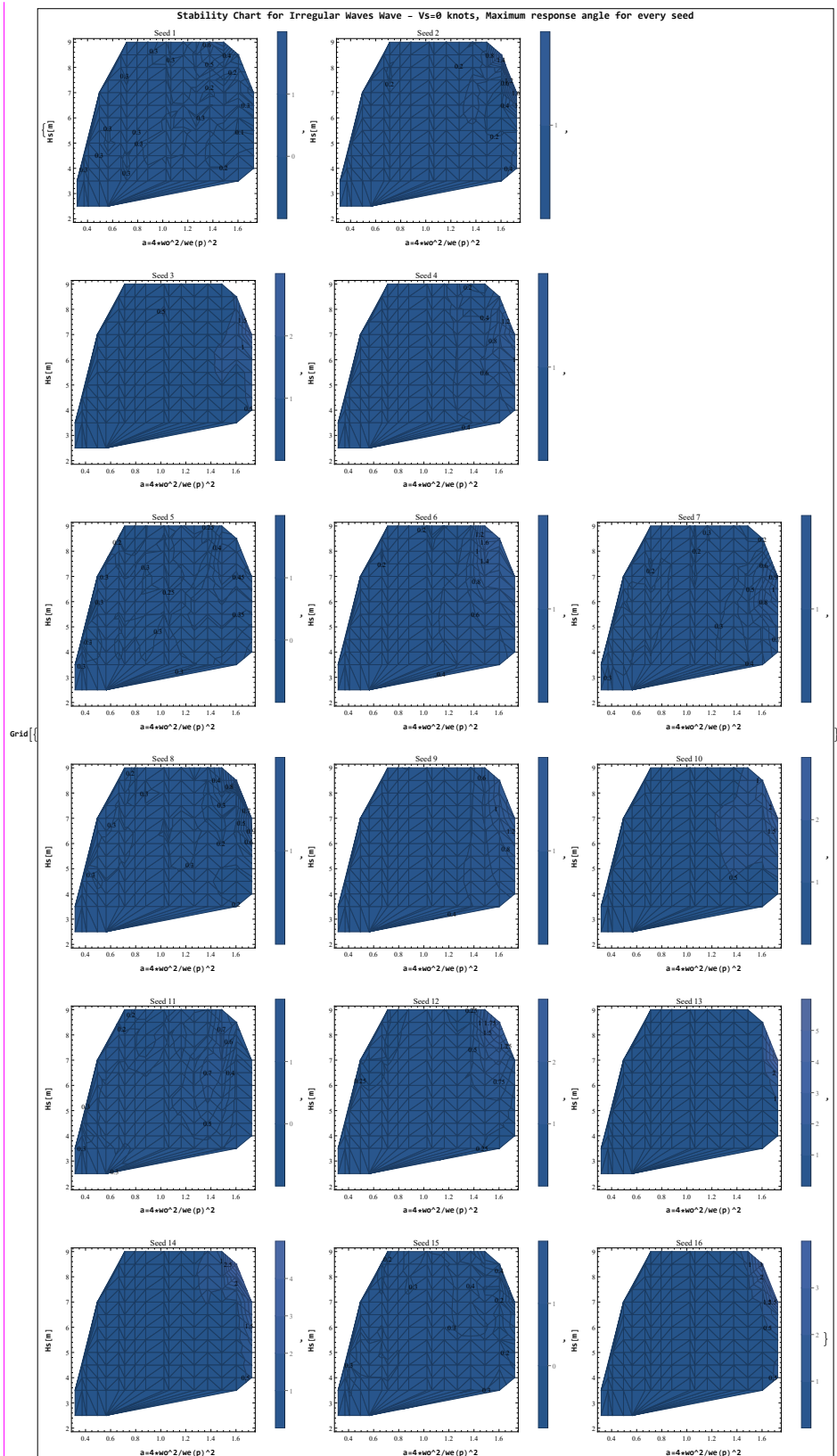


Figure C.9: Diagram for maximum angle response for every seed - constant  $V_s = 0$  knots



## C.4 Ship Responses for different cases

In this appendix, some selected ship responses for each of the 16 seeds are presented. This section provides supplementary material for the section 7: [Results and Discussion](#) of Chapter's 6, for the results of the stability diagrams produced.

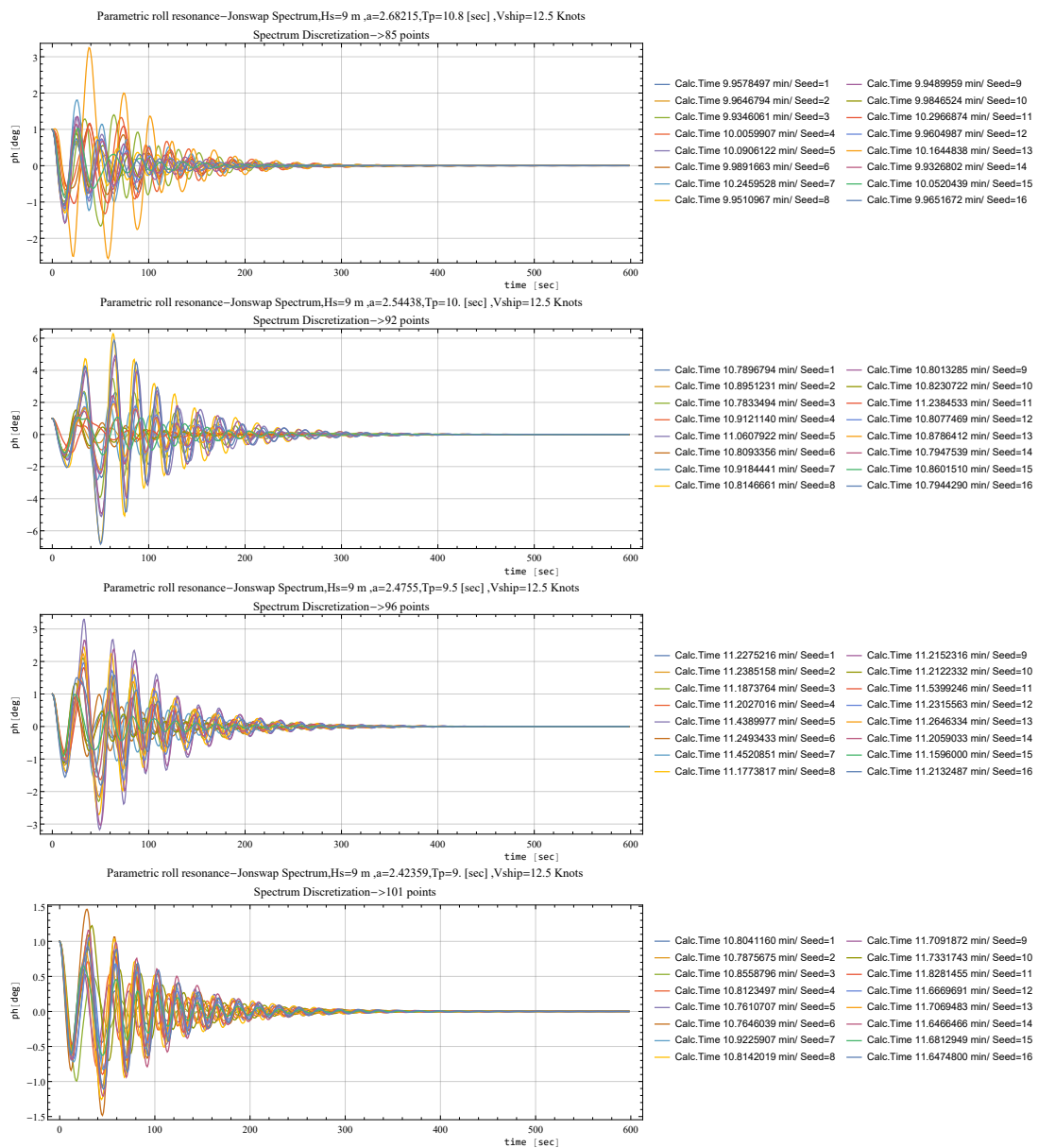


Figure C.10: Parametric roll resonance for  $H_s = 9$  m - constant  $V_s = 12.5$  knots  
 Certain peak periods are presented,  $T_p = 9/9.5/10/10.8$  sec

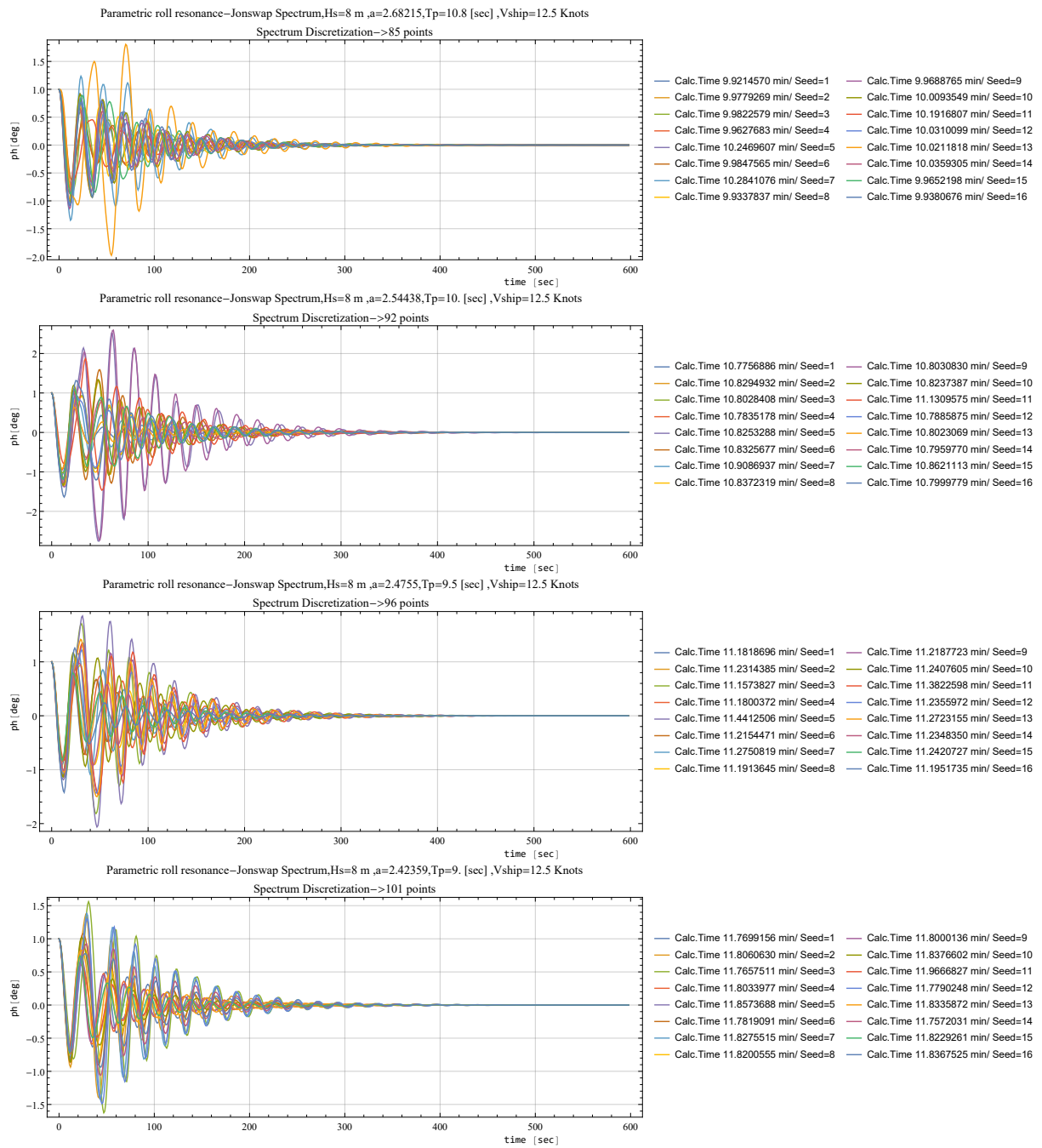


Figure C.11: Parametric roll resonance for  $H_s = 8$  m - constant  $V_s = 12.5$  knots  
 Certain peak periods are presented,  $T_p = 9/9.5/10/10.8$  sec



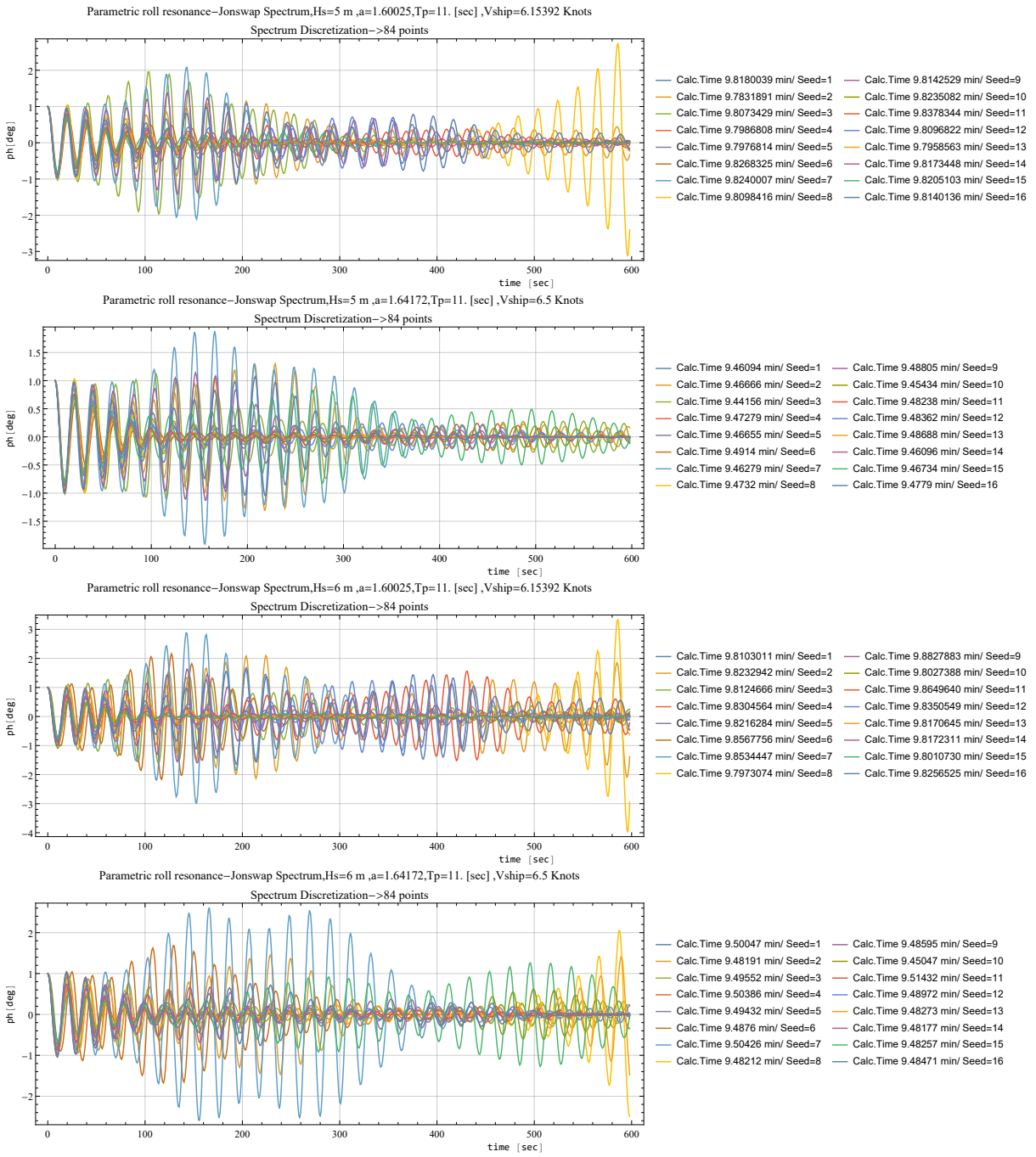


Figure C.12: Parametric roll resonance for  $H_s = 5$  and  $H_s = 6$  m - constant  $T_p = 11$  sec  
 Specific speeds are presented,  $V_s = 6.5/6.15$  knots

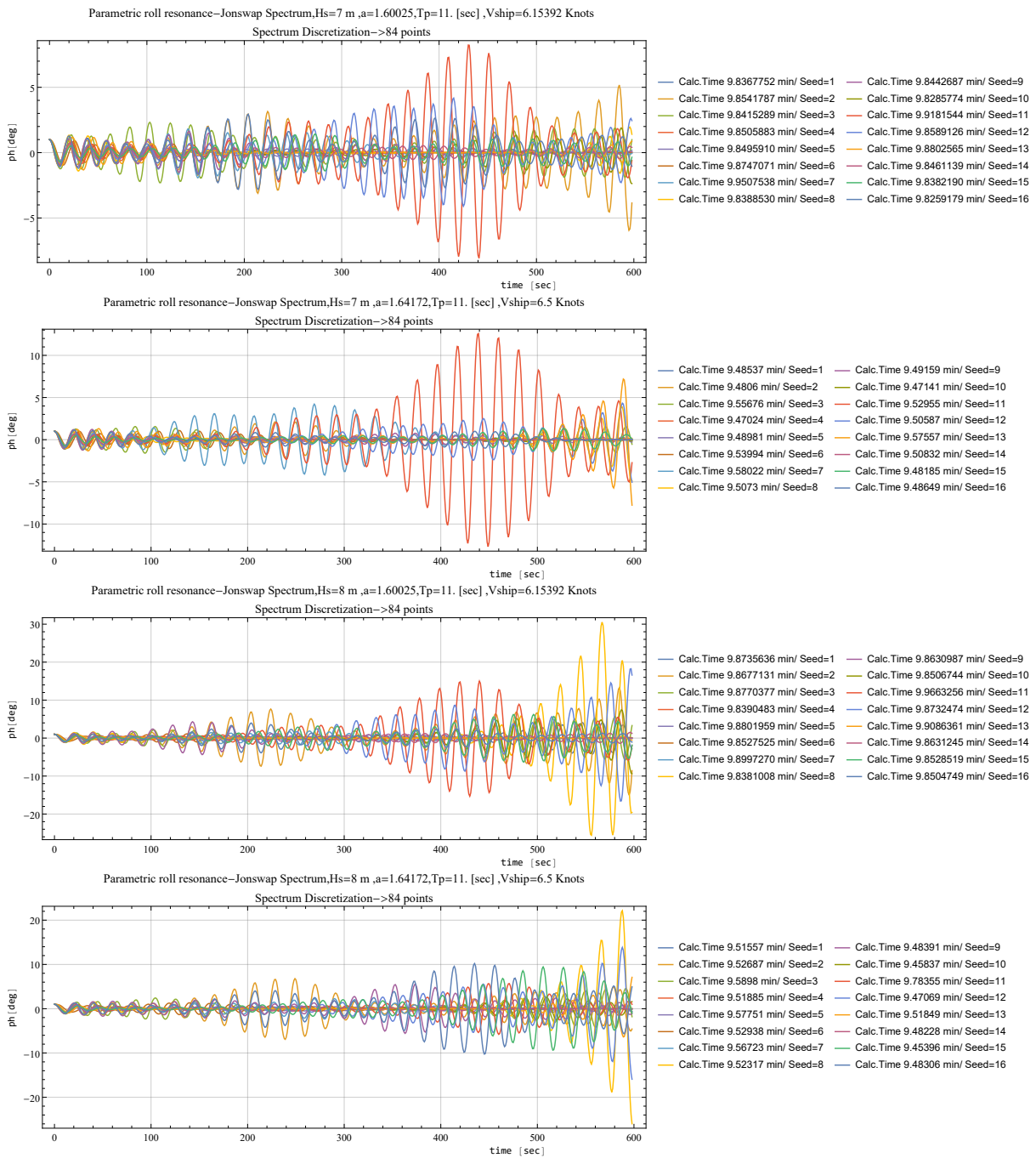


Figure C.13: Parametric roll resonance for  $H_s = 7$  and  $H_s = 8$  m - constant  $T_p = 11$  sec  
 Specific speeds are presented,  $V_s = 6.5/6.15$  knots